ORNL-3167
UC-80 – Reactor Technology

HOMOGENEOUS REACTOR PROGRAM PROGRESS REPORT FOR PERIOD FROM DECEMBER 1, 1960, TO MAY 31, 1961

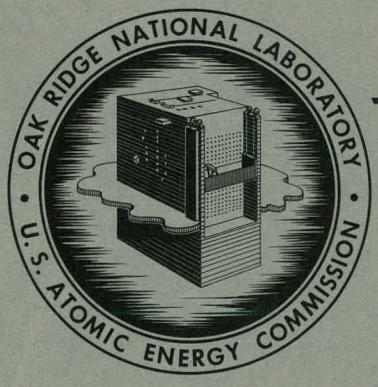

OAK RIDGE NATIONAL LABORATORY
operated by
UNION CARBIDE CORPORATION
for the
U.S. ATOMIC ENERGY COMMISSION

DISCLAIMER

Printed in USA. Price $2.50. Available from the
Office of Technical Services
Department of Commerce
Washington 25, D.C.

ORNL-3167
UC-80 - Reactor Technology
TID-4500 (16th ed.)

Contract No. W-7405-eng-26

HOMOGENEOUS REACTOR PROGRAM

PROGRESS REPORT

FOR PERIOD FROM DECEMBER 1, 1960, TO MAY 31, 1961

Program Director - R. B. Briggs

Homogeneous Reactor Test - S. E. Beall
Reactor Analysis and Engineering Development - R. N. Lyon
Reactor Materials Research - E. G. Bohlmann
Chemical Engineering Development - D. E. Ferguson
Supporting Chemical Research - H. F. McDuffie
Analytical Chemistry - M. T. Kelley

DATE ISSUED

SEP -6 1961

OAK RIDGE NATIONAL LABORATORY
Oak Ridge, Tennessee
operated by
UNION CARBIDE CORPORATION
for the
U.S. ATOMIC ENERGY COMMISSION

THIS PAGE

WAS INTENTIONALLY

LEFT BLANK

SUMMARY

PART I. HOMOGENEOUS REACTOR TEST

1. HRT Operations

Four HRT runs were completed during the report period. The primary objective in each run was to study the reactor behavior with modified (or downward) core flow.

For 314 hr, the reactor operated at its full power of 5 Mw (50% in the core) with no indications of fuel instability. On April 17, while the reactor was subcritical, the mixing rate between core and blanket increased sharply. This increased the blanket concentration, and accordingly the blanket power fraction increased from 50 to 64%. After this incident a power-dependent temperature rise was observed when the power was raised to 5 Mw. This appears to have been a result of uranium deposition in the blanket region.

In May, after the final shutdown, examination of the core interior revealed that the upper patch had fallen out after the patch bolt failed at a point in the blanket region, thereby accounting for the increase in core-to-blanket mixing.

A period of reactor inspection, removal of corrosion specimens, and stand-by storage has been initiated. The reactor will not be operated again.

2. HRT Processing Plant

Final hydroclone-system tests confirmed previous observations that the efficiency of multiclones operated with induced underflow is very low. Solids removal rates with the revised unit averaged only 0.3 g/hr, somewhat less than with the original single hydroclone and substantially less than with the initial multiclone unit. For unknown reasons, the iron content of solids removed following the core-flow reversal was significantly higher than in previous runs.

Reactor off-gas samples were obtained following two periods of constant-power operation for subsequent mass-spectrographic analyses from which Xe^{135} poison fractions may be calculated.

Development of the uranyl peroxide fuel-processing system to remove nickel and other soluble contaminants was concluded with full-scale nonradioactive engineering tests. Decontamination factors of 100 were obtained with three rinses of the precipitate. Losses of uranium due to solubility of uranyl peroxide in the simulated fuel at a concentration of 75 g of U per liter were approximately 3%.

Efficiency tests conducted on the stack-filter iodine traps showed that iodine in very low concentrations is not removed effectively from the ventilation air, but that decontamination factors of at least 1000 would be obtained for large releases into the waste system.

3. HRT Component Design and Development

Runs were made with the HRT flow model to investigate the neutron-level fluctuations observed in the reactor. Power generation was simulated by injecting salt into a number of locations in the core. By analyzing the output concentration as a function of time with the aid of an analogue computer, simulated power-time traces were obtained which were very similar to the power-time trace of the HRT itself. It was concluded that the power (neutron-level) fluctuations of the HRT were caused by flow perturbations.

A flow nozzle was developed for insertion into the HRT which would improve the wall cooling and also reduce the neutron-level fluctuations.

A corrosion-specimen holder and a thermocouple probe for insertion into the HRT core were designed and were tested in the flow model. Excessive bypassing of inlet fluid, observed initially, was corrected by installing a conical baffle at the core inlet.

A run of the HRT mockup with high acid concentration was terminated after the level controller failed.

Omniscope attachments were received. One of these will go through the 3/8-in. holes in the HRT core screens and will permit viewing of the lower nozzle. The other is a 5X magnifying objective for right-angle viewing in the core.

Following a satisfactory pretreatment run, the spare HRT fuel-circulating pump was slightly damaged during inspection. The pump was judged to be still operational and was placed in standby.

4. HRT Reactor Analysis

Power-trace data from the HRT have been subjected to a variety of statistical tests covering both the observed fluctuations and the reactivity changes necessary to produce them. The positive power and reactivity deviations were found to be consistently larger on the average than the negative deviations. The percentage deviation increased with core power level; it was not established whether pressure, temperature, or flow rate affected the deviations. Comparisons of the fluctuations of a hydrodynamic parameter with measurements made in a core mockup showed a strong similarity. While agreement between the mockup measurements and the reactor data is not complete, the comparison offers considerable support to the idea that hydrodynamic fluctuations are a major cause of the power deviations.

On changing the power level in the HRT, temperature transients due to density changes may occur. It was calculated that going from zero power to 5 Mw produces an initial temperature rise of about 0.7°C followed by a gradual decrease over a 2-hr period to an equilibrium point 1.3°C below the initial assumed level of 265°C.

PART II. ENGINEERING DEVELOPMENT

5. Development of Reactor Components and Systems

The alumina bearings of the 200Z pump continued to operate satisfactorily up to a total of 11,072 hr. The hydraulic drive system of the three-stage compressor for contaminated oxygen was modified to eliminate dirt particles which had been causing diaphragm failures.

Further tests of thoria slurries flowing through small-bore capillary tubes showed the presence of a slip effect characteristic of some slurries. Chemically dispersed slurries exhibited no slip effect; it was found that the ratio of dispersed-slurry viscosity to water viscosity was independent of temperature at constant volume fraction solids.

In run 200B-5, it was shown that friction factors for slurry in turbulent flow correlate very well with Reynolds numbers based on the dispersed-slurry viscosity. These tests were conducted in the temperature range 33 to 240°C.

PART III. SOLUTION FUELS

6. Reactions in Aqueous Solutions

Preliminary experiments show that protactinium does not precipitate rapidly in 2 *M* $Th(NO_3)_4$ - 3 *M* HNO_3 or 2.5 *M* $Th(NO_3)_4$ - 0.5 *M* HNO_3 solutions at temperatures ranging from 21 to 180°C. This indicates that protactinium would be available for removal by processing a side stream of a solution blanket. Information in the literature and the results of one preliminary experiment reported here indicate that a solvent-extraction method is an attractive possibility for removing protactinium from solution.

The solubilities of hydrogen in water and of deuterium in deuterium oxide from room temperature to 300°C are reported graphically. The effects on solubility caused by the addition of some inorganic ions to the solvent are shown for the hydrogen-water system.

7. Heterogeneous Equilibria in Aqueous Systems

In a study of the system UO_3-SO_3-H_2O from 150 to 300°C, with particular emphasis on the nature of the UO_3 solid phases, the stable hydrates found corresponded to $\alpha UO_3 \cdot H_2O$ at 150°C, $\beta UO_3 \cdot H_2O$ at 225°C, and $UO_3 \cdot 1/2\ H_2O$ at 300°C. Their identities were established by comparison of x-ray diffraction patterns with known patterns. Upon changing the temperature from 150 to 225 or 300°C, a slow conversion of the solid phase over an 18-hr period was noted. The slowness of this conversion is believed to have been responsible for previous reports that $UO_3 \cdot H_2O$ rather than $UO_3 \cdot 1/2\ H_2O$ was the stable solid at 300°C in this system and in related systems.

The effect of hydrostatic pressure in raising the temperature of liquid-liquid immiscibility of solutions containing UO_2SO_4, H_2SO_4, and H_2O was observed visually for the first time. Easily reproducible values at pressures up to 5000 psi were obtained for a 1.4 *m* UO_2SO_4 in H_2O solution and for a D_2O solution of 0.6 *m* in UO_3 and 1.0 *m* in D_2SO_4. Upon plotting the temperature of liquid-liquid immiscibility against the pressure, a straight line was obtained which gave respective pressure-temperature coefficients of +5.42°C and +8.13°C per 1000 psi. These were in agreement with the expectation that pressure effects would be relatively large in the vicinity of 300°C and could become very large near the critical temperature of the solutions (i.e., near 374°C, the critical temperature of pure H_2O).

Critical temperatures and compositional boundaries for liquid-liquid immiscibility between 300 and 410°C were determined for the system UO_3-CuO-SO_3-D_2O at $m_{CuO}:m_{UO_3}$ = 0.333 = constant, for the system UO_3-NiO-SO_3-D_2O at $m_{NiO}:m_{UO_3}$ = 1 and 0.333, and for the system UO_3-CuO-NiO-SO_3-D_2O at both $m_{CuO}:m_{UO_3}$ and

and $m_{NiO}:m_{UO_3} = 0.25$. In each set of experiments the temperature of liquid-liquid immiscibility was determined for a series of compositions in which the SO_3 component was held constant and the summation of the molal ratios, $\Sigma(m_{\text{metal oxide}}:m_{SO_3})$, was varied from 1.0 to 0.05. The separate families of curves were analogous to those obtained previously for the systems UO_3-SO_3-D_2O and CuO-SO_3-D_2O. High concentrations of metal oxide components were observed to be stable in the supercritical fluids.

A compilation of solubilities of salts in H_2O above 200°C was presented to show that very little published information exists above 374°C for salts having moderate solubilities in the supercritical fluids. The observations at ORNL that metal oxide components such as UO_3, NiO, and CuO were very soluble in supercritical SO_3-H_2O fluids--gaseous mixtures in all respects--open up a new region of temperature for further investigations. Aqueous homogeneous fuel compositions may ultimately be specified which would be stable at 25°C as well as at temperatures considerably above 374°C.

Further solubilities of ThO_2 in HNO_3-H_2O solutions were determined at 200°C and at a new temperature of 150°C. There was little change in the saturation molal ratio, $m_{ThO_2}:m_{HNO_3}$, between 150 and 200°C at HNO_3 concentrations between 1.0 and 10 *M* (at 25°C). These molal ratios were 0.11 in 1.0 *M* HNO_3 and 0.24 in 10 *M* HNO_3. Refractory ThO_2 dissolved moderately fast in HNO_3-H_2O solutions at 150°C as well as at 200 and 300°C. This constituted additional evidence that aqueous solutions of HNO_3 at these temperatures may be useful for dissolving ThO_2 solid in chemical processing.

8. Solution Corrosion

A 0.085 *M* UO_2SO_4 solution in heavy water containing 0.020 *M* $CuSO_4$ and 0.245 *M* D_2SO_4 (room-temperature concentrations) was circulated for 553 hr at 360 to 365°C in a titanium loop. The solution appeared to be stable, but low concentrations of sulfuric acid (and possibly uranyl sulfate) were present in the vapor above the solution. Corrosion of the titanium loop was negligible, but Zircaloy-2 specimens exposed to the solution corroded at rates between 7 and 9 mpy. Corrosion of the front aluminum oxide pump bearing by the highly acid solution forced termination of the run.

9. Radiation Corrosion

One autoclave was operated with a fuel solution, 0.08 *m* UO_2SO_4, 0.02 *m* $CuSO_4$, and 0.24 *m* D_2SO_4 in D_2O for 350 hr out-of-pile at 360°C and for a short time at 280°C in beam hole HB-5 of the LITR. The test was terminated prematurely because of a leak.

The corrosion rate out-of-pile after the initial 50 hr was about 1.3 mpy, which is in line with extrapolations of previous autoclave results at lower temperature. Alpha counting of washed specimens after 124 hr exposure out-of-pile showed a very small amount of uranium sorption (0.24 $\mu g/cm^2$). This is consistent with other information which has shown that uranium sorption is low with a solution of high excess-acid concentration. Deuterium-oxygen recombination rate constants were determined from rates of pressure increase following initiation of irradiation. The K_{Cu} values were 7×10^2, 1.9×10^3, and 6.6×10^3 liters (STP)/mole-hr at 230, 250, and 280°C, respectively. These values verify the decrease in K_{Cu} with increased excess acid which has been shown previously.

Electrochemical measurements using galvanostatic and potentiostatic techniques were made in the temperature range 150 to 300°C on a Zircaloy-2 specimen

passivated in 0.05 *m* H_2SO_4 at 293°C. From the results of the potentiostatic measurements, the activation energy of the anodic reaction (oxidation of zirconium) was 31.1 kcal/mole over the temperature range 180 to 300°C and from -0.700 to +0.300 v to Pt as reference. The activation energy for the cathodic reaction (reduction of O_2) was 10.8 kcal/mole at -1.400 v to Pt over the temperature range 220 to 300°C and 5.4 kcal/mole at temperatures below 220°C. At the potential -1.200 v to Pt as reference the activation energy was 5.4 kcal/mole over the entire temperature range investigated, 180 to 300°C. From the results of the galvanostatic measurements, the self-consistency of the potentiostatic data was verified.

It is considered possible that these results apply to the white-oxide type of corrosion which occurred on a small area (3 to 6% of total area) of the specimen.

PART IV. SLURRY FUELS

10. Thorium Oxide Irradiations

The black vitreous material formed on irradiation in D_2O of 1750°C-fired alumina-coated thoria pellets was spectrographically identified as carbonaceous. It is probably the carbon residue of the polyvinyl alcohol binder used in the pellet fabrication, which was not removed by the 1750°C firing.

A D_2O slurry of classified ThO_2 - 0.4% UO_2 irradiated in a settled condition at 280°C in the LITR to a total nvt of 5×10^{19} neutrons/cm^2 showed pronounced particle damage. Twelve per cent of the irradiated material (initially 2.1 μ average size and 0.5% <1 μ) was recovered as a dispersed suspension with an average particle size of 0.25 μ. A portion of the material (≧6%) that had settled to the bottom of the autoclave and been resuspended by stirring had an average size of 1.6 μ but a very steep size-distribution curve, indicating that nearly all this material had suffered particle damage. Additional material was recovered by drying the autoclave and shaking it to remove solids. Possibly all the oxide was somewhat degraded.

A review of the particle-size information obtained in 18 slurry irradiations made during the past several years suggests particle damage in some cases. Pure ThO_2 fired to 1600°C was resistant to radiation damage for the 200- and 300-hr irradiations to which it was subjected.

Additional facilities are being developed for both dry and wet irradiation of thoria powders and pellets.

11. Development of Gas-Recombination Catalyst

Calibration of the gas-injection apparatus used in the gas-recombination-catalyst development studies continued. In a series of experiments oxygen and deuterium (first O_2 and then D_2) were charged to the capillary system connecting the pressurizable gas burette with the reaction autoclave, were displaced with various quantities of water, and the gases were allowed to recombine to apparent steady state. As the amount of water injected increased, the initial D_2 pressure in the reaction system increased, initial recombination rates increased, and the total quantity of D_2 combined increased until essentially complete reaction of the D_2 added to the reaction vessel was indicated. Water displacement of the gas holdup in the charging system should result in more definitive rate data in future catalyst development studies.

Gas recombination was studied with slurries of the Th - 12.4% U^{235} oxide and added palladium catalyst projected for use in the next in-pile corrosion experiment. The power density in the proposed experiment will be about 26 w/ml. The out-of-pile data indicate that the catalytic activity of the proposed slurry (782 g of Th per kg of D_2O; 1460 ppm Pd, based on Th) will be sufficient to maintain the pressure of radiolytic D_2 gas at ≤100 psi at 280°C during the in-pile experiment. The rate data agreed with a kinetic expression involving a first-order dependence of rate on the hydrogen partial pressure and a half-order dependence on the oxygen partial pressure.

12. Slurry Corrosion and Blanket Materials Tests

Physical characteristics and supplementary attrition data are reported for code P-82 ThO_2 pellets, which are currently being evaluated in an in-pile test. The void volume, determined by mercury intrusion, of the pellets was 5.5×10^{-3} cc/g, and the calculated average pore radius and density were 0.96 μ and 9.49 g/cc, respectively. Microexamination of the interior of the pellets revealed isolated voids.

Only one preparation of a series of 11 new experimental ThO_2 pellet batches which were evaluated in autoclave and accelerated spouted-bed attrition tests displayed a resistance to attrition comparable to code P-82 pellets. The pellets, code P-97, had been fabricated by pressing right cylinders, 0.2-in. diameter and 0.2-in. length, and had been preattrited by milling before the spouted-bed tests.

Autoclave experiment L5Z-155S was performed to evaluate the radiation effect on the degradation of particles in a slurry gently agitated in a rocking autoclave in comparison with that observed in the slurry pumped in in-pile slurry loop experiment L-2-27S. Irradiation of the autoclave in the HB-5 facility of the LITR has been completed. The Zircaloy-2 autoclave contained thoria-urania slurry (0.4% U, based on Th) prepared from the same oxide batch (DT-22) used in the in-pile slurry loop experiment.

The autoclave was irradiated for 453 hr with an effective flux time 87% of the potential. From activation of a cobalt flux monitor located inside the autoclave, the thermal-neutron flux in the autoclave was estimated to be 7.7×10^{12} neutrons/cm^2·sec. At this flux, the slurry particles should develop 5.1×10^{16} fissions per gram of solids.

It is believed that catalytic and gamma recombination were sufficient in the experiment to prevent the development of observable radiolytic-gas pressures. No effect of irradiation on the generalized corrosion was observed in this experiment.

After irradiation, the surface area of the slurry was 30 m^2/g, as compared to a surface area of 8 m^2/g for the unirradiated mixture of the original thoria-urania and palladium-thoria catalyst. No degradation of slurry particles was observed from particle-size analyses.

Radiochemical data on slurry samples from the entire course of the first slurry in-pile loop experiment indicated the development of 7×10^{16} fissions per gram of solids, corresponding to an estimated exposure of 1.6×10^{19} nvt at a flux averaged over the total slurry volume of 2.4×10^{12}.

Particle degradation was exhibited throughout the irradiation period in a number of ways. Particle size and crystallite sizes decreased progressively, while surface area increased correspondingly. Electron micrographs of the particles at various stages of the experiment substantiated the particle breakdown.

Postirradiation examination of the core region of the loop showed no significant deposits of solids in this region. Small amounts of solids (1 to 3 mg/cm^2) were removed from corrosion coupon specimens by scrubbing. Zircaloy-2 corrosion specimens showed weight gains of 1 to 2 mg/cm^2, indicating low corrosion rates. Zircaloy-2 coupons in holder entrance positions showed weight losses at 22 fps.

PART V. FUEL MANUFACTURE

13. Thorium Oxide Production

Large, rounded ThO_2 particles have been prepared by the sol-gel process. This process consists of partial denitration of thorium nitrate with superheated steam and subsequent dispersion in water to form a ThO_2 sol. The sol is then evaporated at 70 to 80°C to form a gel, which breaks up into large particles. These particles are converted to dense ThO_2 by calcination at 1150°C. The particles thus formed are irregular in shape but can be rounded by grinding. To date, efforts to prepare rounded pellets by forming the gel into spheres and calcining have been unsuccessful.

PART VI. METALLURGY

14. Metallurgy

A study has been made to determine to what extent Knoop hardness was affected by and could be correlated with the deformation characteristics and anisotropy of properties of Zircaloy-2 sheet exhibiting a high degree of preferred orientation. It was found that there was a strong dependence of Knoop hardness on texture. A simple model was proposed to describe the deformation that occurs when a Knoop hardness indentation is made. The variations in hardness could be correlated with this model and with the preferred orientation of the material.

Two methods for forming rounded bodies of thorium oxide have been investigated. A method in which dome-ended pellets were pressed directly was found unsatisfactory for producing a sound lamination-free product from modified batches of starting powder. A method for producing spheres was successfully developed in which powder is formed into cubes, the cubes are abraded into a spherical shape, and the spheres are sintered to final densities. Batches of ThO_2 - 1% UO_2 spheres have also been prepared by using this pressed-cube technique.

PART VII. ANALYTICAL CHEMISTRY

15. Analytical Chemistry

An amperometric method used for the titration of thorium with ethylenediaminetetraacetic acid in which Fe(II) is used as the indicator has been extended to the determination of copper and some of the rare-earth elements. The method, adaptable to remote operations, provides an alternative method for the determination of copper in samples of irradiated homogeneous-reactor fuel solutions.

THIS PAGE

WAS INTENTIONALLY

LEFT BLANK

CONTENTS

PART II. ENGINEERING DEVELOPMENT

PART III. SOLUTION FUELS

PART IV. SLURRY FUELS

PART I. HOMOGENEOUS REACTOR TEST

1. HRT OPERATIONS

S. E. Beall, P. N. Haubenreich, J. W. Hill, Jr.

H. F. Bauman, J. R. Buchanan, S. R. Buxton, J. R. Engel, D. F. Frech, R. H. Guymon, P. H. Harley, R. J. Harvey, J. O. Kolb, H. B. Piper, J. L. Redford, D. M. Richardson, H. C. Roller

Four HRT runs were completed during the report period. The end of the final run (No. 25) was a scheduled permanent shutdown.

1.1 RUN DESCRIPTIONS

1.1.1 Run 22

The first run with downward flow through the HRT core vessel (run 22) was in progress at the start of the report period. The main objective of the run was to raise the reactor power in steps and to observe the reactor behavior for several days at each level, until the design power of 5 Mw was reached. The power level had reached 1.8 Mw with no indications of fuel instability. However, the magnitude of the reactor noise, or small neutron-level fluctuations, was about double that in previous operation with upward flow in the core. It was decided, therefore, to study the nature and causes of the fluctuations before the power was raised higher. To this end, the reactor operating conditions were varied to observe the effect on the power fluctuations. The basic operating conditions for run 22 were: core average temperature, 260°C; blanket average temperature, 230°C; core pressure, 1400 psig. Variations during the experiments included reducing the core flow rate from the normal 460 gpm to 300 gpm, raising the core temperature to 280°C and lowering it to 240°C, and lowering the pressure to 1200 psig. At each condition the neutron level was recorded at 1-sec intervals on punched tape for at least 4 hr. Analysis of the data is described in Sec. 4.1.

On December 4, while the reactor was operating at 1200 psig and 1.8 Mw, the cell air activity began to rise, and fresh fission products were detected in the shield sumps. The reactor was shut down, and the source of the activity was found to be a leak in a feed-pump head (see Sec. 1.3.1). After the pump was replaced, experimental operation (now run 23) of the reactor was resumed on December 16.

1.1.2 Run 23

During the 12-day shutdown, run 22 data had been studied sufficiently to make clear that all the nuclear power fluctuations were part of a single normal distribution. That is, the largest fluctuations were basically not different from the very small, frequent fluctuations. For this reason, and because the

relative standard deviation of the power was found to increase in an orderly manner with power from very low powers, the fluctuations were not symptomatic of fuel instability. Furthermore, the fluctuations were not serious in themselves because heat capacities and mixing effects smeared them out so that there were no detectable fluctuations in the steam heat removal system. Therefore the stepwise increase in power toward 5 Mw was resumed without delay at the beginning of run 23. All operating conditions were the same as for the previous run.

At each power level four pairs of samples were analyzed, and the reactor nuclear average temperature (NAT) was observed carefully for changes. The statistical distributions of the fluctuations in neutron level and pile period were determined soon after each new power level was reached. The normal distribution was then used as a reference to permit detection of abnormalities which might indicate fuel instability.

The power was raised to 5 Mw on January 4, and during the next week, 89 hr was spent at this power. At no time was there any evidence of fuel instability.

1.1.3 Fuel Replacement

Corrosion of stainless steel over a 22-month period had raised the concentration of nickel in solution to the point where there was some concern over the possibility of hydrolytic precipitation. About 5 moles of acid was added on December 26, to help prevent this, but it was decided to replace the fuel charge before prolonged operation at high power was undertaken.

Before the old fuel charge, with its accumulated fission and corrosion products, was removed, three days were spent in determining the catalytic activity of the solution for internal recombination of radiolytic gases (see Sec. 1.2.2). Experiments were conducted at 1000 psig and five different core temperatures. In each the power was raised and bubbles were allowed to form in the core for a brief time.

On January 13, the reactor was made subcritical by dilution. The temperature was held at 180°C by external heating, while the old fuel was concentrated in the dump tanks and then isolated in the fuel storage tanks.

Fresh fuel solution was charged into the dump tanks, on January 16, thus effecting a complete refueling in three days, without interruption of circulation.

1.1.4 Run 24

During run 24, after two days of circulating the fresh fuel (to improve the protective oxide film on the piping), a new series of recombination experiments was initiated. The new fuel contained only half the normal copper, and after the catalytic activity was measured with this amount, the copper was brought up to normal and the measurements were repeated before full-power operation was resumed.

During the next few days, the letdown heat exchanger was found to be bypassing part of the feed stream into the letdown stream through a leak in the concentric-tube heat exchanger. This made it impossible to obtain good fuel inventories (one measure of performance); so plans were made to replace the heat exchanger. Furthermore, the cell activity again increased (from a few curies to 10 to 20 curies), and samples from the cell sumps showed fresh fission products. On February 8 the reactor was shut down to locate the source of the fresh activity.

The leakage was found to be escaping from a crack in a stainless steel forged tee in the fuel-dump-tank drain line. Since the tee could not be replaced,

the leak was stopped by freezing each side of the tee. Several other equipment replacements were made during the shutdown also (see Sec. 1.3.2).

Before operations were resumed, the integrity of the fuel low-pressure system was confirmed by hydrostatically testing the fuel dump tanks and associated equipment at 500 psig for 1 hr. No leakage to the outside could be detected.

The reactor high-pressure system was successfully hydrostatically tested to a pressure of 2675 psig.

1.1.5 Run 25

The main purpose of run 25 was to obtain more information on the reactor behavior at full power (5 Mw). Temperatures and pressure were the same as during the preceding runs: 260°C core, 230°C blanket, and 1400 psig core pressure.

On April 6 the power was raised to 5 Mw and held without difficulty for most of the next 11 days. Then the NAT began to decrease sharply, and the power was reduced to heat loss. The heat-balance flowmeter showed that the fuel feed rate had fallen off by an amount which would account for the NAT decrease. The reactor was subcritical for 9 hr while the feed pump was readjusted. When the reactor was made critical again, the blanket concentration was found to have increased from 1.8 to 2.9 g of U per kg of D_2O, indicating an increase in core-blanket mixing from 2 to 14 lb/min. (This change was explained later when inspection showed that the upper patch in the core wall had fallen out; the patch bolt had melted on the blanket side.) The mixing rate had been practically steady at 2 lb/min since the patches were installed prior to run 22.

With the high blanket concentration, about 64% of the power was generated in that region. At a 5-Mw total power and a 230°C blanket average temperature, steam pressure in the blanket heat exchanger was only 190 psig, and the capacity of the blanket steam valve was reached. The blanket temperature was therefore increased to 240°C to raise the steam pressure and permit 5-Mw operation. At the same time, 14 moles of sulfuric acid was added to raise the fuel acid-to-sulfate molar ratio to 0.43.

When the power was next raised to 5 Mw, a noticeable NAT rise of 2 or 3°C occurred during and after the power increase. This was observed three times at 1400 psig. Then, to investigate the possibility of boiling deposition on the core tank, the pressure was raised to 1700 psig. After similar behavior was observed at 5 Mw at this pressure, the pressure was reduced to 1250 psig. The NAT again rose a few degrees when the power was raised to 5 Mw. An addition of $CuSO_4$ was made which nearly doubled the fuel copper concentration, and the 5-Mw experiment was repeated twice with the same results. Neither the large pressure variation nor the increase in copper concentration had a noticeable effect on the observed temperature increase. The blanket temperature was reduced to near 230°C, and on the last day of power operation the power was raised to 5 Mw for 4 hr. The NAT rose and leveled off as before. At 4:30 p.m. on Friday, April 28, the experimental program of the HRT was terminated.

1.2 ANALYSIS OF EXPERIMENTS WITH MODIFIED (DOWNWARD-FLOW) CORE

Experimental effort in the four runs described above was devoted to a detailed study of fuel stability and internal recombination with downward flow through the core.

1.2.1 Fuel Stability

During runs 22 through 25, between November 1960 and April 1961, the reactor was critical for 2371 hr, at powers above heat loss for 1177 hr, and at 5 Mw for a total of 347 hr. Nearly all the high-power operation was with a system pressure of 1400 psig and a core average temperature of 260°C. These conditions were the same as those which existed during much of runs 20 and 21; the operation in runs 22 through 25 differed in that the core flow was downward, the blanket temperature was lower, and the fuel acid level was generally higher. The combination of these changes was evidently effective, for the reactor was operated for long periods with no signs of fuel instability at 5 Mw, twice the power at which instability had been evident before the changes.

It is very likely that the improvement in the fuel stability was attributable in large part to more effective removal of separated uranium (if present) from the core and better cooling of surfaces of the core tank. The better cooling of the core tank resulted largely from increased velocities and a higher heat transfer coefficient on the core side. The lower blanket average temperature (230°C instead of equal to the core) also contributed to keeping the core tank cool.

The fuel composition may have been another significant factor. Ratios of acid-to-sulfate of 0.34 or greater were maintained in all operation at above 2 Mw. This assured that the two-liquid-phase minimum temperature was always higher than the pressurizer temperature at 1400 psig by at least 10°C (ref. 1). Before the flow was reversed, unstable operation occurred in run 21 at 1400 psig and 4 Mw at an acid-to-sulfate ratio of 0.32. At that time the core and blanket solutions were near the five-component solubility limits at 300°C. On the other hand, in run 25, the reactor was repeatedly stable at 1400 psig and 5 Mw with an acid-to-sulfate ratio of 0.34.

On April 17, after over 300 hr at 5 Mw, the upper core-patch bolt melted on the blanket side (see Sec. 1.1.5). The failure is attributed to overheating and deposition of uranium under the low-velocity conditions in the blanket.

After reversal of the core flow, the only indication of fuel instability ever observed was the power-dependent temperature rise (1 to 2°C) which was observed during the last ten days of operation, after the core patch had fallen off. This small rise in reactor nuclear average temperature, which was observed repeatedly at 1400, 1700, and 1250 psig, whenever the power was raised above about 4 Mw, does not appear to have been caused by solution mixing transients, changes in temperature patterns, or fuel instability in the core. Because of the unusually high blanket concentration, the power density on the blanket side of the core wall was higher than at any other time in the history of the reactor. These new conditions apparently caused uranium deposition on the blanket side of the core tank, with a resultant increase in reactor average temperature.

The corrosion rates for type 347 stainless steel ranged from 0.4 to 0.9 mpy until the final 150 hr of operation. In this period the acid-to-sulfate ratio was raised to 0.43, and the corrosion rate was 2.4 mpy.

1.2.2 Results of Internal-Recombination Experiment

Internal-recombination experiments were performed with the old fuel charge at the end of run 23 and with the new charge at the beginning of run 24. One set of experiments was performed with the old charge to obtain the effective recombination rate constants in the presence of significant concentrations of fission and corrosion products. Two sets of experiments were performed with the

fresh fuel charge, at different levels of acid and copper, to measure the rate constants without long-lived fission products and corrosion products. Each set consisted of four or five experiments at different core average temperatures. All experiments were with downward core flow.

For each experiment, the reactor power level was raised until a sharp drop in critical temperature indicated the formation of radiolytic-gas bubbles. The power was lowered about 500 kw to allow the temperature to recover and then raised again to check the bubble point. In each set, one experiment was performed in which the power was held just below the bubble threshold for several hours to see if there was any effect of short-lived fission products on the effective recombination rate.

Evaluation of the recombination constants was based on the calculation model which considered the temperature distribution in the external piping of the core loop as well as in the core itself. The core temperature distribution used was that predicted from experiments on a full-scale hydraulic model of the vessel. Preliminary calculations indicated that, with reverse flow in the core, radiolytic-gas bubbles would appear first in the core vessel, where they would be detectable by their effect on the reactor critical temperature. Letdown of radiolytic gas could not be expected, and was not observed.

In evaluating the recombination rate constants, all the recombination was attributed to copper catalytic activity. The rate constants were evaluated in terms of the effective specific rate constant at 250°C and the activation energy of the reaction. When five experiments were performed, ten independent values were obtained for each constant. Table 1.1 presents the results of the three sets of experiments. For the specific rate constant, both the average value and the range of the several independent values are given. The units of the specific rate constant express the absolute reaction rate, in gram molecules per second of deuterium reacted per liter of 250°C solution, at unit molar deuterium concentration and unit molar copper concentration, with molarity expressed at the temperature in question. Only average values are given for the copper and acid concentrations and the activation energy. In the last set of experiments, one value differed appreciably from the others. If this point is discarded, the average specific rate constant is 1.97 liters/g-mole·sec, and the average activation energy is 23.3 kcal/g-mole.

Table 1.1. Results of Recombination Experiments in Runs 23 and 24

Fuel Charge	No. of Expts.	Cu Concentration (g-moles/kg D_2O), Average	Acid Concentration (g-moles/kg D_2O), Average	Specific Rate Constant at 250°C (liters/g-mole·sec) Average	Specific Rate Constant at 250°C (liters/g-mole·sec) Range	Activation Energy (kcal/g-mole), Average
Old	5	0.0138	0.0288	2.04	1.99-2.07	23.8
Fresh	4	0.0077	0.0195	2.25	2.16-2.32	22.1
Fresh	5	0.0133	0.0239	2.00	1.93-2.27*	22.8

*One value, out of ten, was above 2.02.

The results of the last two sets of experiments indicate lower copper activity at the higher copper and acid concentrations. If it is assumed that this effect is due only to the acid concentration, and if this acid dependence is extrapolated to the acid level of the old fuel experiments, an enhancement of the catalytic activity by the fission and/or corrosion products is indicated. There

was no detectable effect on the catalytic activity of short-term operation at power levels just below the bubble point.

The results reported here are based on deuterium and oxygen solubilities reported by Battelle Memorial Institute.[2] If the same solubilities are applied to the out-of-pile data of McDuffie and Stone,[3] the rate constants determined in the reactor are larger by a factor of 1.5 to 2.

1.3 MAINTENANCE ACTIVITIES

During the report period there were two interruptions of reactor operation for maintenance. The first followed run 22 and the other run 24.

1.3.1 Elimination of Primary-System Leak Following Run 22

Within six days after detection of the primary-system leak that ended run 22, the system had been shut down, the leaking component had been located and replaced, and closure of the containment shield had begun. The leaking component was found by smearing cell equipment systematically while working through the dry-maintenance facility.[4] Hot smears localized the leak, which was found to be at a weld between the head and discharge check-valve chamber of the east fuel feed pump. The weld will be examined to determine why it failed.

1.3.2 Activities Following Run 24

Although run 24 was terminated because of a primary-system leak, the shutdown afforded an opportunity for some major maintenance activities in conjunction with the leak hunt and repair. Within 30 days after the end of run 24, the maintenance and leak repair activities were completed--sooner than had been estimated.

The smear technique used to locate the earlier system leak (see Sec. 1.3.1) was used to locate the second one also. This leak originated in a cracked tee fitting in the feed line (line 107) from the east fuel dump tank. The configuration of the feed lines from the east and west dump tanks was such that the line containing the leaking fitting could be deactivated while use of the line from the west tank continued. Therefore, freeze jackets were remotely installed on each side of the leaky fitting so that it could be isolated by ice plugs during reactor operation. For additional protection, a clamp was placed on the fitting to make the crack less likely to increase in size.

The fuel letdown heat exchanger was replaced because of an internal leak between the feed and letdown portions. Because of its configuration, the heat exchanger was a very formidable component for remote replacement. Although only 2 in. at its maximum diameter, it was quite long and covered a wide area (see Fig. 1.1). In order to get the old heat exchanger out of position and the new one in, it was necessary to remove temporarily the two fuel space coolers, to disconnect the air lines to the fuel letdown and dump valves, and to disconnect several thermocouples. Even with these difficulties the job was completed rapidly without spread of contamination or overexposure of personnel to radiation.

Both remote heads of the fuel feed pump, the blanket dump valve (PCV-252), and both chemical-plant isolation valves (HCV-141 and -142) were routinely replaced during the same shutdown. The east diaphragm head of the feed pump had failed during run 23. The west head was replaced because a trace of fresh

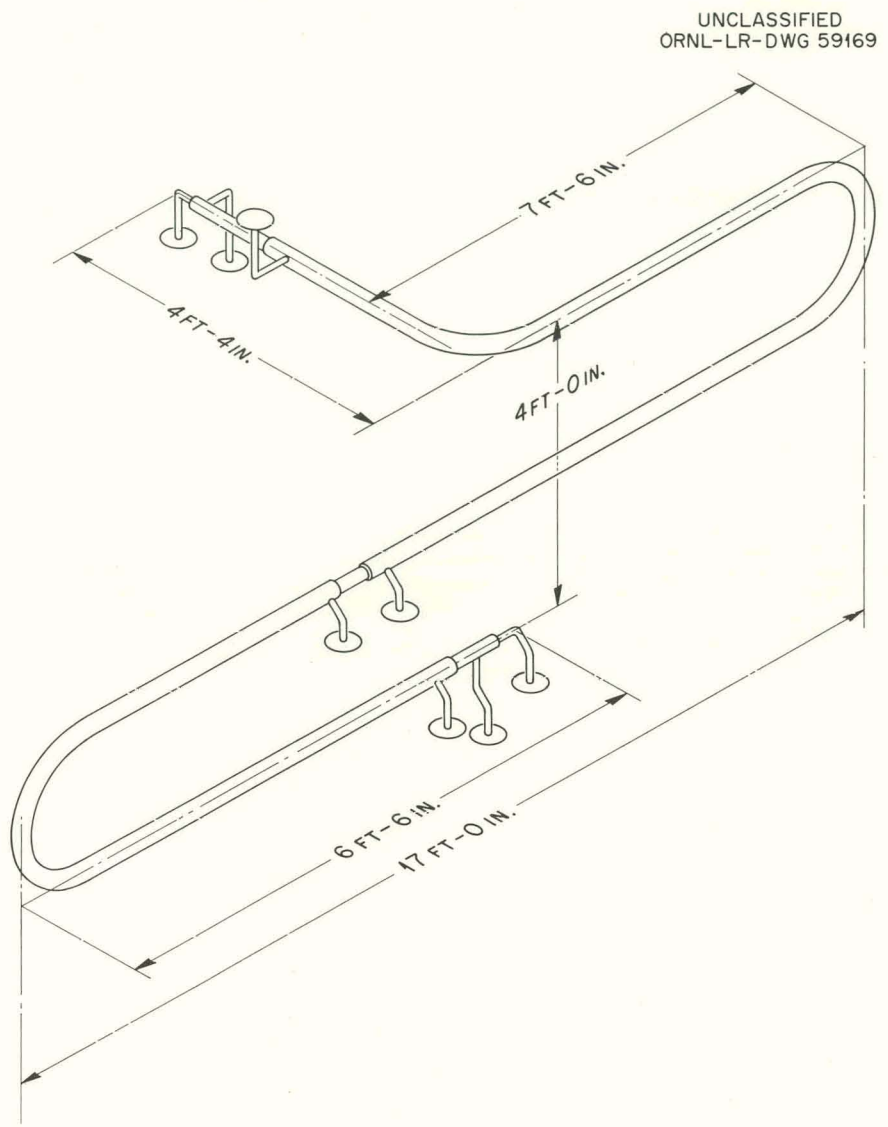

Fig. 1.1. Schematic of the Fuel Letdown Heat Exchanger.

fission products was detected in its intermediate system after run 24 was completed. The three valves were replaced because of excessive leakage through the seats.

1.4 POSTOPERATIONAL PERIOD

After the run-25 shutdown an inspection of the interior of the core vessel revealed that the upper Zircaloy patch had become detached from the vessel and was lying on the upper diffuser screen along with a portion of the bolt from the patch. The lower patch was in place, but its gold gasket was loose. Core-vessel surfaces appeared as they had prior to run 22.

The detached patch and bolt fragment were removed from the core for examination. Preliminary macroscopic investigations revealed that the bolt had

melted on the blanket side near the toggle nut (see Figs. 1.2 and 1.3). There was no evidence of attack on the core side of the patch or on its surfaces which contacted the vessel or bolt. The blanket side of the patch, however, exhibited some of the same attack found on the bolt. Microscopic examinations will be made of both the bolt and patch.

Operations necessary for removal of corrosion specimens and for inspection and storage of the reactor (in an assembled state) are now in progress.

Fig. 1.2. Remnant of Zircaloy-2 Bolt Sticking Through Upper Patch.

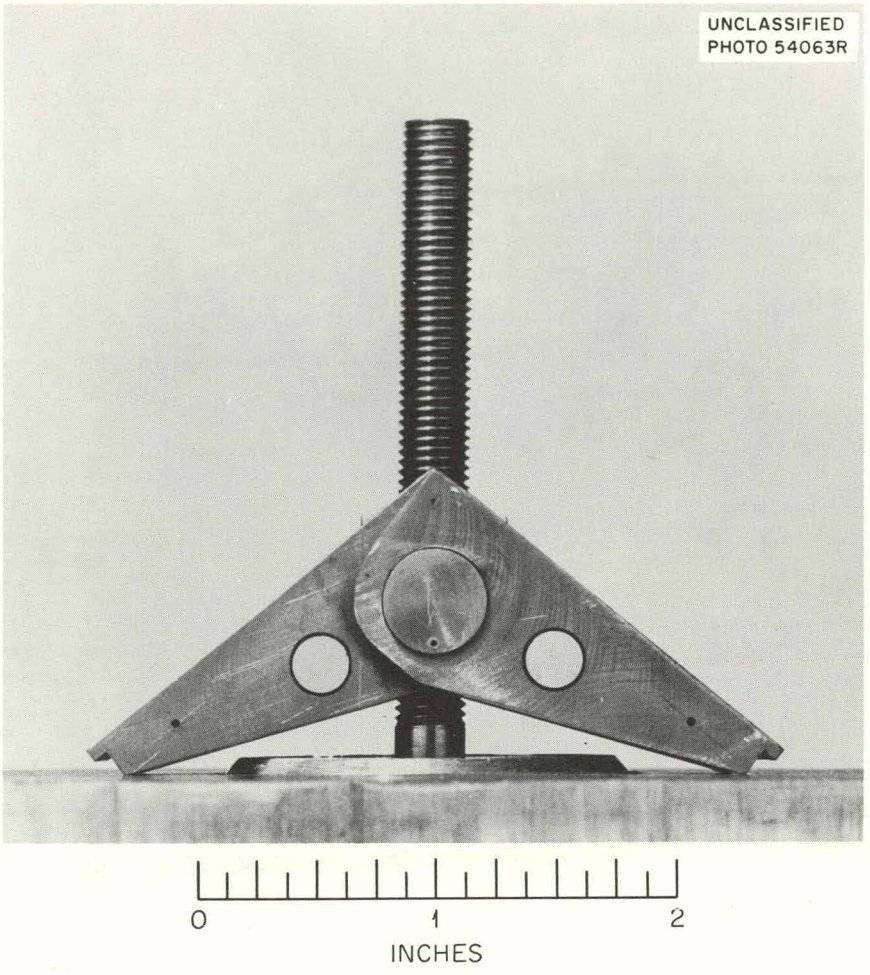

Fig. 1.3. Scale Model of Upper-Hole Patch Assembly.

REFERENCES

1. W. L. Marshall and E. V. Jones, Temperature of Second Liquid Phase Formation for Two Aqueous Homogeneous Reactor Fuel Compositions and Their Concentrates; Estimation of Temperatures for Liquid-Liquid Immiscibility, HRP-60-142 (Nov. 9, 1960).

2. E. H. Stephan et al., Resolubility of Gases in Water and in Aqueous Uranyl Salt Solutions at Elevated Temperatures and Pressures, BMI-1067 (Jan. 23, 1956).

3. H. F. McDuffie and H. H. Stone, HRP Quar. Prog. Rep. Jan. 31, 1958, ORNL-2493, p 181-183.

4. P. P. Holz, Dry Maintenance Facility for the HRT, ORNL CF-60-10-85 (Oct. 11, 1960).

2. HRT PROCESSING PLANT

W. D. Burch O. O. Yarbro

2.1 PERFORMANCE OF REVISED MULTIPLE HYDROCLONE

In three additional operating periods, totaling 2059 hr, the relatively inefficient performance of the revised multiple hydroclone was confirmed. Cold tests with this unit and with other similar parallel-hydroclone systems, reported previously,[1] had shown that efficiencies with such systems dropped drastically when underflow ratios were decreased. In these final tests the revised multiclone unit was installed to operate with induced underflow; with this method of operation the effective underflow ratio is only 2 to 3%. The basic improvements obtained with the smaller hydroclones (0.4-in. diameter, compared with 0.6 in. for the original multiclone) and higher pressure drop across the unit were completely offset by the reduction in efficiency attributed to the induced-underflow operation. Data from the final three runs are presented in Table 2.1.

Table 2.1. Removal Rates and Solids Composition for Final Multiclone Runs

	Run No.		
	22-27	22-28	24-29
Date run began	11/7/60	11/30/60	1/30/61
Operating hours	603	564	892
Solids collected (g)	162	224	300
Removal rate (g/hr)	0.27	0.40	0.39
Solids composition (%)			
Fe	30	30	25
Cr	8	13	18
Zr	33	27	28
Ti	0.7	0.6	0.9

Comparisons of the revised multiclone with the original multiclone and single hydroclone are somewhat clouded by possible effects of the core-flow reversal on circulating-solids concentrations. Removal rates are considerably lower than with the first multiclone unit and appear somewhat lower than with the original single hydroclone. This latter observation can be true even

with comparable circulating-solids concentrations in the main reactor flow loop. The single hydroclone, processing the multiclone underflow receiver on a 2-min cycle, will maintain an average solids concentration in that circuit below the concentration in the reactor if the multiclone efficiency does not exceed 10%.

Solids compositions were somewhat different from those of previous runs. The iron-to-zirconium ratio is approximately 1 in these runs, compared with an average value of about 0.5 throughout most of the period from reactor runs 17 through 21. Several factors, such as the higher acid concentration in recent runs, a somewhat higher stainless steel corrosion rate, or some hydrodynamic mechanism connected with the reversed core flow, may be responsible for the variation in composition, but the data are too limited to permit positive deductions. The uranium and copper content of the solids could not be determined because of the leakage of an undetermined amount of fuel through a valve isolating the reactor and chemical plant during the chemical-plant rinse operations.

2.2 XENON BEHAVIOR STUDIES

Efforts were continued to improve the measurements which determine the behavior of Xe^{135} in the reactor system. A system was installed for sampling the reactor off-gas upstream of the charcoal adsorber beds, and several samples were obtained in the final reactor run. In this sampling system, approximately 100 liters of off-gas was routed to the vapor space above the chemical-plant decay tanks, and an aliquot was subsequently removed via the tank-bubbler instrument lines. Techniques for removing small samples for analysis of the radioactive isotopes by gamma spectrometry had not been perfected when reactor operations were terminated. Several samples of this type were removed and analyzed, but only the rubidium daughter of Kr^{88} could be detected. The facility was not adequately shielded or contained to permit removal of undiluted samples until after the samples had cooled for two days, and some unexplained mechanism preferentially separated the Rb^{88} from its parent and other gaseous isotopes when only a small quantity of activity was collected in the sampling system.

Two sets of samples (six per set) were removed following periods of constant reactor power. These samples will be analyzed by mass spectrometry for the ratio of Xe^{136} to Xe^{134} following the decay of Xe^{133} to acceptable levels. From these measurements the Xe^{135} poison fraction will be calculated for comparison with a previous similar measurement.[2]

2.3 FUEL PROCESSING BY PEROXIDE PRECIPITATION

The development of a process for removing nickel and other soluble impurities from reactor fuel solutions by precipitating the uranium as uranyl peroxide and filtering off soluble contaminants was continued on a full engineering scale. Three 4-kg batches of natural uranium in simulated HRT fuel were precipitated in a 6-in.-diam 20-ft-high column equipped with external cooling and heating coils and two sintered stainless steel filters. A 2-in.-diam 3-ft-long cylindrical filter extended up from the column bottom, which contained a 5-in.-diam flat filter disk. The peroxide could not be retained on the finest available sintered filter (nominal 3-μ pore size) without the use of filter aids. A charge of 700 g of diatomaceous-earth filter aid was added to the column and remained there throughout the runs.

Uranium losses of 6% without precipitate washing were lowered to 3% by two washes. Recycling the initial portion of filtrate, which contained high uranium concentrations, would further decrease the losses. Decontamination factors for soluble impurities were 8 without washing and 100 with three rinses.

Reprecipitation of the uranium from one run, followed by two rinses, reduced the activity by a factor of only 2. Uranium losses in this run were only 0.4%, probably because excess acid had been removed in the initial precipitation, making the uranyl peroxide less soluble. Plans to study this effect by partially neutralizing the acid initially were dropped when the cylindrical filter failed by corrosion. The filter had been contacted with simulated fuels almost continuously for a period of about three months and ruptured at a pressure of 25 psi, compared to its nominal rating of 50 psi.

2.4 EFFICIENCY MEASUREMENTS OF THE 7500 AREA STACK IODINE TRAPS

Prior to run 22, several improvements were made to the 7500 building ventilation system to reduce the potential hazard from uncontrolled releases of radioactivity.[3] Included in these improvements was a new stack fan and filter system, which incorporated a 4-in.-thick silver-plated mesh bed and a charcoal cannister system as iodine traps. When routine measurements of the stack I^{131} release in March showed occasional daily releases as high as 5 millicuries (highest release, 19 millicuries) and an external radiation survey of the traps showed that they probably retained less than 1 curie, a limited program was undertaken to measure the efficiency under controlled conditions. Two 10-millicurie charges of I^{131} were volatilized into a helium stream and discharged into the waste vent system. Following the first addition, to the vapor space above the 1000-gal waste tank, no significant increase in the iodine concentration was detected either upstream or downstream of the iodine traps. In the second test, in which the I^{131} was discharged directly upstream of the stack filter system, 10% of that charged was found in the air stream upstream of the iodine traps (implying that 90% was removed on the first absolute filter), and a further reduction in concentration by a factor of 100 was noted downstream of the traps.

The tests indicate that in normal day-to-day operations, where iodine concentrations in ventilation air are very low, no substantial reduction is achieved on the iodine traps, but following a major release, reductions of greater than a factor of 1000 should be obtained, partly by deposition on ventilation pipe walls and partly by adsorption on the stack iodine traps.

2.5 HEAVY-WATER DECONTAMINATION

It is planned that the 7000-lb D_2O inventory now in the reactor will be decontaminated by two-stage distillation and a final ion-exchange treatment. The initial distillation in the reactor dump tanks and a second distillation in the waste evaporator will lower the contamination level to the range of 10^3 to 10^4 counts/min/ml. A laboratory test with a representative sample of evaporator distillate and equivalent portions of Dowex-1 in the hydroxide form and Dowex-50 in the hydrogen form demonstrated decontamination factors of 10^3 and bed capacities of approximately 750 cc of D_2O per cubic centimeter of resin. This should reduce the contamination of the D_2O to < 10 counts/min/ml. A simple system, employing an airlift, was designed to raise the waste-evaporator condensate continuously for gravity flow through a 6-in. column. Processing will be done later in the year.

REFERENCES

1. W. D. Burch *et al.*, HRP Prog. Rep. Nov. 30, 1960, ORNL-3061, p 21-23.

2. W. D. Burch *et al.*, HRP Quar. Prog. Rep. Jan. 31, 1960, ORNL-2920, p 9.

3. S. E. Beall *et al.*, HRP Prog. Rep. Nov. 30, 1960, ORNL-3061, p 17.

3. HRT COMPONENT DESIGN AND DEVELOPMENT

I. Spiewak

R. Blumberg
R. H. Chapman
E. C. Hise
J. E. Jones Jr.
C. G. Lawson
W. R. Mixon
W. Terry

3.1 HRT CORE

3.1.1 Effect of Flow Variations on Neutron Level in the Reactor

Experiments were performed in a full-scale mockup to determine the extent to which flow disturbances within the HRT core are responsible for the variations in neutron level observed in HRT power operation with the flow reversed.

The basic process is believed to operate as follows: oscillations in position of the jet, which passes from the top to the bottom of the core, create a slight variation in the temperature of the fluid leaving the core, while the inlet temperature remains constant. This produces a slight variation in the core average temperature; since the reactor has a negative temperature coefficient, a reactivity variation is produced. The neutron level then changes continuously to compensate for the varying reactivity.

The variation of the residence time (average temperature) was analyzed by considering that the fluid entering the core took one of two paths. The first path was a short-circuit path that went directly from the inlet to the outlet. Measurements of step changes in salt concentration by means of salt conductivity probes sensed by a Sanborn recorder showed that about 30% of the incoming fluid took this path, and that the transport time was about 0.6 sec. The remaining 70% of the fluid was "well mixed" and took about 14 sec on the average to leave the core.

The following equations were used to describe the kinetics of the system

1. Neutron balance:

$$\frac{d(P/P_0)}{dt} = \frac{1}{\ell} \left(\gamma\Delta\overline{T} - \beta k\right) \frac{P}{P_0} + \frac{\beta k}{\ell} \qquad (1)$$

For variations in $\gamma\Delta\overline{T}$ or Δk which are small relative to β, Eq. (1) is modified to:[1]

$$\frac{d\left[(P - P_0)/P_0\right]}{dt} = \frac{\Delta k}{\ell} - \frac{\beta(P - P_0)}{P_0} . \qquad (1a)$$

2. The average core temperature is obtained from a heat balance and is related to k with the temperature coefficient of reactivity:

$$\frac{1}{\gamma}\frac{dk}{dt} = \frac{d\bar{T}}{dt} = \frac{Q_1}{V}(T_1 - \bar{T}) - \frac{Q_1}{V}[\alpha_0 + \Delta\alpha(t)]\left[T_1 + t_S\left(\frac{\partial T}{\partial t}\right)_P - \bar{T}\right] + \frac{P}{\bar{\rho}\,\bar{C}V}. \quad (2)$$

Neglecting the heat removed by the short-circuit fraction (about 5% of the total heat), this becomes:

$$\frac{1}{\gamma}\frac{dk}{dt} = \frac{d\bar{T}}{dt} = \frac{Q_1}{V}(T_1 - \bar{T}) - \frac{Q_1}{V}[\alpha_0 + \Delta\alpha(t)](T_1 - \bar{T}) + \frac{P}{\bar{\rho}\,\bar{C}V}. \quad (2a)$$

3. The value of $\Delta\alpha(t)$, the variation in the short-circuit fraction, was measured continuously with salt conductivity probes in an experiment where a constant salt input was added to the recirculated fluid within the core mockup while fresh water was passed through the core continuously. The relationship between the salt concentration and the short-circuit fraction was calculated from a material balance of the salt stream added and removed from the core:

$$\frac{\Delta\alpha(t)}{\Delta S_0(t)} = \frac{1}{S}, \quad (3)$$

where

P = instantaneous power level in core,

P_0 = average power level in core,

t = time,

T_1 = core inlet temperature,

$\bar{T}$ = time-varying core average temperature,

Δk = change in reactivity due to change in $\bar{T}$,

γ = temperature coefficient of reactivity = $1.5 \times 10^{-3}/^{\circ}C$,

ℓ = neutron generation lifetime (6×10^{-4} sec for core),

β = fraction of neutrons produced which are delayed neutrons (it is assumed that the precursor concentration is constant); β was calculated to be 0.006 for HRT core,

k = multiplication constant,

Q_1 = volume flow rate into core, constant at 1 cfs,

V = core volume, 10.3 ft^3,

$\bar{\rho}\,\bar{C}$ = volumetric heat capacity of core solution,

t_S = transit time of short circuit fluid = 0.6 sec,

$\left(\frac{\partial T}{\partial t}\right)_P$ = temperature rise rate of fluid in core = 0.78 P (Mw), °C/sec,

α_0 = average short-circuit fraction = 0.3,

$\Delta\alpha(t)$ = variation in short-circuit fraction about α_0,

$S_0(t)$ = time-varying outlet salt concentration,

$\overline{S}$ = average salt concentration in core.

A special-purpose analogue computer was used to calculate the time variation of the "power" and of core average temperature, $\overline{T}$, from the salt concentration in the outlet stream of the model and from Eqs. (1a), (2a), and (3). Samples of the simulated power traces, $\overline{T}$ traces, and the outlet salt concentration as recorded are shown in Figs. 3.1, 3.2, and 3.3. The calculated power traces are similar to HRT power traces. Figure 3.4 shows a comparison of the frequency of large peaks with data obtained from the HRT.[2] Figure 3.5 shows a comparison of the root-mean-square deviation from mean power of the positive and negative peaks calculated by the flow-model analogue with those obtained from the reactor data (calculations by M. Tobias and D. Vondy). The fact that the negative power peaks from the reactor are lower than the positive peaks from the reactor while the model shows a more symmetrical behavior is attributed to the treatment of the delayed neutrons in Eq. (1a). For the more rigorous Eq. (1) the response would be asymmetrical. Assuming that the delayed-neutron precursors remained constant, a change of the reactor core temperature of 0.4°C would result in a change of about 11% on a positive Δk and about 9% on a negative Δk from Eq. (1), while from Eq. (1a) the change would be 10% for both positive and negative changes.

The calculated power response to sinusoidal changes in short-circuit fraction is shown in Fig. 3.6 with power as a parameter. At low powers the high-frequency oscillations have little effect on the power level. As the power level is increased, the reactor power responds to smaller oscillations.

The frequency distribution of flow disturbances was determined from the outlet salt concentration of the flow model. The result is shown in Fig. 3.7, which shows the oscillation that exists in the range of periods from 2 to 48 sec (frequencies between 11 and 0.13 radian/sec). According to the frequency response diagram (Fig. 3.6), all such oscillations should produce an observable power fluctuation when the core power is 2.5 Mw; more rapid fluctuations should produce very little effect on the power trace.

If the distribution of flow disturbances shown in Fig. 3.7 occurs also in the reactor at 2.5 Mw core power, then the frequency of occurrence of positive oscillations in power would be expected to look like the cumulative frequency curve. At a total power of 5 Mw in the HRT (2.5 to 3 Mw in the core) one would expect to see about 0.22 oscillation/sec (or about 0.11 positive peak per second and 0.11 negative peak per second). The value of 0.11 positive peak per second observed in the model compares favorably with the 0.12 per second observed for the HRT at higher powers (see Sec. 4.1.2).

It was concluded from this flow experiment and comparison with the HRT power behavior that the oscillations in neutron level were caused by hydrodynamic oscillations.

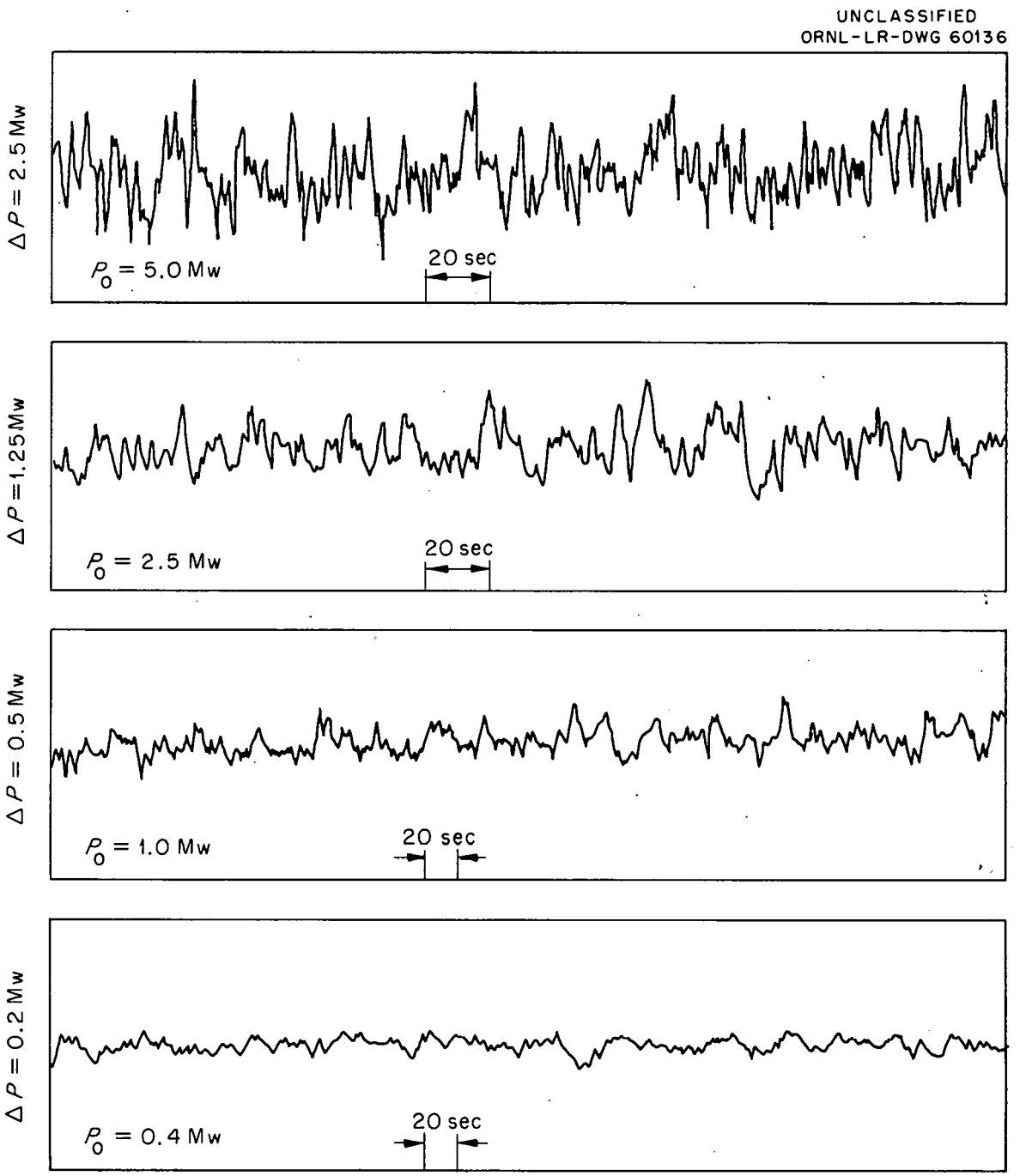

Fig. 3.1. Effect of Power Level on Flow-Model Power Oscillations.

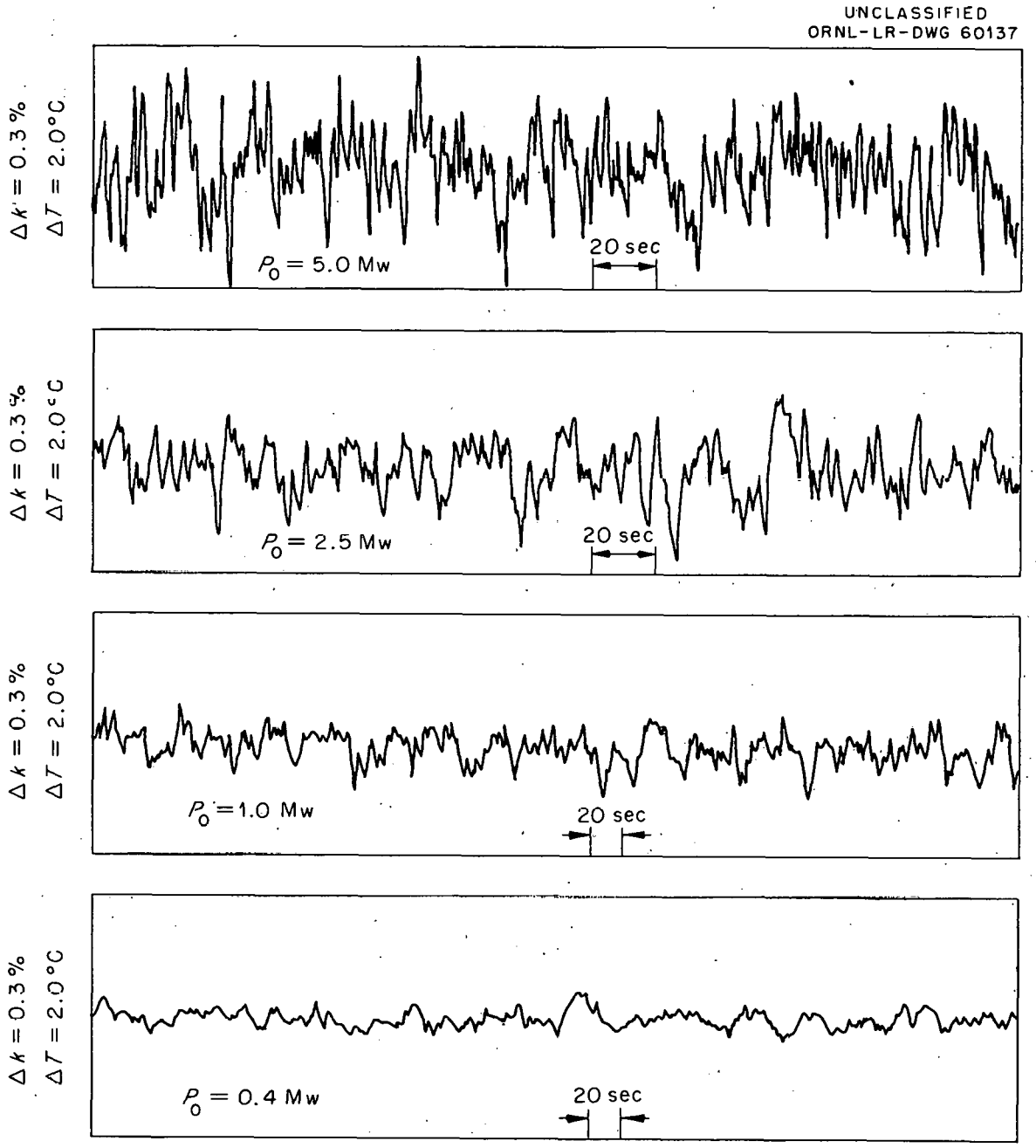

Fig. 3.2. Effect of Power Level on Deviations in Flow-Model Core Average Temperature and Changes in Multiplication Constant.

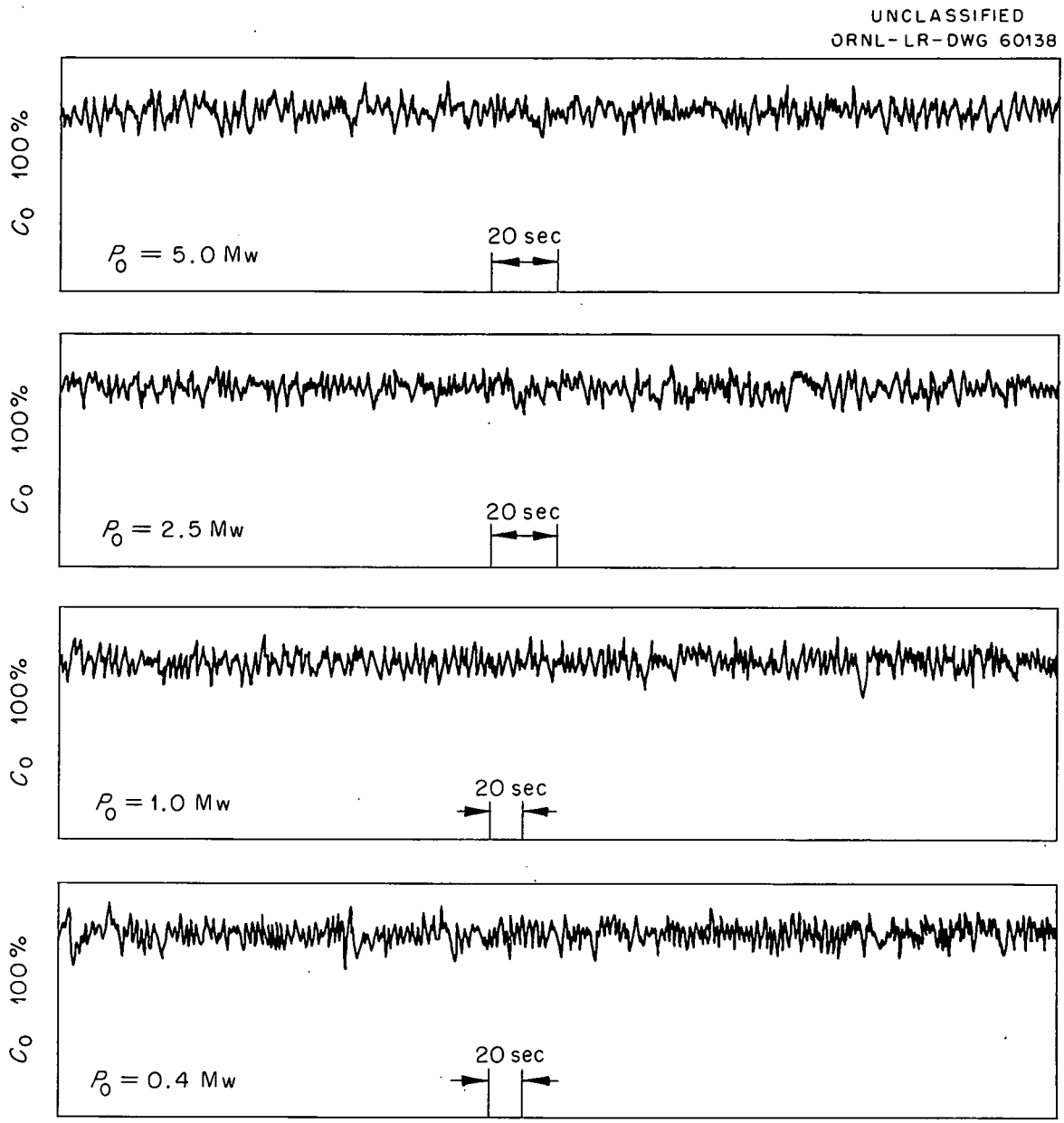

Fig. 3.3. Outlet Salt Concentration During Power and $\Delta k(\Delta \bar{T})$ Traces Shown in Figs. 3.1 and 3.2.

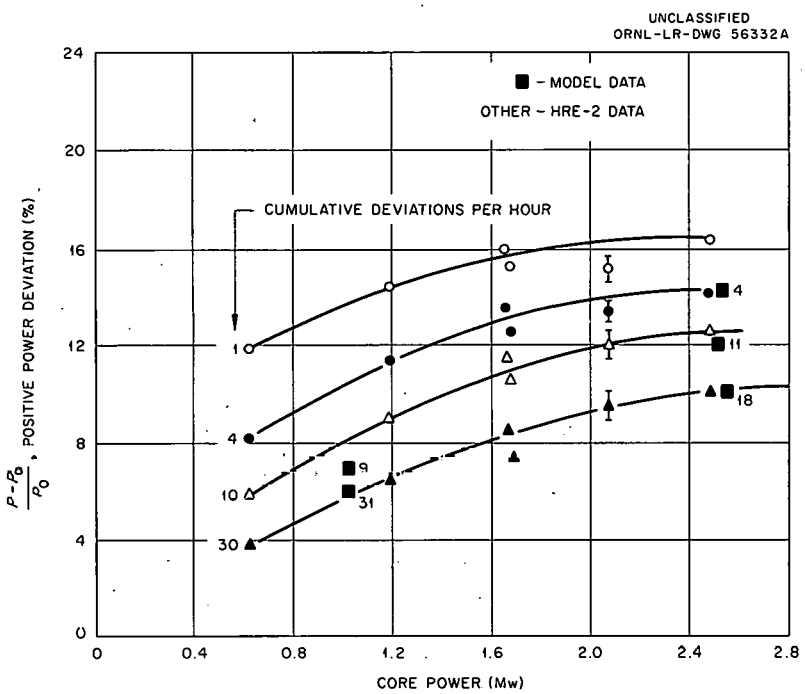

Fig. 3.4. Comparison of the Frequency-Amplitude of Positive Power Deviations in the Flow Model with HRT Data.

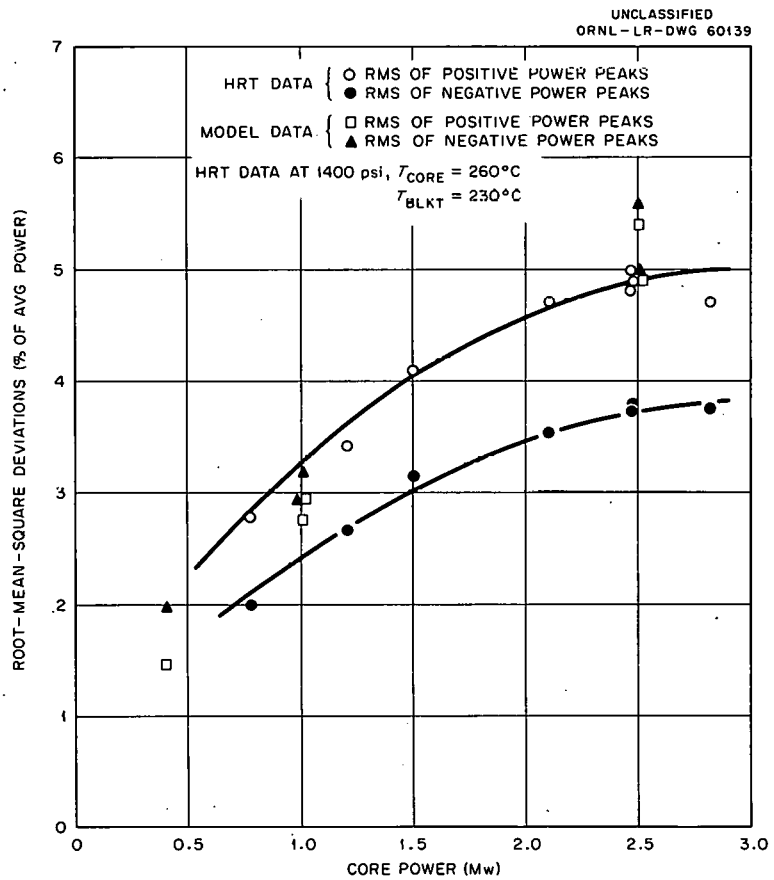

Fig. 3.5. Comparison of HRT Power Average Oscillations with Amplitudes Calculated from Flow Model.

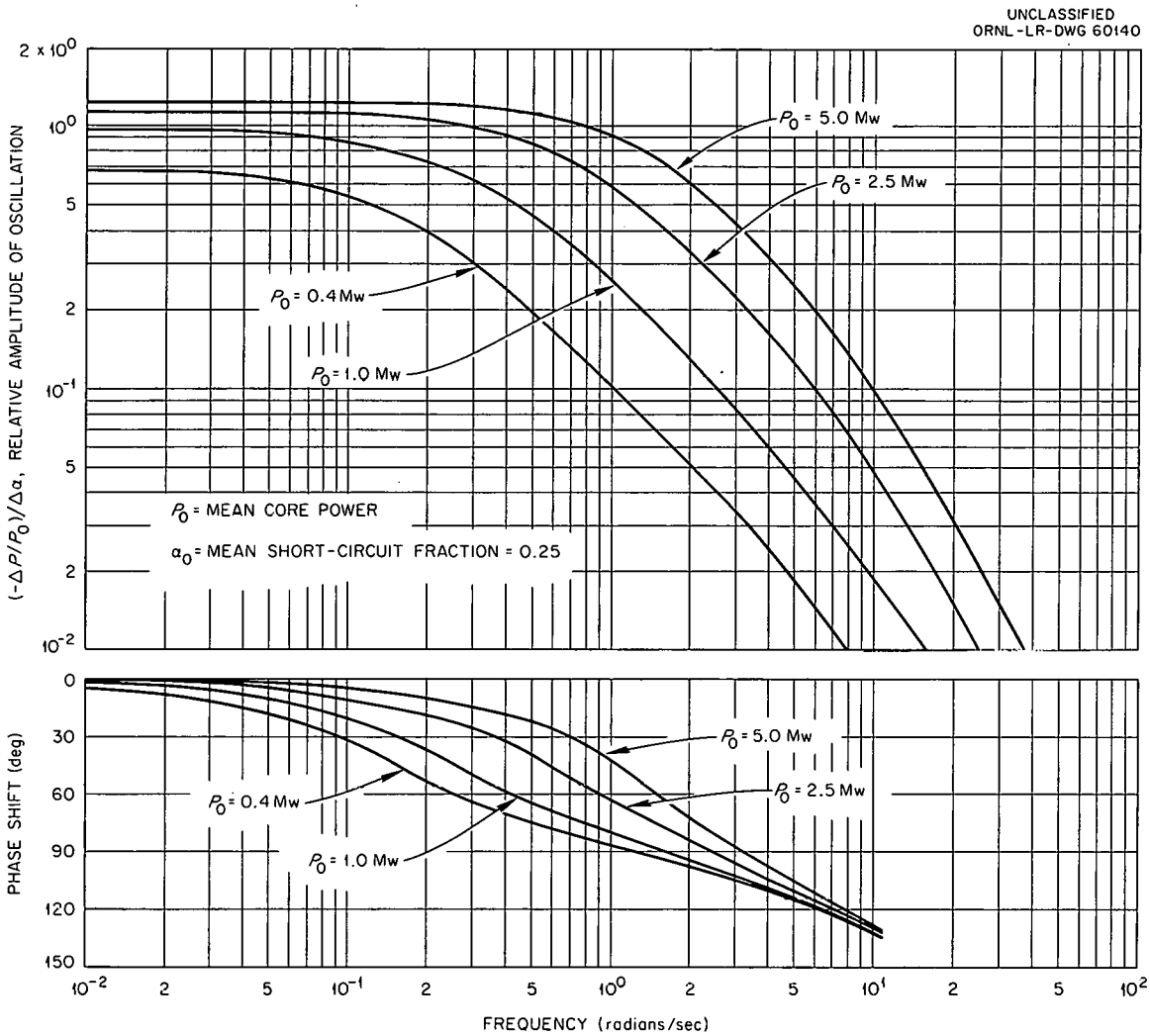

Fig. 3.6. Calculated Frequency Response of HRT Core Power to Flow Short-Circuit Oscillations.

3.1.2 Flow Test of Proposed HRT Flow Diffuser

A flow diffuser was installed in the HRT flow model to test its effectiveness in reducing core wall temperature and core power oscillations. The diffuser (Fig. 3.8) was designed to direct the incoming fluid down the wall of the core through radial swirl vanes. Five 1/4-in. holes were provided at the center section of the diffuser to cool the region just beneath the diffuser.

The diffuser decreased the bypass fraction from 0.30 to 0.16, and decreased the magnitude of the simulated power-trace oscillations by at least a factor of 2. Fluid-age traverses indicate that the ratio of the local fluid temperature rise above the core inlet temperature to the average core temperature rise is as indicated in Table 3.1.

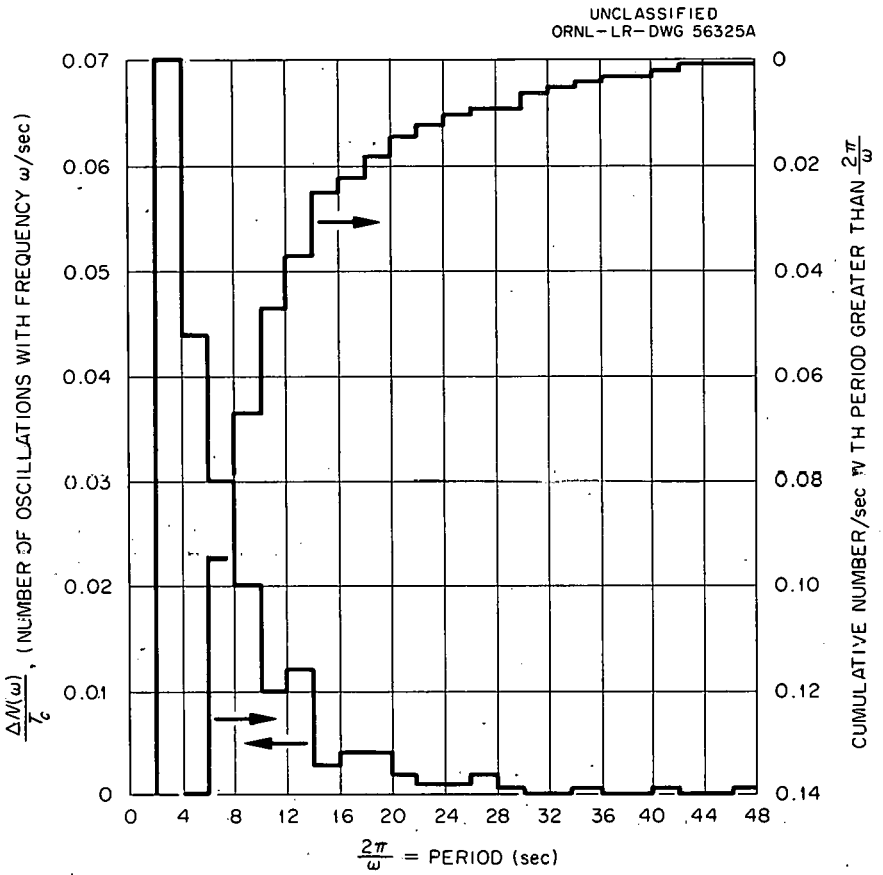

Fig. 3.7. Frequency of Occurrence of Flow Oscillations.

Table 3.1. Minimum and Maximum Values of Ratio of Local Temperature Rise at Several Elevations to Average Temperature Rise

Elevation	Minimum (at wall)	Maximum	Location for Maximum Value
Outlet (bottom)	1.0	1.0	
Intersection of cones	0.96	1.04	Center line
2 in. above 90° cone	0.90	1.04	5 in. from wall
Equator	0.92	1.14	4 in. from wall
7 1/2 in. above equator	0.72	1.10	Under diffuscr edge
12-1/2 in. above equator	0.54	1.20	Under diffuser edge

UNCLASSIFIED
PHOTO 36948

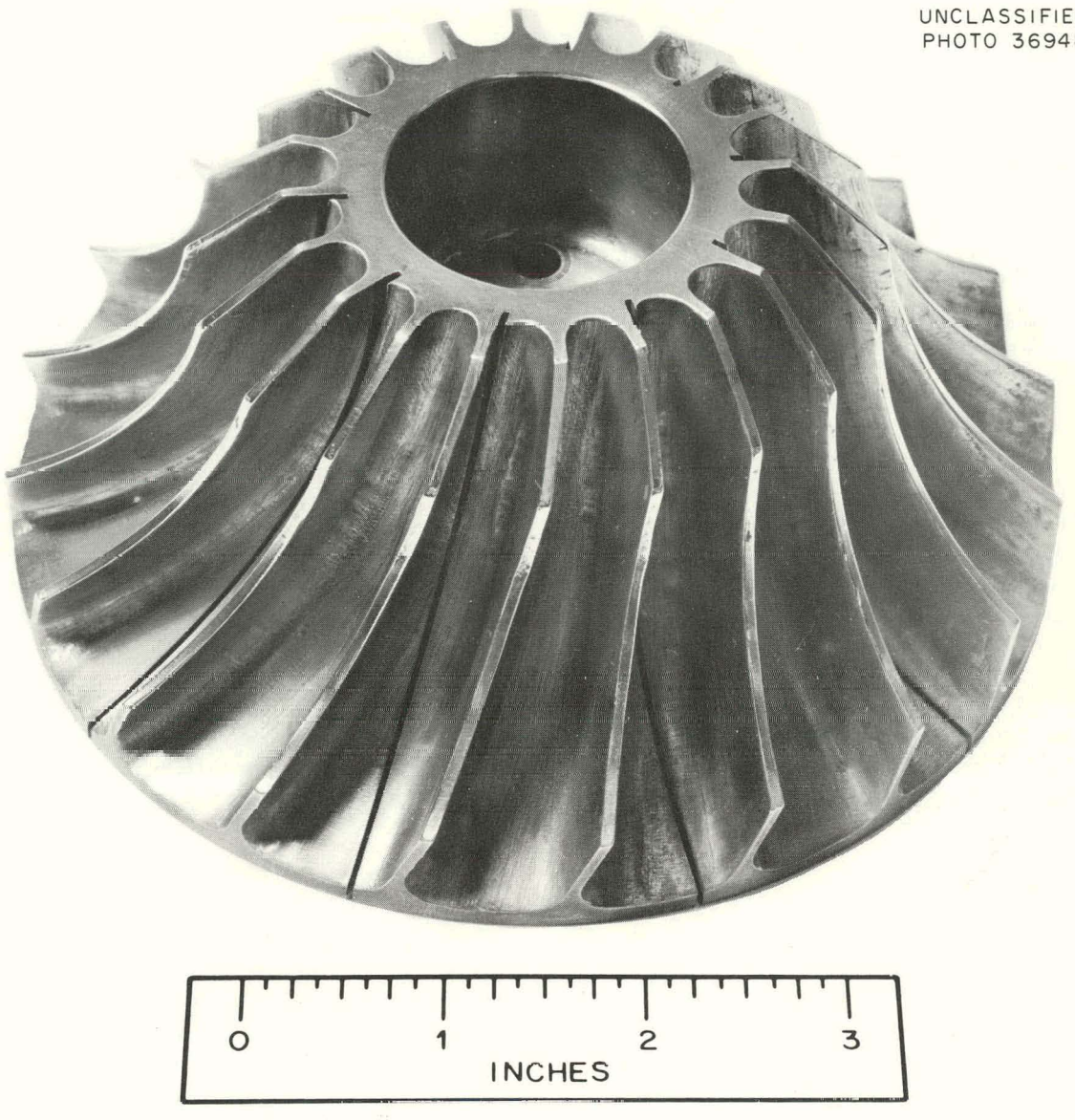

Fig. 3.8. Proposed HRT Core Diffuser.

It was noted that flow oscillations occurred below the cooling holes at the center of the baffle, and at times the flow was upward through the holes and into the incoming stream. These holes were plugged, and ten 1/32-in.-wide radial slots were cut equally spaced in the diffuser to simulate conditions of a collapsible diffuser as proposed for installation in the HRT. These alterations did not change the bypass ratio appreciably.

Maximum fluid velocities, which occurred 1/16 to 3/8 in. from the wall are compared with those in the present HRT core in Table 3.2.

Table 3.2. Fluid Velocity in Vicinity of Core Wall

Elevation	Maximum Fluid Velocity (fps)	
	HRT Reverse Flow	Reverse Flow with Diffuser
7 1/2 in. above equator	1.5	5.0
Equator	1.9	3.7
10-in. below equator	3.2	2.3

The flow model with diffuser was tested for solids removal by addition of sand, metal chips, and small polyethylene balls. All solids remained fluidized and were swept out of the vessel. No additional measurements were made since the HRT program was curtailed. However, the diffuser tested appears to provide better flow conditions than those in the present HRT core.

3.1.3 HRT Core Corrosion Specimen Holder and Thermocouple Probe

The corrosion-specimen holder[3] was developed to permit a direct measurement of the corrosion rate under HRT core conditions with the flow reversed. The thermocouple probe is a device for positioning a number of thermocouples in certain regions of the HRT core. Its development was undertaken to aid in the investigation of the oscillations in neutron level observed following the reversal of flow. Because of curtailment of reactor operation, neither device was actually installed in the reactor.

A prototype specimen holder was installed in the HRT flow model to determine its effect on flow patterns. It was noted that the assembly produced an increase in the direct bypass fraction from 0.30 to 0.45. This increase is logical because the holder was located at the vertical center line directly between the inlet and outlet nozzles. At a very high bypass fraction, core power would be limited by the small amount of fluid recirculating into the bulk of the core.

With a 2-in. cone placed at the center of the 3 1/2-in. inlet, it was possible to reduce the bypass fraction to 0.36; a 2-1/2-in. cone indicated 0.30. Other configurations tested were less promising.

The design of the thermocouple probe is shown in Fig. 3.9. The probe consists of a central Y-shaped structural member with three folding arms. Each of the folding arms and the central mast position three thermocouples (for a total of 12) in regions of interest when the device is erected within the core. One of the thermocouples attached to the central mast extends through the screens to the straight section of the core outlet. In order to guide this thermocouple through the screens as the device is being erected, a thin (about 5-mil-thick) collapsible copper funnel is prepositioned in the center holes of the screens. During the process of erecting the device, the funnel is collapsed. It is subsequently dissolved by the fuel solution. The stainless steel sheath of the thermocouples is seal-welded to the core-access cover flange, and the leads are sealed by packing glands.

The thermocouple probe induced a bypass fraction of 0.46, which could be reduced to 0.26 with the use of the 2-1/2-in. cone at the inlet.

Both the corrosion-specimen holder and the thermocouple probe appear to be practical devices, but some additional flow tests would be needed.

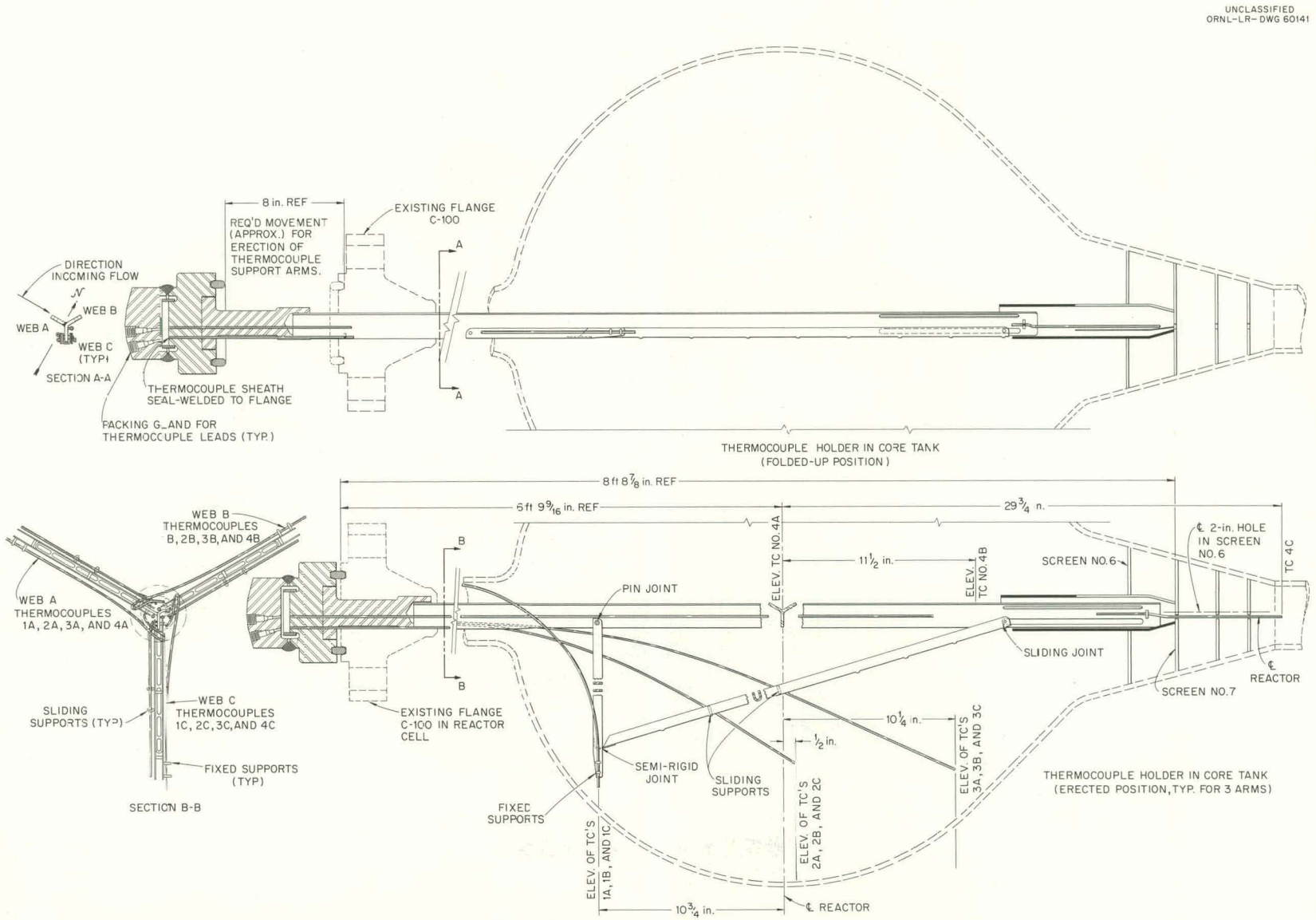

Fig. 3.9. HRT Thermocouple Probe.

3.2 HRT MOCKUP OPERATION[4]

Shortly after beginning a run on simulated HRT fuel solution, except that 0.045 M acid was used instead of the normal 0.030 to 0.035 M, the mockup level controller failed; so the run was discontinued. The system was drained, rinsed, and placed in standby condition. The controller will not be repaired.

3.3 HRT REPLACEMENT REACTOR VESSEL

The design study of a replacement reactor vessel for installation in the present reactor system was terminated early in the report period. A summary report, describing in detail the design, was written.[5] The conceptual design at the termination of the study is essentially as reported previously.[6]

3.4 HRT REMOTE MAINTENANCE AND INSPECTION

Development of tools for improving the patching of the HRT core tank was discontinued.

A special attachment for the Omniscope, capable of passing through the 3/8-in. holes of the screens in the core vessel, was received from Lerma Engineering Corporation. This device provides the capability of viewing the lower portion of the screen diffuser. A new objective lens, which provides up to 5X magnification, was also received.

A new ultrasonic thickness gage was designed and fabricated to obtain the final measurements of the core wall thickness. The tool is similar to the one used earlier to measure the conical portion of the vessel,[7] but it is capable of measuring the spherical portion as well.

3.5 REINFORCING CLAMP AND FREEZERS FOR HRT LINE 107

After locating a leak in a tee in HRT line 107 (between the two fuel dump tanks), a reinforcing clamp was designed and installed to prevent rupture of the faulty tee. Temporary freezers were modified and installed on the connecting lines to isolate the faulty tee during operation.

3.6 SPARE HRT FUEL-CIRCULATING PUMP

The spare HRT circulating pump, with stainless steel parts replacing the titanium parts in the hydraulic end of the pump,[8] and with piping attached to fit the HRT fuel system, was given a 100-hr pretreatment run-in. Operation of the pump during the pretreatment at 250°C and 750 psi was without incident. Upon disassembly of the pump for a dimensional check after the pretreatment run-in, the lower Graphitar bearing was slightly damaged. However, it is believed that the bearing usefulness is not impaired. The pump was reassembled and placed in standby condition for possible use in the HRT.

REFERENCES

1. A. M. Weinberg and E. Wigner, The Physical Theory of Neutron Chain Reactors, p 609, University of Chicago Press, Chicago, 1958.

2. J. A. Kolb and P. N. Haubenreich, personal communication.

3. I. Spiewak et al., HRP Quar. Prog. Rep. Nov. 30, 1960, ORNL-3061, p 29.

4. J. E. Jones Jr., HRT Mockup Runs CS-25 and CS-26, ORNL CF-61-4-96 (April 26, 1961).

5. R. H. Chapman, (in preparation).

6. I. Spiewak et al., HRP Quar. Prog. Rep. Nov. 30, 1960, ORNL-3061, p 30-33.

7. S. E. Beall et al., HRP Quar. Prog. Rep. July 31, 1960, ORNL-3004, p 5.

8. I. Spiewak et al., HRP Quar. Prog. Rep. Nov. 30, 1960, ORNL-3061, p 25.

4. HRT REACTOR ANALYSIS

P. R. Kasten

M. L. Tobias D. R. Vondy T. B. Fowler

4.1 STATISTICAL TREATMENT OF HRT POWER-TRACE DATA

The power-trace data from the HRT with downward flow have been subjected to a variety of statistical studies with the aim of obtaining an explanation for the cause of the observed fluctuations. The variables observed were (1) the size of the fluctuations; (2) their frequency; (3) the reactivity changes necessary to produce the fluctuations; and (4) a hydrodynamic parameter α, the so-called short-circuit fraction. The first two items are obtainable directly from the power trace; the other two must be computed. The fourth item was compared with experimental measurements made by C. G. Lawson in a mockup of the HRT core.

The principal computational tools of this analysis were the IBM 7090 programs PIP and SNAVELY. Through the cooperation of R. K. Adams and J. O. Kolb, the power trace of the HRT Sanborn recorder was digitized principally at the rate of one number per second in the form of a paper tape. The paper tape was checked for gross errors by an Oracle code and converted to IBM cards. The cards were then treated by either or both of the IBM 7090 programs.

The PIP program is designed to obtain frequency distributions of the input data. The digitized power data were averaged in arbitrary batches of approximately 5 min worth of data, and the deviations from this average were used to compute such items as the following:

1. The average positive and negative deviation.
2. The average positive and negative peak.
3. The standard deviation, kurtosis, and momental skewness of all points and of all peaks.
4. The standard deviation, momental skewness, and kurtosis of positive and negative peaks separately.
5. The frequency distributions of positive and negative peaks and of positive and negative deviations; that is, the fraction of the deviations which were in excess of a certain size was computed and tabulated.

The SNAVELY program computes the reactivity changes necessary to produce the observed power traces, assuming that the variation in power is linear with time between digitizer readings. The rates of reactivity addition are also computed, as well as the variation in the bypass fraction α which would be required to provide the reactivity changes. The equations used in SNAVELY are:

$$\frac{dP}{dt} = \frac{\Delta k(1 - \beta) - \beta}{\ell} P + \sum_{i=1}^{5} \lambda_i C_{ic} + \sum_{i=1}^{5} \lambda_i C_{iB} , \tag{1}$$

$$\frac{dC_{ic}}{dt} = f_c \frac{\beta_{ic} P}{\ell} - \lambda_i C_{ic} \quad (i = 1,2,3,4,5) , \tag{2}$$

$$\frac{dC_{iB}}{dt} = (1 - f_c) \frac{\beta_{iB} P}{\ell} + \lambda_i C_{iB} \quad (i = 1,2,3,4,5) , \tag{3}$$

$$S_c \frac{d\bar{T}_c}{dt} = f_c P - \frac{W_c C_{pc}}{m} (\bar{T}_c - T_{ic}) , \tag{4}$$

$$S_B \frac{d\bar{T}_B}{dt} = (1 - f_c) P - \frac{W_B C_{pB}}{0.7} (\bar{T}_B - T_{iB}) , \tag{5}$$

$$\bar{T}_c = T_{ic} + m(T_{oc} - T_{ic}) , \tag{6}$$

$$m = \frac{1}{1 - \alpha} , \tag{7}$$

$$\bar{T}_B = T_{iB} + 0.7(T_{oB} - T_{iB}) , \tag{8}$$

$$\Delta k = \Delta k_{DF} + \alpha_c[\bar{T}_c - \bar{T}_c(0)] + \alpha_B[\bar{T}_B - \bar{T}_B(0)] , \tag{9}$$

where

C_{ic}, C_{iB} = concentration of i-th group of delayed-neutron precursors in core and blanket, respectively, in power units

C_{pc}, C_{pB} = heat capacity of core and blanket fluids, respectively (energy per degree per unit mass)

f_c = fraction of power generated in the core

Δk = excess reactivity

Δk_{DF} = any reactivity addition "driving force"; some reactivity addition to the reactor

ℓ = prompt-neutron lifetime

m = a constant used to relate inlet, outlet, and nuclear average temperatures

P = total reactor power at time t

S_c, S_B = total heat capacity of core and blanket, respectively (energy per degree)

t, Δt = time and time increment, respectively

$\bar{T}_c$, $\bar{T}_B$ = nuclear average temperature in core and blanket, respectively

$\bar{T}_c(0)$, $\bar{T}_B(0)$ = equilibrium nuclear average temperatures in the core and blanket, respectively

T_{ic}, T_{oc}, T_{iB}, T_{oB} = inlet and outlet temperatures of the core and blanket, respectively

W_c, W_B = mass flow rate through core and blanket, respectively

α = bypass fraction (fraction of flow through the core which does not undergo recirculation)

α_c, α_B = temperature coefficients of reactivity for changes in the temperatures of the core and blanket, respectively

β_{ic}, β_{iB} = fraction of delayed neutrons in i-th group in core and blanket respectively

λ_i = decay constant of i-th group of delayed-neutron precursors

Difference analogs of Eqs. (1), (4), and (5) are used, while (2) and (3) are integrated under the assumption that P is a broken-line function. Given the digitized power-trace data, Δk may be calculated from Eqs. (1), (2), and (3) as a function of time and may be subjected to the statistical treatment given to the power trace itself. Also, using the remainder of the equations, we can calculate (a) the variation in m and α required to produce the calculated Δk's, or (b) the Δk_{DF} required to produce the observed power trace assuming that m is fixed. The rates of reactivity addition and the time between zeros of reactivity addition may also be obtained.

Other mathematical tools employed to some degree have been Fourier analysis and auto- and cross-correlation techniques.

4.1.1 Results of Examination of Power Trace with the PIP Code

The PIP code results confirm the visual impression of unsymmetry given by the power trace. Positive peaks are on the average larger than negative troughs, and the average positive deviation is larger than the average negative deviation. Further, the variable which affects the magnitude of the peaks most is the core power level. A few experiments have been done in which the pressure, the flow rate, and the temperature have been varied individually, all with ambiguous results. Figure 4.1 shows the relative root-mean-square deviation of positive and negative deviations as a function of core power. The data show a considerable amount of scatter, but there is a clear, almost linear, upward trend which seems to curve over at 3 Mw. The points for 1000 and 1200 psi lie above the corresponding 1400-psi points. However, the points at 280 and 240°C, which represent substantial changes in overpressure, lie below or on the line drawn for the 260°C core, which at least partially contradicts the idea that pressure is having any effect. As for reduced flow rate, the changes in the deviations appear slight, and as with the pressure and temperature tests, there is too little evidence to draw firm conclusions.

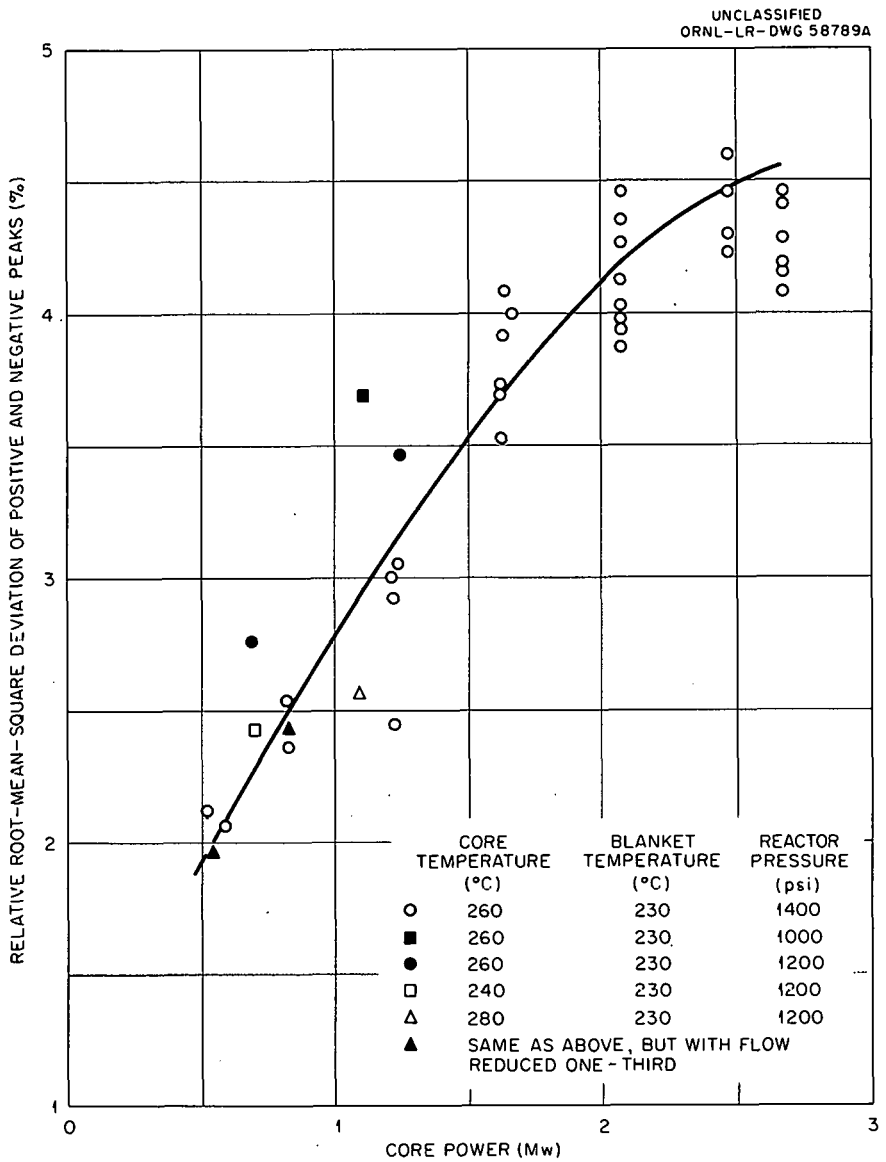

Fig. 4.1. Relative Root Mean Square of Power Peaks vs Core Power for Downward Flow.

Most of the data are from run 23 when digitizing was done as one point per second. Some data were taken in run 25 at four points per second and show a definitely lower deviation than the information from run 23. No explanation for this difference is available.

The frequency distributions which have been made by using PIP reveal the highly random character of the deviations. When the HRT was operated in upward flow, the average deviation was small, but there were some large excursions. In downward-flow operation, in contrast, although the average deviation was about four times greater, an excursion as large as 20% was a rarity. These facts are illustrated in Figs. 4.2 and 4.3. Figure 4.2 is a typical frequency-distribution plot, with probability scales on which a Gaussian distribution would appear as a straight line; Fig. 4.3 is a plot of the frequency of positive-peak occurrence vs total power.

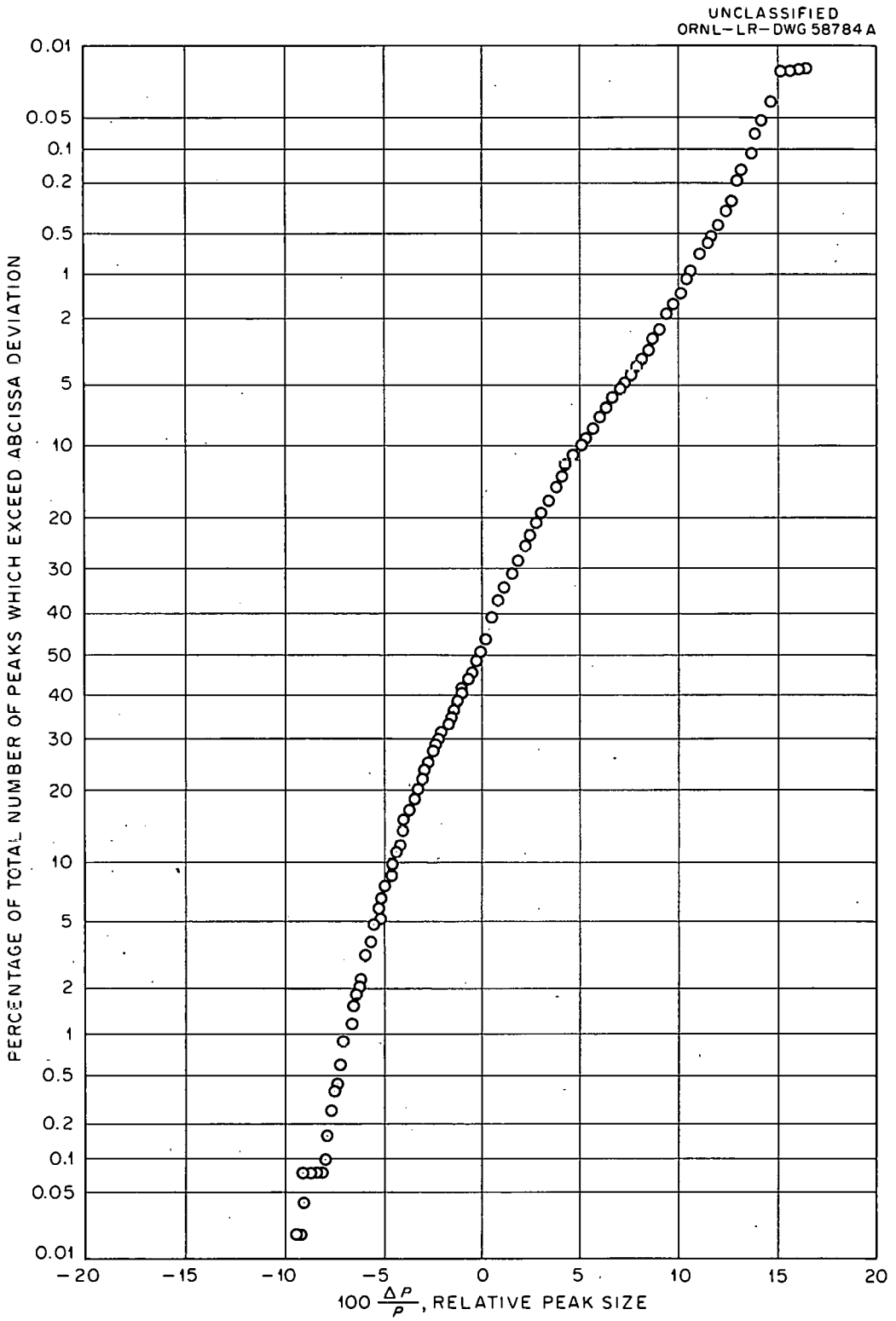

Fig. 4.2. Frequency Distribution of Peaks Observed During HRT Operation at 5 Mw for 6 Hours on Jan. 7, 1961.

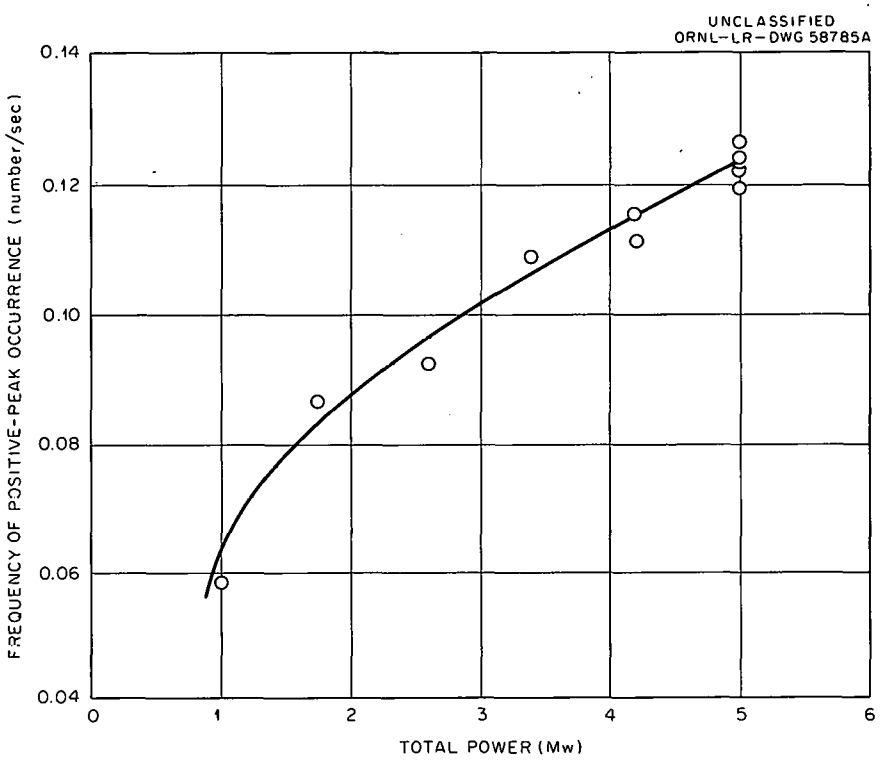

Fig. 4.3. Number of Positive Peaks per Second vs Total Reactor Power at 1400 psi, 260°C Core (Downward Flow), 230°C Blanket.

4.1.2 Results of Examination of Power-Trace Data by Using the Kinetics-Analysis Code SNAVELY

The computed reactivity additions (Δk_{DF}) which would be required to produce the observed fluctuations in power were found to be unsymmetric also. The positive reactivity additions were, on the average, somewhat larger than the negative reactivity additions. The same was true of positive and negative rates of reactivity addition. Referring to Figs. 4.4 and 4.5, it is seen that the principal variable is the core power; the effects of changing temperature, flow rate, or pressure are far less evident. Also of interest is the fact that the relative standard deviation of the reactivity addition appears to be independent of core power as shown in Fig. 4.6, whereas the relative standard deviation of the power itself (given in Fig. 4.1) increased with increasing power. This suggests strongly that while the reactivity additions increase with core power, the fluctuating mechanism which produces the additions is independent of power level.

Changes in the temperature distribution in the core produced by fluctuations in the fraction of fluid recirculated could produce these reactivity additions. To test this hydrodynamic hypothesis, it was assumed (in effect) that Δk_{DF} in Eq. (9) was zero, and the time variation of $\overline{T}_c$ was computed. Using Eq. (4), it was possible to obtain the time dependence of the variable m given in Eq. (6). By a simple argument (C. G. Lawson, personal communication), m can be related by Eq. (7) to the bypass fraction α (i.e., that fraction of the flow into the core which does not recirculate). The frequency distribution of deviations from the average m obtained from the reactor power trace could then be compared with a similar frequency distribution obtained from a full-scale model of the HRT core in measurements made by Lawson (see Sec. 3.1). The results are shown in Fig. 4.7 for several core power levels.

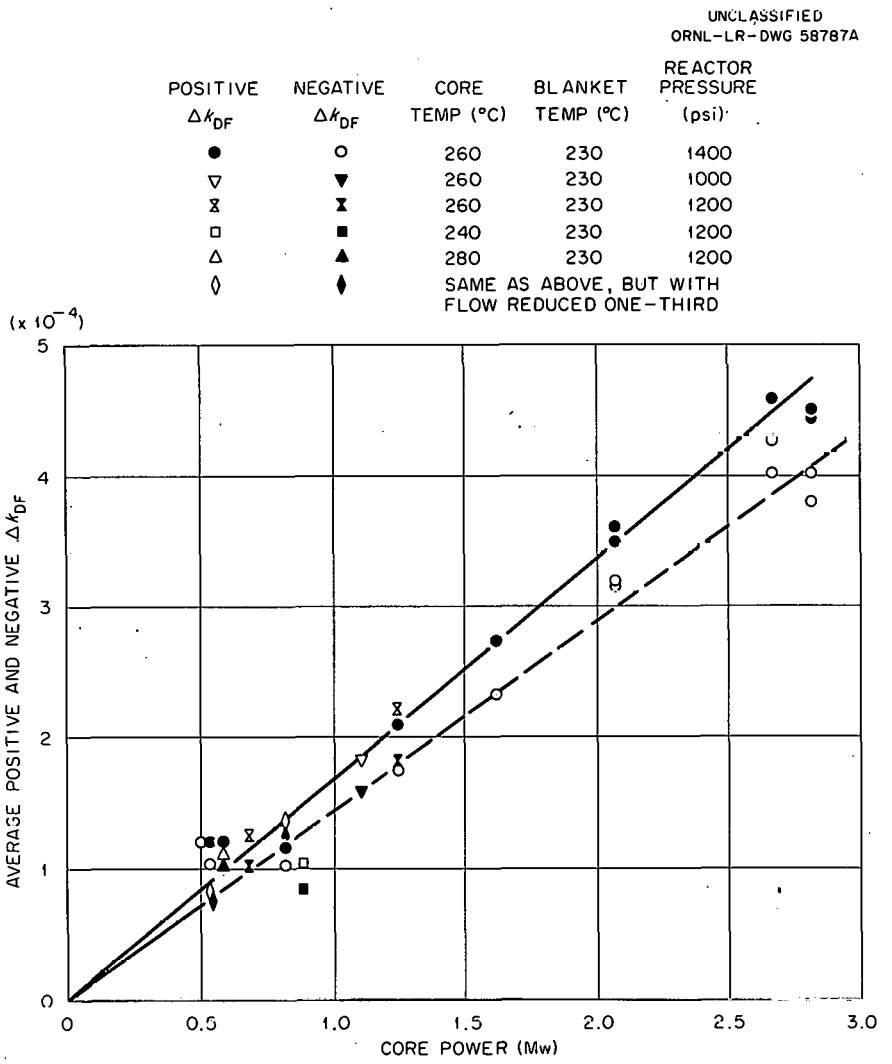

Fig. 4.4. Average Positive and Negative Excess Reactivities vs Core Power.

It is seen that the variation in m obtained with the model is very similar to that obtained with the reactor except for the ever-present asymmetry which is noted at the larger deviations in m. (These correspond to the asymmetry in the power trace.) No consistent dependence of the degree of this asymmetry upon core power can be perceived. At the present time, explanations for the asymmetry are available, but they rest upon unverifiable conjectures. It is of interest to note that Lawson, using analogue-computer equipment, was able to construct an artificial power trace using continuously obtained salt trace measurements of m (or α) obtained in the HRT core model as the driving function. This "power trace" was much like the actual power trace. It is true that any randomly varying driving function could produce a qualitatively similar power trace, but the standard deviation of m observed in the reactor is in good agreement with the salt trace m; this strongly supports the hypothesis that the HRT power fluctuations originate hydrodynamically.

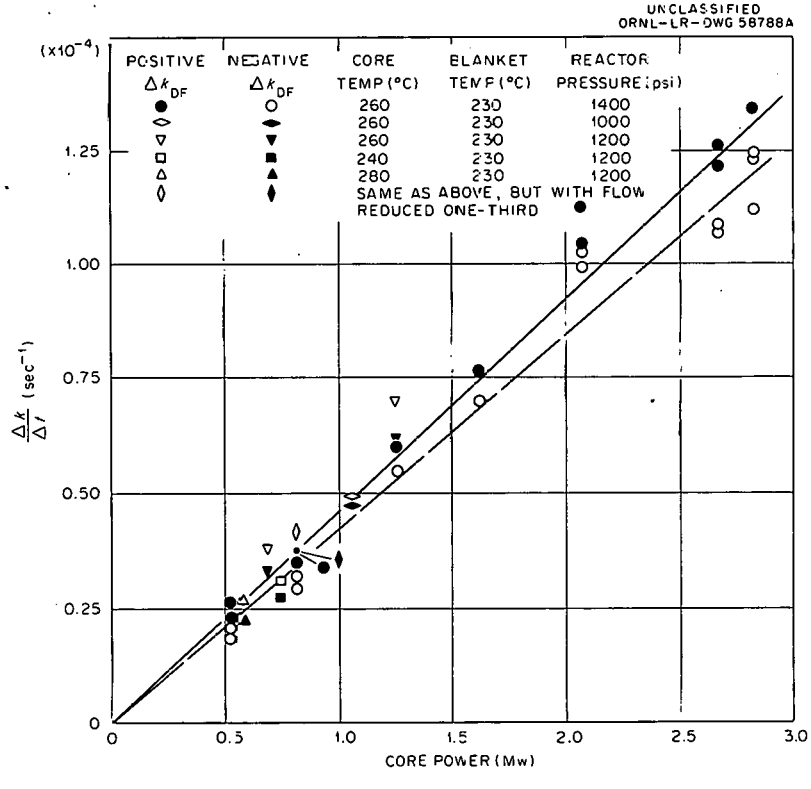

Fig. 4.5. Average Rate of Excess Reactivity Additions.

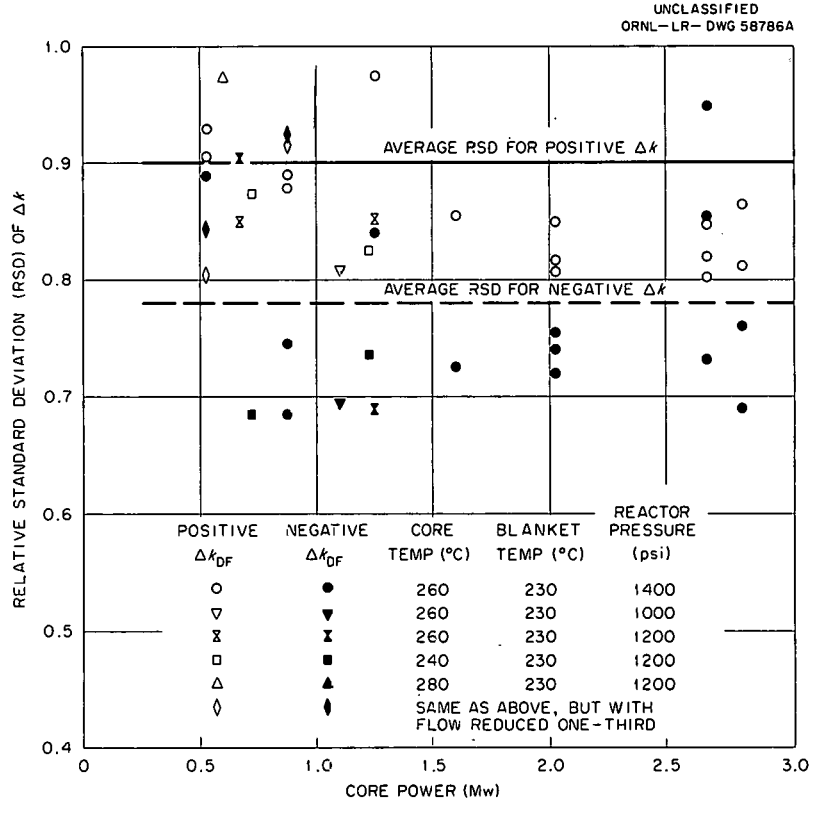

Fig. 4.6. Relative Standard Deviation of Positive and Negative Reactivity Additions.

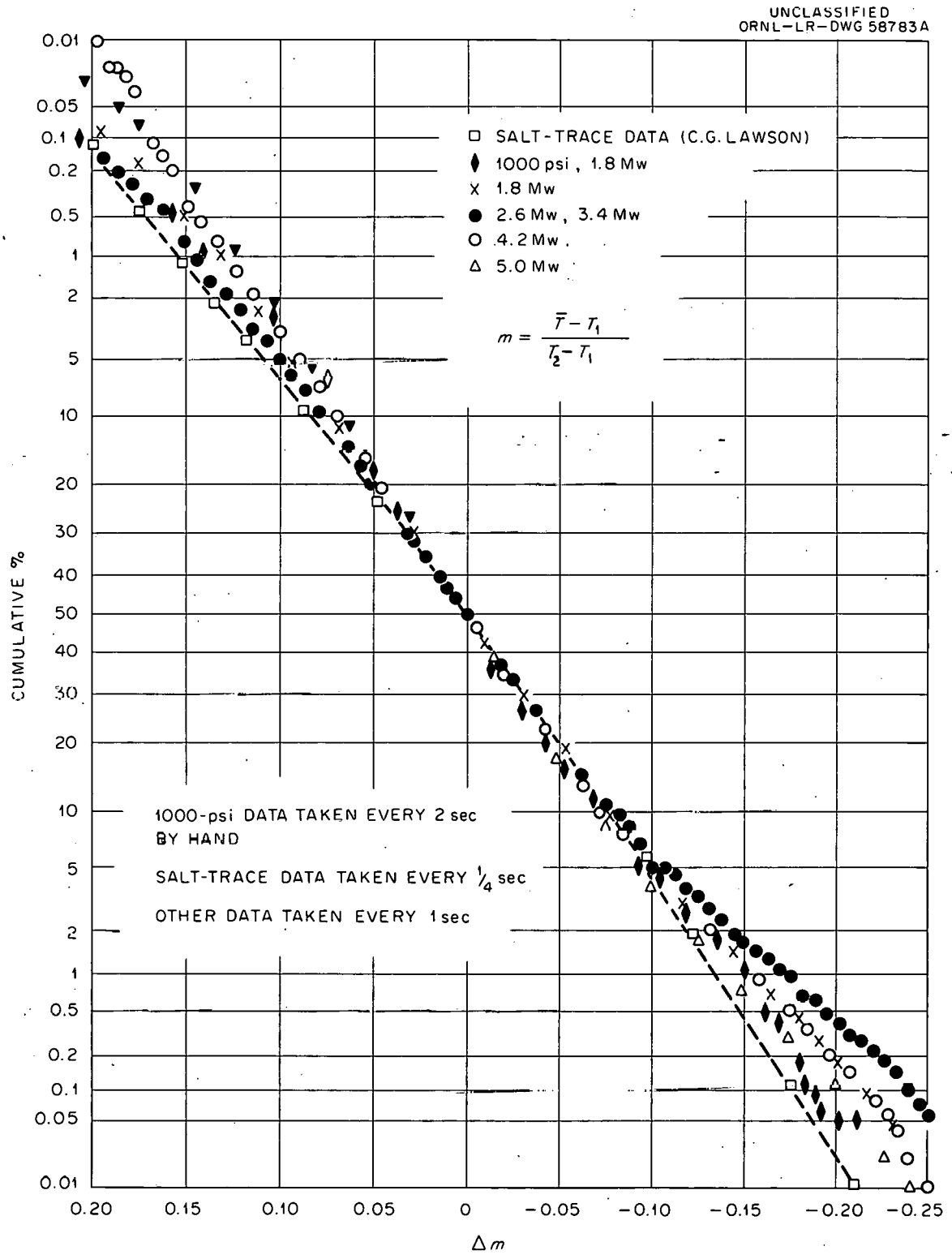

Fig. 4.7. Cumulative Frequency Distributions of Deviations in the Parameter m Obtained from Reactor Power Traces Compared with Measurements Made in Core Mockup.

4.1.3 Fourier Analysis and Cross-Correlation Techniques

Another means of detecting resemblances between the salt trace observations and the reactor power traces might be by means of Fourier analysis. The Fourier series of the power trace was constructed, treating the digitized data as points on a broken-line function. The "fractional power" due to each frequency was obtained, that is, the sum of the squares of the sine and cosine coefficients of a given frequency divided by the sum of the squares of all the coefficients. No particular frequency or narrow band of frequencies was observed as being of special importance.

Use of an auto- and cross-correlation program based upon the ideas of J. W. Tukey[1] has as yet shown nothing striking in the way of particular frequencies.

4.2 TEMPERATURE TRANSIENTS DUE TO DENSITY CHANGES ACCOMPANYING VARIATIONS IN HRT POWER LEVEL

One of the causes for a drifting of the nuclear average temperature in the HRT appears to be associated with a density change in the core circulating system of the HRT as the reactor power is changed. The mechanism is briefly the following. At heat-loss power, the core, the heat exchanger, and the inlet and outlet lines to the core are all at almost the same temperature. On going to 5 Mw, the average core temperature remains the same, but the inlet and outlet temperatures fall below this temperature, so that liquid must be added to the core system to make up for the contraction in the core external volume. This liquid comes ultimately from the blanket dump tank, which contains water only. In this process, fuel was first fed to the core from the core dump tank so that the core concentration and temperature was slightly raised initially. (The other streams to the core were disturbed so as to permit this rise in concentration.) To keep the core dump-tank weight constant, condensate was added to it. At this point the ratio of core-to-dump-tank concentrations was higher than that which corresponded to equilibrium conditions with the various pumping rates; as the equilibrium ratio was gradually restored, the core concentration and temperature fell below the original values at zero power.

This process was analyzed[2] based on the following assumptions and restrictions:

1. The fraction of power generated in the blanket is constant.
2. The weight of water in the core dump tank is held constant.
3. The blanket temperature is constant.
4. The back-mixing rate from core to blanket is constant.
5. The reactor is critical at all times, and the total amount of uranium in the reactor is a fixed quantity.
6. Metal expansion is neglected.
7. Zero-power rather than heat-loss power is used as the starting condition.

Using specific reactor conditions (core temperature 265°C, blanket 230°C, 60% of power generated in the core), it was assumed that 15 min was required to go from zero power to 5 Mw. It was estimated that the core temperature would

rise initially about 0.7°C, followed by a gradual fall over a 2-hr period to an equilibrium point 1.3°C below the initial level of 265°C. Figure 4.8 gives the calculated time-temperature variation during and following the power rise.

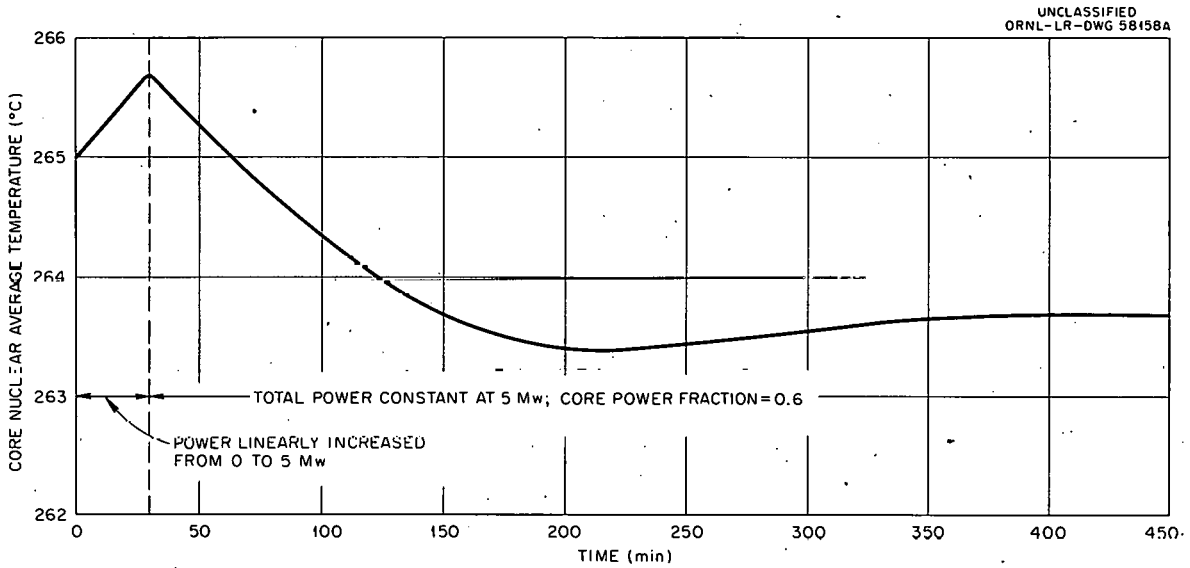

Fig. 4.8. Core Temperature vs Time Following a Power Increase from Zero to 5 Mw.

REFERENCES

1. Nancy Clark, Share Subroutine CS TUKS - Tukey Spectrum Estimation, Convair, San Diego (Dec. 5, 1958).

2. M. L. Tobias and D. R. Vondy, Temperature Transients Due to Density Changes on Changing Power Level in the HRT, ORNL CF-61-4-63 (Apr. 6, 1961).

PART II. ENGINEERING DEVELOPMENT

5. DEVELOPMENT OF REACTOR COMPONENTS AND SYSTEMS

I. Spiewak

R. H. Chapman
D. M. Eissenberg
J. E. Jones Jr.
J. C. Moyers

5.1 CIRCULATING-PUMP DEVELOPMENT

The 200Z canned-motor pump, which has a motor similar to those used in the HRT circulating pumps but which contains parts more suitable for use in circulating thoria slurries, continued to operate in high-temperature water in a test of its alumina radial bearings. The pump has operated satisfactorily for 11,072 hr to date.

5.2 OXYGEN COMPRESSOR

Modifications were completed on the three-stage oxygen compressor,[1] designed to recycle radioactive oxygen, and the unit was placed in standby. A status report was written summarizing the development of the compressor.[2]

The unit operated 2000 hr without a first- or second-stage diaphragm failure. Six third-stage diaphragm failures occurred; all but one can be attributed to the presence of foreign matter in the system. The packed-piston drive unit, believed to be the source of the foreign matter, was replaced with an oil-operated triplex unit. The triplex drive actuates the intermediate water system through Neoprene pulsator units. The system was not operated following these modifications because of changes in the program.

5.3 SLURRY ENGINEERING

5.3.1 Wall Slip Phenomena in Viscometer Tubes

Tests were reported previously for a slurry of pumped 1600°C-fired 1.5-micron thoria flowing through five vertical capillary tubes.[3] That particular slurry did not appear to exhibit a wall-slip phenomenon at 30°C.

Additional runs made in laminar flow with other slurries revealed a slip effect characteristic of particular materials. This effect takes the form of separate pseudoshear diagrams for different diameter tubes, as illustrated in Fig. 5.1. The effect seems to be most pronounced at intermediate shear rates where forces are great enough to lift flocs away from the wall but not great enough to completely disrupt the floc structure. The slip effect appears to decrease with decreasing concentration. Because slurries in the large tubes, which theoretically show less slip, go into turbulent flow at relatively low

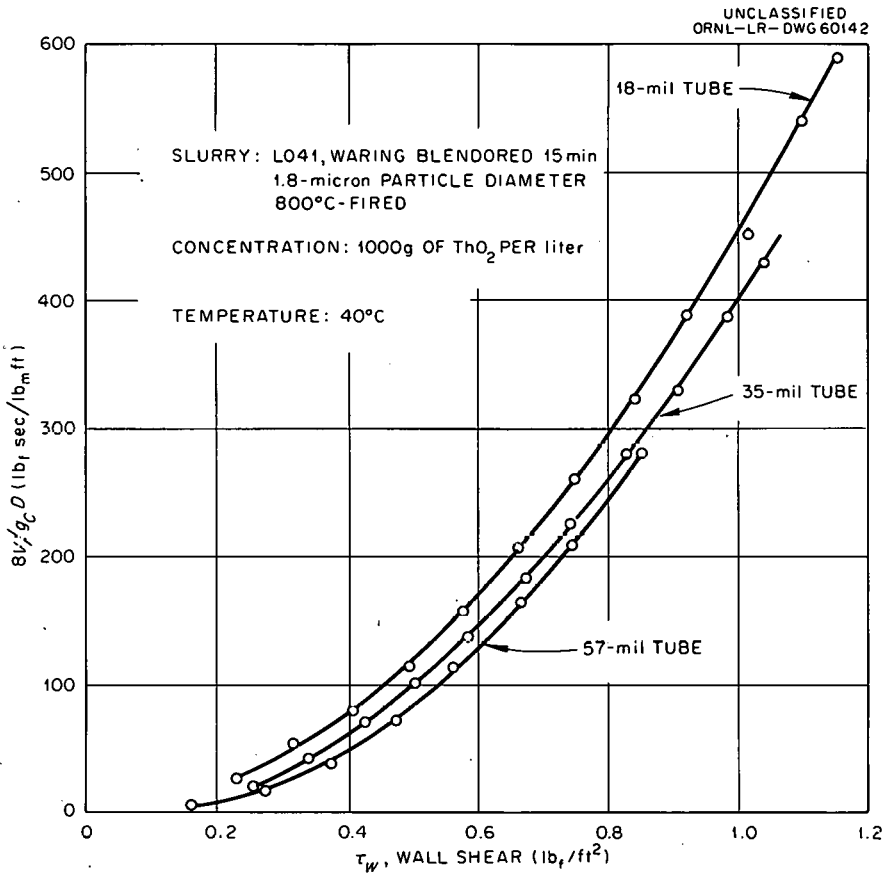

Fig. 5.1. Example of Wall Slip Effect at High Concentration of a Low-Fired Slurry.

shear rates, it is not possible to demonstrate whether at high shear rates the slip effect would disappear entirely. However, it was noted that chemically dispersed slurries exhibit no observable slip effect.

The shape of the small-tube pseudoshear diagram is such that an estimate of the coefficient of rigidity taken at high wall shear rates would not be affected by the presence of the slip effect. The slip effect causes an apparent lower value of the yield stress at high shear rates.

This discrepancy is much less, however, than the error produced by limiting rheometers to tubes which do not show slip (0.125 in. and larger). A slurry in a 0.125-in. tube is usually in turbulence with a rate of shear of 100-125 $(lb_f \text{ sec})/(lb_m \text{ ft})$. Referring to Fig. 5.1, the yield value and coefficient of rigidity, based on wall shear rates less than 125 $(lb_f \text{ sec})/(lb_m \text{ ft})$, would be in error by as much as a factor of 2 or 3; the yield value based on the various viscometers would be different by at most 20%.

A study was made of the shear diagrams of chemically dispersed slurries in the temperature range 20 to 80°C. It was found that the behavior was as predicted for nonflocculated suspensions by Happel.[4] That is, the specific viscosity, (viscosity of slurry)/(viscosity of water), of dispersed slurries is dependent essentially on the volume concentration of solids and is not a function of temperature. The volume concentration dependence given in ref 1 was related to the experimental values for dispersed thoria slurries when appropriate corrections were made[5] for the particle bulk density.

The general conclusion from this work is that small-bore capillary viscometers should be preferred for rheological measurements in spite of the slip effect noted with some slurries. The great advantage of the small tubes is their ability to reach high rates of shear in laminar flow.

5.3.2 200B Loop Operation

The 200B loop piping was modified (Fig. 5.2) to permit measurement of pressure drop in turbulent flow across a vertical section of loop piping. The test section is 12 ft 6 in. long and 1-1/2 in. in inside diameter, giving an L/D of 100. The section is preceded by a 4-ft calming section containing a cruciform baffle. A second electrically insulated test section has been provided for later use for measurement of burnout heat flux to a slurry flowing turbulently past a heated surface. In addition, a high-temperature vertical-tube capillary viscometer has been installed in the loop (Fig. 5.3) and is being tested.

One run (200B-5) was completed in which turbulent pressure-drop measurements were obtained for a slurry of 1.8-micron 1600°C-fired oxalate-precipitated thoria (DT-12 and DT-13). Measurements of pressure drop vs flow rate were obtained with water and at six slurry concentrations in the range 400 to 1400 g of ThO_2 per liter and in the temperature range 33 to 240°C. The results have been correlated by using the conventional Fanning friction-factor - Reynolds number plot.

The primary difficulty in applying the correlation was the selection of an appropriate viscosity in the Reynolds number term. The viscosity selected was that of chemically dispersed slurry, believed to be approximately equal to the viscosity of the flocculated slurry at very high rates of shear. In Fig. 5.4

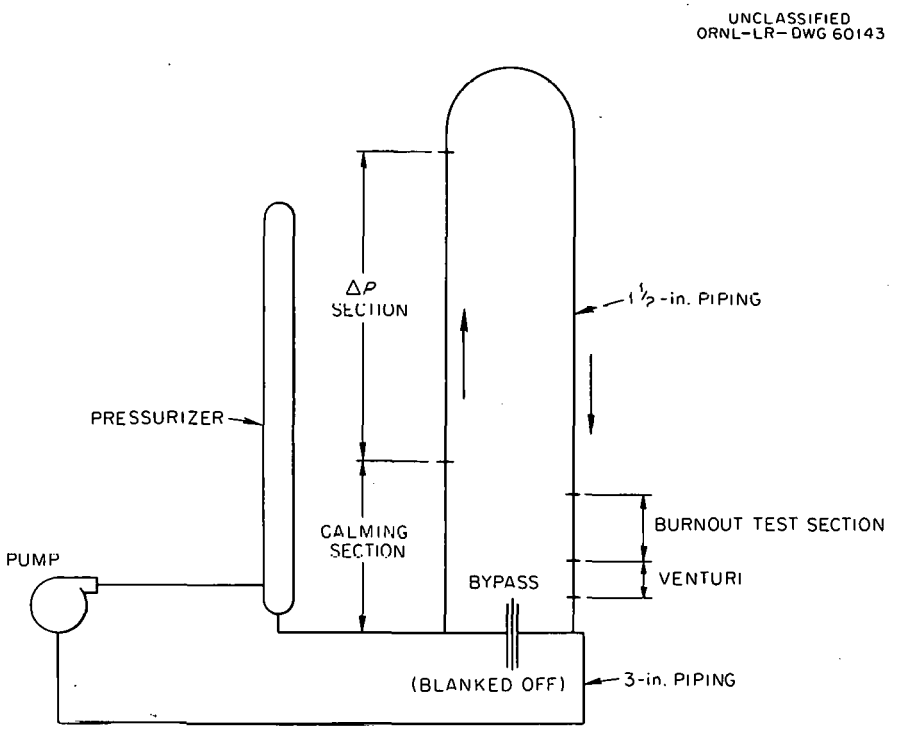

Fig. 5.2. Schematic Diagram of Revised 200B Loop Piping.

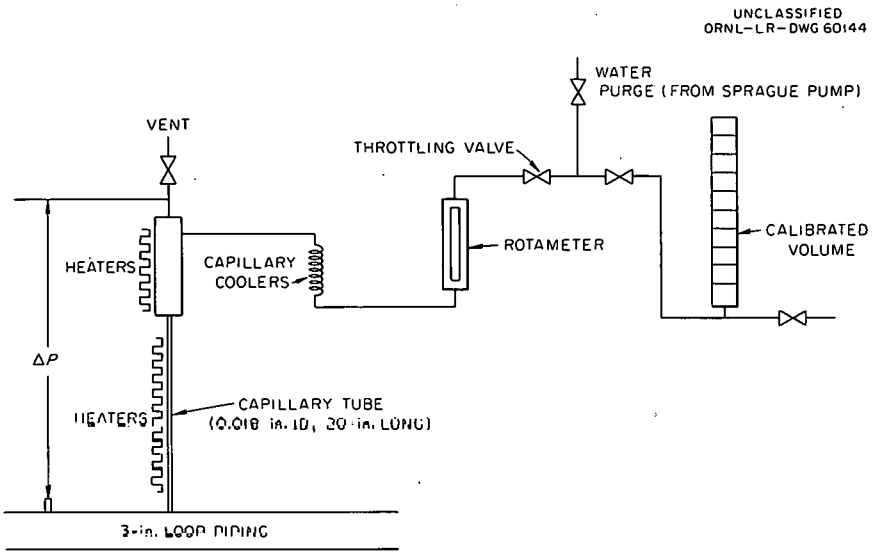

Fig. 5.3. Schematic Diagram of High-Temperature Loop Viscometer.

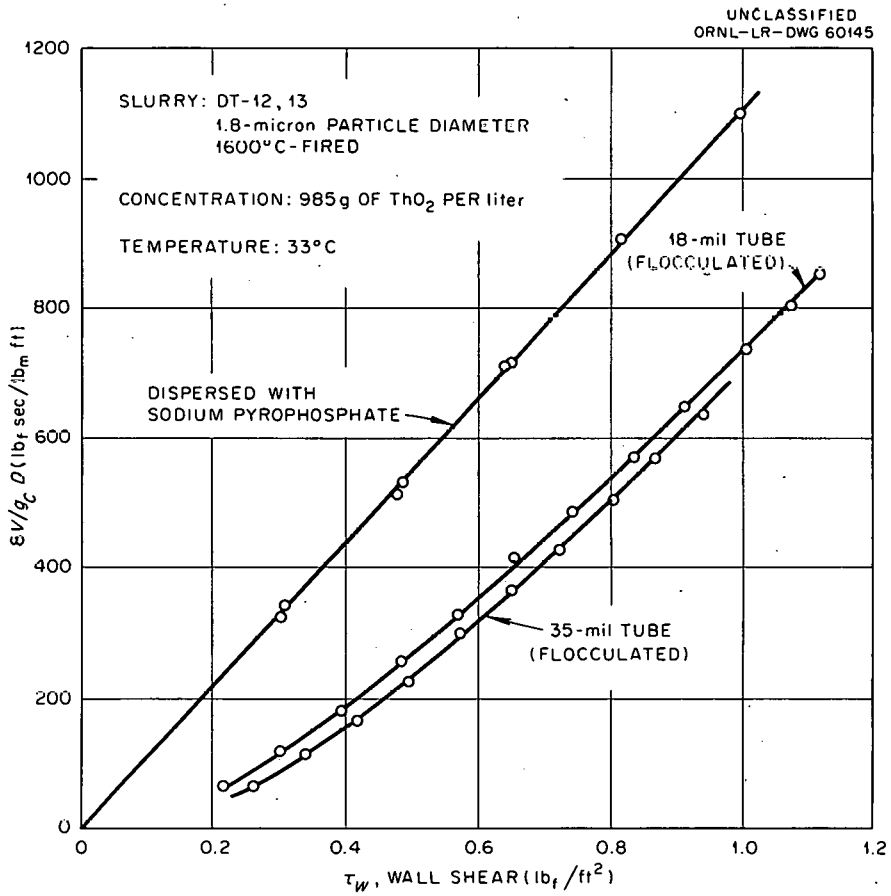

Fig. 5.4. Comparison Between Dispersed and Flocculated Experimental Pseudoshear Diagrams.

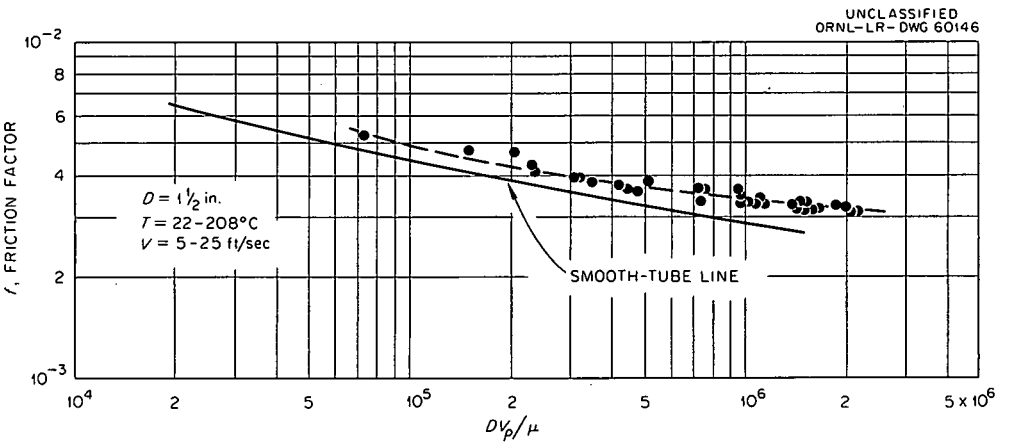

Fig. 5.5. Water Calibration Curve for 200B Loop Friction-Factor Section.

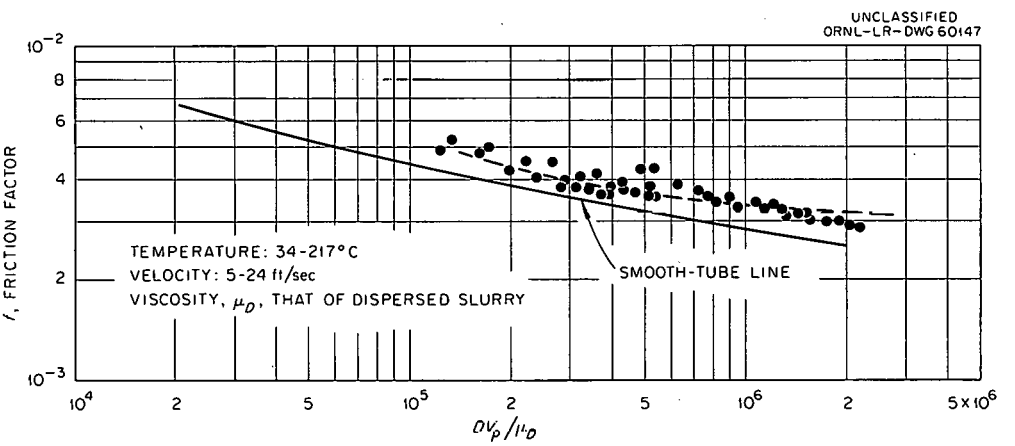

Fig. 5.6. Friction-Factor Plot for DT-12,13 Slurry (1.8-Micron Particle Diameter, 1600°C-Fired); Concentration, 600 g of ThO_2 per Liter.

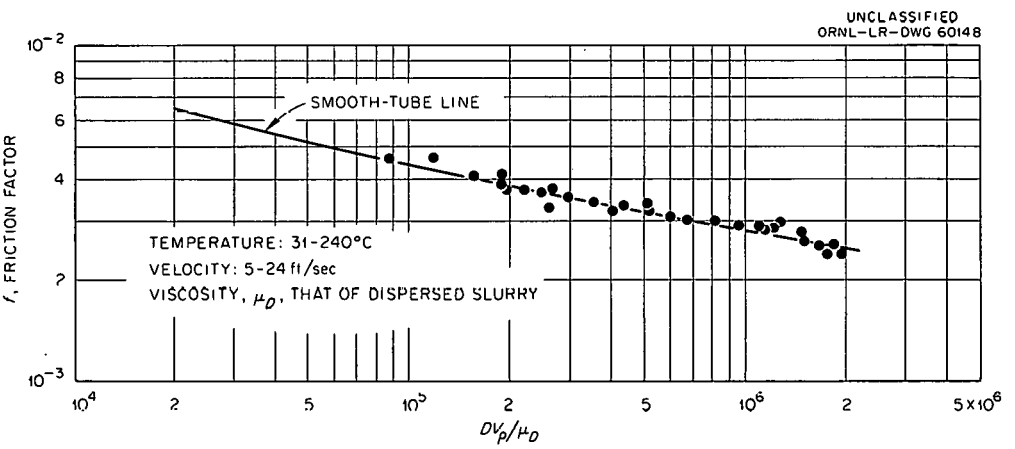

Fig. 5.7. Friction-Factor Plot for DT-12,13 Slurry (1.8-Micron Particle Diameter, 1600°C-Fired); Concentration, 1230 g of ThO_2 per Liter.

it can be seen that the slope of the pseudoshear diagram (inverse coefficient of rigidity) of the flocculated 200B-5 slurry tends to approach the slope obtained with the dispersed slurry (inverse viscosity) at high rates of shear. At the elevated temperatures the viscosity was calculated by assuming (viscosity of slurry)/(viscosity of water) to be independent of temperature at constant volume fraction solids.

When correlated in the manner indicated, the slurry turbulent friction factors fell between the experimental water calibration line and the conventional smooth-tube line (Figs. 5.5, 5.6 and 5.7).

No attempt was made in this run to correlate the transition and laminar-flow pressure drop because of the problem of slurry dropout in horizontal sections of the loop at the lower flow rates. The loop is equipped with a bypass line around the friction-factor section which will enable, in the future, measurements of transition and laminar-flow pressure drops while maintaining good suspension in the horizontal loop sections.

REFERENCES

1. I. Spiewak et al., HRP Quar. Prog. Rep. July 31, 1960, ORNL-3004, p 39; I. Spiewak et al., HRP Quar. Prog. Rep. Jan. 31, 1960, ORNL-2920, p 24-25.

2. J. E. Jones Jr., Status Report of Development of Three Stage Oxygen Compressor for Aqueous Homogeneous Reactor Service, ORNL CF-61-5-77, (May 3, 1961).

3. I. Spiewak et al., HRP Quar. Prog. Rep. Nov. 30, 1960, ORNL-3061, p 41.

4. J. Happel, J. Appl. Phys. 28, 1288 (1957).

5. D. M. Eissenberg, Concentration of Settled Beds of Thoria Slurry, ORNL-3107 (Apr. 18, 1961).

PART III. SOLUTION FUELS

6. REACTIONS IN AQUEOUS SOLUTIONS

M. J. Kelly

C. J. Barton
D. R. Cuneo
L. O. Gilpatrick
H. H. Stone
J. E. Strain

6.1 STABILITY OF PROTACTINIUM IN THORIUM NITRATE - NITRIC ACID SOLUTIONS AT 21 TO 200°C

6.1.1 Introduction

Thorium nitrate solutions are attractive for use as a breeder blanket in an aqueous two-region homogeneous reactor if the N^{15} isotope can be produced at a cost below $1.25 per gram, according to Lindsey.[1] He suggested that a blanket of this type be operated at a maximum temperature of about 175°C to avoid hydrolytic precipitation of thorium but had no information concerning the stability of protactinium in thorium nitrate - nitric acid solutions under proposed blanket operating conditions. Lindsey also lacked data necessary to determine the feasibility or cost of removing uranium and protactinium from the blanket. Kelly *et al.*[2] reported that protactinium can be effectively removed from solution along with about 2% of the thorium by peroxide precipitation.

The purpose of the present investigation, from which only preliminary results are yet available, is to provide data on the stability of protactinium in thorium nitrate - nitric acid solutions and to continue the study of methods of removing protactinium and uranium from such solutions. During the past quarter, most of the experimental effort was applied to the stability problem.

6.1.2 Experimental Procedure

A simple experimental arrangement was devised to heat protactinium-containing thorium nitrate solutions in a glove box. An 8-ml stainless steel bomb containing about 4 ml of the test solution was connected to a stainless steel filter unit by a short U-shaped length of 6- or 20-mil-ID stainless steel tubing. The filter was connected by means of 6-mil-ID stainless steel tubing to a high-pressure needle valve to which another short length of capillary tubing was attached to permit flush liquid and samples to be transferred from the bomb into suitable containers. The bomb and filter were placed in a 400-ml beaker after the apparatus was loaded and leak tested with oxygen at about 1000 psi. The beaker was then filled with a heat-conducting medium and heated on a small hot plate equipped with a thermostat. Temperatures were measured by means of a 250°C mercury thermometer inserted in the heat transfer medium.

Thorium nitrate - nitric acid solutions containing Pa^{231} and Pa^{233}, the latter added as a tracer, were prepared in the following manner. Protactinium-233 tracer was produced by irradiating several hundred milligrams of $Th(NO_3)_4 \cdot 4H_2O$

in the Oak Ridge Research Reactor for about 2 min. After cooling overnight, this material was dissolved in 9 N H_2SO_4 - 6 N HCl, as recommended by Kirby,[3] and was extracted with a mixture of diisobutyl carbinol (DIBC) and xylene (63-37 vol %). The organic layer containing Pa^{233} was washed twice with 9 N H_2SO_4 - 6 N HCl solution and then transferred to a glove box where it was contacted with an aqueous phase containing Pa^{231} and its daughter products in 9 N H_2SO_4 - 6 N HCl solution. After extracting the Pa^{231} into the DIBC, the latter was washed with 9 N H_2SO_4 - 6 N HCl, and then a portion of the DIBC was removed from the glove box for alpha and gamma counting. These counts established a ratio between the Pa^{231} content of the mixture and the gamma count resulting from the Pa^{233} tracer so that the gamma count could be used as a means of determining the protactinium content of solutions containing a high concentration of thorium.

The effectiveness of the above procedure in separating Pa^{231} from its daughter products, some of which are short-lived alpha emitters, was demonstrated by pulse-height analysis of a DIBC extract. Peaks attributable to other alpha emitters could not be detected, indicating that more than 99.3% of the alpha-active material in the DIBC was Pa^{231}. The protactinium was then washed out of the DIBC by contacting it with dilute HNO_3 solution containing a trace of fluoride to complex the protactinium and prevent it from hydrolyzing. In preparing the solution for experiment 5 (Table 6.1), oxalic acid was used as the complexing agent instead of fluoride to eliminate the possibility of carrying traces of fluoride ion into the final solution. The protactinium was precipitated along with a small amount of thorium carrier by addition of NH_4OH and was then separated from the supernatant liquid by centrifuging and decanting. The precipitate was washed with distilled water and again centrifuged to permit removal of the wash solution by decantation. The precipitate was finally dissolved in 4 ml of a $Th(NO_3)_4$-HNO_3 mixture of the desired composition, and an aliquot of the solution was removed for a gamma count to determine its protactinium content before transferring the solution to the bomb.

Sufficient oxygen was admitted to the bomb assembly after it had been sealed and leak tested to give a pressure of 600 psi at room temperature. After surrounding the bomb and filter with a heat-transfer medium as described above, the rheostat on the hot plate was adjusted to give the desired temperature, and samples of the bomb solution were removed at intervals for gamma counting after first flushing the line with a small amount of the solution. In some experiments aliquots of the solution were dried and ignited at 800°C to determine their thorium content, and total nitrate concentrations were determined by titration with dilute NaOH after passing an aliquot of the solution through a Dowex-50 ion-exchange column.

6.1.3 Results and Discussion

Data obtained in five separate experiments conducted to date are contained in Table 6.1. In experiment 1, some loss of protactinium occurred on standing at room temperature, but the rather rapid drop in protactinium concentration that occurred on heating the bomb probably resulted from precipitation of thorium at a temperature above the limit of stability of this solution composition. Examination of the bomb contents at the end of the experiment revealed a large amount of solids which contained a significant fraction of the starting amount of protactinium.

The unexpectedly high temperature reached by the solution in this experiment was attributed to the large vertical temperature gradient resulting from the use of sand as the heat-conducting medium. In experiments 2, 3, 4, and the first part of experiment 5, powdered aluminum was used as the heat transfer medium. This material is a much better heat conductor than sand, but a fairly large

Table 6.1. Stability of Protactinium in $Th(NO_3)_4$-HNO_3 Solutions at Temperatures in the Range from 21 to 200°C

Experiment 1			Experiment 2			Experiment 3			Experiment 4			Experiment 5		
2 *M* $Th(NO_3)_4$ + 3 *M* HNO_3			2 *M* $Th(NO_3)_4$ + 3 *M* HNO_3			2 *M* $Th(NO_3)_4$ + 3 *M* HNO_3			2.5 *M* $Th(NO_3)_4$ + 0.5 *M* HNO_3			2.5 *M* $Th(NO_3)_4$ + 0.5 *M* HNO_3 + Zircaloy		
Time (hr)	Temp. (°C)	Pa Conc. (ppm)	Time (hr)	Temp. (°C)	Pa Conc. (ppm)	Time (hr)	Temp. (°C)	Pa Conc. (ppm)	Time (hr)	Temp. (°C)	Pa Conc. (ppm)	Time (hr)	Temp. (°C)	Pa Conc. (ppm)
0	21	5.3	0	21	13.5	0	21	109	0	21	23.7	0	21	95.6
17	21	2.4	62	21	11.7	4	21	109	18	21	21.6	19	21	103.8
19.6	>200	1.5	66	113	11.5	7	154	109	24	181	22.6	43	~125	101.6
20.3	>200	1.1	68	113	11.8	25	153	108	44	179	21.3	50	~125	99.6
21.3	>200	0.9	86	113	10.9	33	183	*	67	180	21.7	67	~125	91.8
22.8	~123	0.7	89	147	11.1	34	21	110	74	200	20.4	74***	181	73.4
23.5	~123	0.7	92	149	11.0	49	21	109	101	200	20.8**	80	181	67.0
41	~123	0.2	110	150	10.5	56	178	109				92	180	68.2
			117	180	10.2	75	180	104				95	180	-
						96	180	109				98	200	29

*Sample line plugged; insufficient sample.

**Sample line plugged; sample removed from bomb at room temperature.

***Heat transfer medium changed from aluminum powder to mercury just before taking this sample.

vertical heat gradient existed in the bomb environment so that the solution temperatures are not accurately known. Since the thermometer bulb was placed near the bottom of the containing beaker just above the heat source, the bomb, which was further away from the heat source, was probably 20 to 40°C cooler than the higher temperatures recorded for these experiments in Table 6.1. This temperature uncertainty was eliminated during the latter part of experiment 5 by replacing the aluminum powder with mercury. This experiment is considered the most significant of the series because of the improved temperature control, the presence of Zircaloy-2, a part of which had an oxide coating, and elimination of the possibility of trace amounts of fluoride ions in the solution.

It seems clear from the results obtained in the latter part of experiment 5, which show only about an 8% decrease in protactinium concentration over a period of 18 hr at 180°C, that protactinium in a solution containing a high concentration of thorium and a low concentration of free nitric acid does not precipitate rapidly when the solution is in contact with stainless steel, Zircaloy-2, and oxidized Zircaloy-2 at this temperature. Insufficient data have been obtained at 200°C to justify a definitive statement concerning the stability of protactinium in 2.5 *M* $Th(NO_3)_4$ - 0.5 *M* HNO_3 at this temperature. Data reported by Marshall et al.[4] indicate that thorium might precipitate from a solution of this composition at 200°C. Although the protactinium concentration dropped rather drastically in 3 hr at this temperature, there was no detectable change in the thorium concentration. This indicates that protactinium may hydrolyze at a slightly lower temperature than thorium under the conditions prevailing in this experiment.

Total nitrate determinations showed a small but significant decrease in nitrate concentration during the experiment. This may have been due to reaction with stainless steel. It was noted that portions of the solution removed for sampling through the stainless steel filter, which has a very large surface area as compared to the bomb, were dark green while the solution remaining in the bomb at the conclusion of the experiment were almost colorless. This seems to indicate that nitrate attack on stainless steel was strongly dependent on the surface-to-volume ratio. Further experiments of this type will be performed in the near future with apparatus which will permit better control and measurement of the solution temperature.

A portion of the solution remaining in the bomb at the conclusion of experiment 3 was used to check the effectiveness of protactinium recovery by peroxide precipitation. A 0.5-ml aliquot of the solution was mixed at room temperature with 0.2 ml of 30% H_2O_2 and centrifuged. The supernatant liquid was found by counting to contain only about 4% of the calculated protactinium content of the 0.5-ml aliquot. Another portion of the solution was diluted with 2 *M* $Th(NO_3)_4$ - 3 *M* HNO_3 solution and extracted with twice its volume of DIBC. After shaking for 2 min, 38% of the protactinium was found in the organic phase; shaking for another 5 min resulted in 74% extraction.

A number of investigators have studied the removal of trace amounts of uranium and protactinium from concentrated thorium nitrate solutions in connection with the production of U^{233}. Oliver, Meriwether, and Rainey[5] reported a study of the variables affecting the extraction of protactinium from thorium nitrate solutions by means of DIBC. Batch tests and countercurrent batch extractions performed with Pa^{233} tracer demonstrated effective separation of protactinium from thorium, uranium, and several typical fission-product activities. It was also shown that exposure of DIBC to a high level of gamma activity and heating to the boiling point of the material (172 to 175°C) did not impair its ability to extract protactinium. These investigators found that protactinium was not deposited on either glass or stainless steel walls when $Th(NO_3)_4$-$Al(NO_3)_3$-HNO_3 solutions were concentrated by boiling to 0.5 of the original volume and then diluted to the

starting volume. Although this investigation was directed toward the objective of obtaining selective separation of protactinium from uranium as well as thorium, it seems likely that conditions can be found that will permit extraction of both uranium and protactinium from $Th(NO_3)_4$-HNO_3 solutions. Since tests reported by Kelly et al.[2] indicate that small amounts of uranium cannot be precipitated as the peroxide in the presence of a high concentration of thorium, further study of the extraction method appears to be warranted.

6.1.4 Conclusions

Based upon the preliminary experiments reported here, there seems to be no reason to believe that precipitation of protactinium in a thorium nitrate - nitric acid solution blanket at 180°C would be sufficiently rapid to prevent its removal by processing in a side stream at a moderate rate. Information in the literature and the results of a preliminary experiment reported here indicate that a solvent-extraction method may be suitable for recovery of protactinium from a solution blanket, and it is possible that such a method may be effective in removing uranium also.

6.2 STUDIES ON GAS SOLUBILITY IN VARIOUS SOLVENTS

6.2.1 Introduction

Studies on gas solubility in aqueous systems provide data of direct interest to operations and design activities. These studies, when broadened in scope, may provide insight into the mechanism of the homogeneous hydrogen-oxygen recombination reaction catalyzed by copper. The effect of concentrations of inorganic species on solubility has been studied only slightly, particularly with changes in the temperature parameter as well as concentration. These studies, therefore, have both applied and fundamental interests.

The experimental procedures and some previous data have been reported elsewhere.[6,7]

6.2.2 Results and Discussion

Figure 6.1 shows the solubilities of hydrogen in H_2O and deuterium in D_2O from room temperature to 300°C. The data are suitable for engineering purposes as shown. Tabulated data, including the observed experimental deviation, from room temperature to 250°C are available elsewhere.[7] Figure 6.2 shows the effect of some ionic solutions on the solubility. "Salting-out" effects are particularly noticeable at low concentrations, with smaller effects noted at higher temperatures.

6.2.3 Conclusions

The data presented are useful to those concerned with design and operation of reactor systems using aqueous solutions or slurries. Preliminary data on the effect of added ionic constituents show that a precise determination can be made of the effect of various ions on the solubility of the gas. It is believed that sufficient data of this type will provide insight into the solution process.

REFERENCES

1. E. E. Lindsey, Thorium Nitrate as a Breeder Blanket, ORNL CF-60-8-150 (August 1960).

2. M. J. Kelly et al., HRP Quar. Prog. Rep. Nov. 30, 1960, ORNL-3061, p 43-47.

3. H. W. Kirby, The Radiochemistry of Protactinium, NAS-NS-3016 (December 1959).

4. W. L. Marshall et al., Reactor Chem. Div. Ann. Prog. Rep. Jan. 31, 1961, ORNL-3127, p 47-50.

5. J. R. Oliver, J. R. Meriwether, and R. W. Rainey, Extraction of Protactinium with Diisobutylcarbinol, ORNL-2668 (Apr. 1959).

6. L. O. Gilpatrick and H. H. Stone, HRP Quar. Prog. Rep. Nov. 30, 1960, ORNL-3061, p 47-48.

7. L. O. Gilpatrick and H. H. Stone, Reactor Chem. Div. Ann. Prog. Rep. Jan. 31, 1961, ORNL-3127, p 60-61.

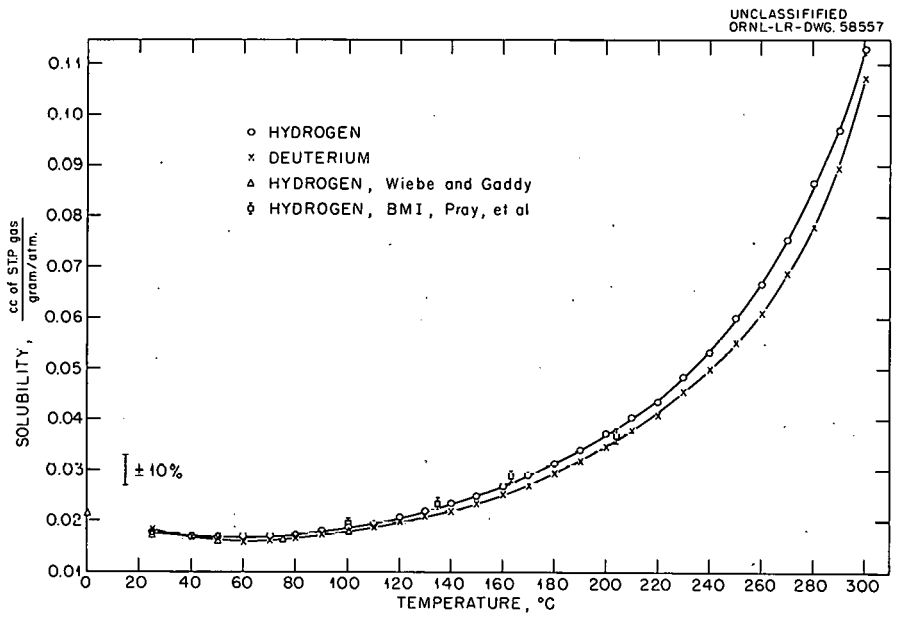

Fig. 6.1. Hydrogen in H_2O and Deuterium in D_2O.

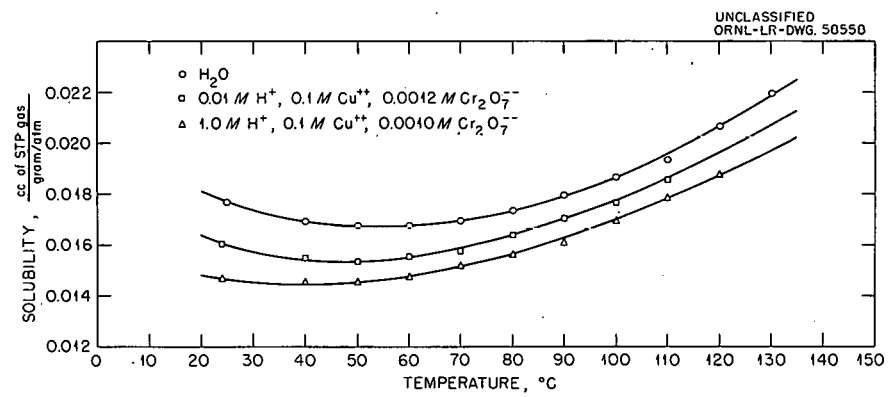

Fig. 6.2. Hydrogen Solubility in Aqueous Perchlorate Solutions and Water.

7. HETEROGENEOUS EQUILIBRIA IN AQUEOUS SYSTEMS

W. L. Marshall

J. S. Gill
E. V. Jones
J. E. Savolainen
R. Slusher

7.1 SOLUBILITY AND NATURE OF THE UO_3 HYDRATES IN THE SYSTEM UO_3-SO_3-H_2O, 150-300°C

In a previous investigation[1] the solubilities of UO_3 hydrates were determined in solutions of SO_3 and H_2O at temperatures between 150 and 290°C and at concentrations of SO_3 from 10^{-3} to 1.0 *m*. In the majority of experiments the concentrations of the saturating component UO_3 and component SO_3 were determined by a method involving the direct measurement at 25°C of the pH of solution samples drawn from the equilibration vessel. Many of the past determinations were repeated in the current investigation, and additional solubilities at 300°C were obtained. Particular attention was directed to the various hydrates of UO_3 and the region of temperature and concentration of SO_3 at which each one was stable. Apparatus used in the experiments and analytical procedures were reported previously.[2] The overall work is incorporated into a paper which will appear shortly.[3]

In one set of experiments the solubilities of UO_3 hydrates were determined at 150, 225, and 300°C in water solutions from 0.001 to 0.1 *m* in total SO_3 (Table 7.1). Mixtures were equilibrated for 16 hr at each temperature before sampling the solution phases. After the solubility determinations at 300°C the solid phases were removed from many of the vessels and identified by x-ray diffraction.

In another set of experiments solubilities of UO_3 hydrates in H_2SO_4-H_2O solutions were determined from liquid-phase samples obtained in less than an hour at 225 and 300°C and after 18 hr at 150, 225, and 300°C (Table 7.1). A pair of vessels was removed after each 18-hr sampling. The solid phases were dried between sheets of filter paper within 10 min after removal from a vessel and were identified by x-ray diffraction within 2 hr after drying. A second pair of vessels was also removed and opened after 30 min at 300°C in order to identify the solid phases after a short length of time.

Saturation molal ratios, $m_{UO_3}:m_{SO_3}$, obtained by extrapolation from 290 to 300°C of previous data[1] for the system UO_3-SO_3-H_2O yielded ratios approximately 10% higher than those reported here. In the present study of the system UO_3-SO_3-H_2O most solution-solid mixtures were rocked at 300°C for a minimum of 16 hr. Previously, although experimental data were reproducible after 15 min at one temperature, an entire run--at several temperatures--was usually finished in 10 hr. The stable solid phase at 300°C in the current investigation was identified as the hemihydrate, $UO_3 \cdot 1/2\ H_2O$, by the use of an accepted x-ray diffraction pattern for this solid.[4] However, in the earlier investigation up to 290°C, UO_3 monohydrate was stated to be the solid phase. In pure water under a saturation vapor pressure the exact temperature for a transition from Dawson's et al. $UO_3 \cdot 1.0\ H_2O$ orthorhombic II phase, in this report designated $\beta UO_3 \cdot H_2O$, to $UO_3 \cdot 1/2\ H_2O$ is in doubt but is reported[4] to be between 280 and 325°C.

Table 7.1. Solubilities at 150, 225, and 300°C of UO_3 Hydrates in H_2SO_4-H_2O Solutions

Time at Temperature (hr)	SO_3 (m)	UO_3 (m)	Ratio $\left(\frac{M, \text{ at } 25°C}{m}\right)$	Solid Phases[a]
	At 150°C (Stable Solid = $\alpha UO_3 \cdot H_2O$)			
16	0.0954	0.1157	0.992	
18	0.0704	0.0834	0.993	A
16	0.0295	0.0345	0.995	
18	0.01589	0.01829	0.996	A + D[b]
16	0.00964	0.01063	0.997	
16	0.00120	0.00119	0.997	
	At 225°C (Stable Solid = $\beta UO_3 \cdot H_2O$)			
16	0.0967	0.1077	0.992	
0.25	0.0677	0.0730	0.993	
18	0.0689	0.0741	0.993	B + A[b]
16	0.0303	0.0307	0.995	
0.25	0.01583	0.01549	0.996	
18	0.01614	0.01590	0.996	B + A[b]
16	0.01039	0.00913	0.997	
16	0.00324	0.00279	0.997	
16	0.00134	0.00098	0.997	
	At 300°C (Stable Solid = $UO_3 \cdot 1/2\ H_2O$)			
16	0.2204[c]	0.2125	0.990	
16	0.1758[c]	0.1731	0.990	
16	0.1248[d]	0.1314	0.992	
16	0.1031	0.1053	0.992	C
16	0.0974	0.0974	0.992	
16	0.0969	0.1000	0.992	
0.50	0.0697	0.0712	0.993	C + B[b] + A[b]
0.50	0.0677	0.0696	0.993	C + B[b] + A[b]
18	0.0736	0.0729	0.993	C
16	0.0491	0.0477	0.995	
16	0.0490	0.0470	0.995	
16	0.0312	0.0284	0.995	C[b]
0.50	0.01584	0.01417	0.996	B[b] + A[b]
0.50	0.01675	0.01450	0.996	B[b] + A[b]
18	0.01691	0.01450	0.996	C
16	0.01208	0.00922	0.997	
16	0.01092	0.00847	0.997	C
16	0.00347	0.00233	0.997	C
16	0.00155	0.00068	0.997	C
16	0.00113	0.00044	0.997	C

[a] Where A = $\alpha UO_3 \cdot H_2O$, B = $\beta UO_3 \cdot H_2O$, C = $UO_3 \cdot 1/2H_2O$, D = $UO_4 \cdot 2H_2O$. Established by comparison of x-ray diffraction patterns.

[b] Metastable solids, decomposing.

[c] Points on ternary 2L curve (no solid phase present).

[d] Isothermal invariant point S + 2L.

In view of the disagreement at 300°C, further solubilities were determined at 150, 225, and 300°C; these are included in Table 7.1 and Fig. 7.1. After 15 min at 150°C, attempts to obtain clear samples of two solution phases, approximately 0.016 and 0.07 *m* in SO_3, produced a lemon-white and a yellow solid suspended in the samples. These solids presumably were a UO_4 hydrate formed upon the addition at 25°C of H_2O_2 and a UO_3 hydrate, respectively. The two vessels containing these solution and solid mixtures were opened after 18 hr at 150°C. Only the yellow solid was found in the vessel containing 0.07 *m* SO_3 solution, but both the yellow solid and a small amount of the lemon-white solid were found in the vessel containing 0.016 *m* SO_3. The x-ray diffraction pattern for the yellow solid was that for Dawson's et al. $UO_3 \cdot 0.8\ H_2O$ orthorhombic I phase,[4] in this report designated $\alpha UO_3 \cdot H_2O$. The pattern for the lemon-white solid was that for $UO_4 \cdot 2H_2O$ identified by Watt et al., found in contact with aqueous solutions above 64°C by Gilpatrick and McDuffie and confirmed by Silverman and Sallach.[5]

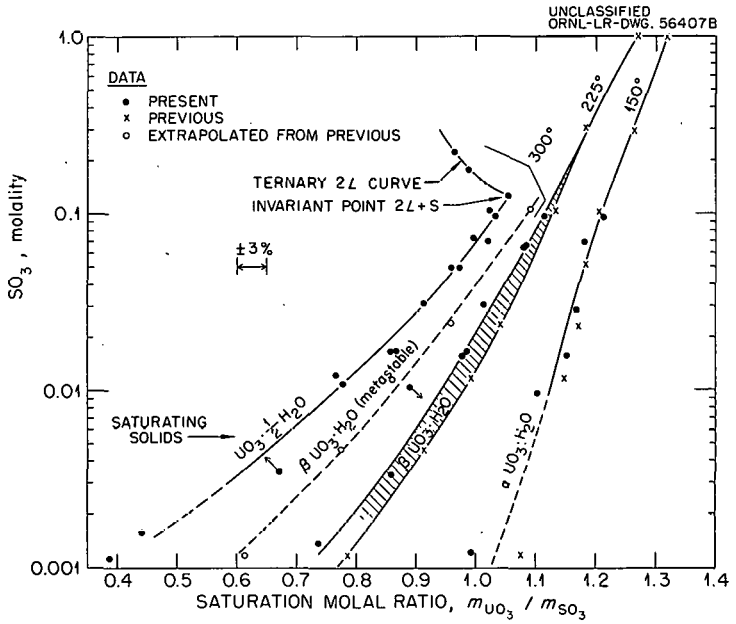

Fig. 7.1. Saturation Molal Ratios at 150, 225, and 300°C for the Solubility of UO_3 Hydrates in H_2SO_4-H_2O Solutions.

Decreased acidity of a solution phase containing dissolved UO_4 will reduce the solubility of UO_4 hydrate and lower its rate of decomposition.[6] The acidity of an SO_3 solution is lowered by saturating it with UO_3;[1] thus the rate of decomposition of dissolved UO_4 is reduced. At the higher temperatures all UO_4 hydrate was decomposed, leaving only the UO_3 hydrates.

Results in Table 7.1 where indicated show that $\alpha UO_3 \cdot H_2O$ is a stable solid phase at 150°C, presumably $\beta UO_3 \cdot H_2O$ at 225°C, and $UO_3 \cdot 1/2\ H_2O$ at 300°C. If at any temperature a metastable solid is present but is converting to the stable solid, the observed solubility should be that for the metastable solid which has the higher solubility. The previous data at 270 and 290°C and the extrapolated data at 300°C (Fig. 7.1) should be those for the solubility of $\beta UO_3 \cdot H_2O$, which at least at 300°C is metastable. In Fig. 7.1 even the previous data at 225°C may represent the solubility of metastable $\alpha UO_3 \cdot H_2O$, while the present data at 225°C are for the solubility of stable $\beta UO_3 \cdot H_2O$. Two curves at this temperature are drawn although there is at most only a 5% difference in molal ratio between the two sets of data. A low heat

of transition between the three solid hydrates of UO_3 may be expected, and therefore it appears that metastability by one or the other could very easily occur in the above range of temperature.

7.2 EFFECT OF HYDROSTATIC PRESSURE ON LIQUID-LIQUID IMMISCIBILITY TEMPERATURES OF A UO_3-SO_3-H_2O SOLUTION AND A UO_3-SO_3-D_2O SOLUTION

In previous investigations[7] on the two-liquid-phase regions of the system UO_2SO_4-$CuSO_4$-H_2SO_4-H_2O, the second liquid phase was observed to occur momentarily at temperatures several degrees below that observed under equilibrium conditions. This phenomenon was first observed in 1957 by J. S. Gill when tubes containing selected compositions of solution were quickly inserted into a liquid-salt bath held 5 or 6°C below the expected temperature (~310°C) for the occurrence of liquid-liquid immiscibility. A second liquid phase would appear momentarily but would disappear immediately upon vibrating a tube. This effect may be considered a negative-pressure effect, which Timmermans tried to find in other systems by experimental means.[8] (The vapor pressure had not increased to the saturation value, and therefore a pressure less than the equilibrium pressure existed momentarily.) Since at 310°C the saturation vapor pressure for these solutions was approximately 97 atm and since the initial pressure could not be less than the saturation vapor pressure at 25°C, the relative effect of hydrostatic pressure on this system was considered to be large. Furthermore, application of a hydrostatic pressure should raise rather than lower the temperature of liquid-liquid immiscibility.

Later, a relatively large effect of pressure on a similar system was shown when a solution volume containing UO_3, SO_3, N_2O_5, and H_2O components expanded in a sealed tube, as the temperature rose, to fill completely the cavity. This occurred 1°C below the expected temperature (near 351°C) for liquid-liquid immiscibility. As the temperature rose further, the volume of liquid phase was constant, and therefore the pressure increased considerably beyond that of saturation vapor. Liquid-liquid immiscibility was not observed.[9] In another set of experiments, the effect of pressure on liquid-liquid immiscibility in the system UO_2SO_4-H_2O and its D_2O analog was observed indirectly and was reported[10] to be greater than approximately +1.9°C/1000 psi but less than +8.7°C/1000 psi.

In the study of the effect of pressure it was desirable to make direct visual observations of the occurrence of liquid-liquid immiscibility as well as quantitative measurements of pressure and temperature. In order to make visual observations, a metal-to-glass connection unit was developed. By means of this connection unit, solutions of UO_3, SO_3, and H_2O were subjected to quantitative, hydrostatic pressures at selected temperatures, and the effect of pressure on liquid-liquid immiscibility was determined. Preliminary results are given in Figs. 7.2 and 7.3 for an H_2O solution 1.4 *m* in UO_2SO_4 and for a D_2O solution 0.6 *m* in UO_3 and 1.0 *m* in SO_3. These easily reproducible results are the first obtained by the visual method. The changes of immiscibility temperature with pressure, $\Delta t/\Delta P$, calculated from the slopes in Figs. 7.2 and 7.3 were +5.42°C/1000 psi for the 1.4 *m* UO_2SO_4 solution and +8.13°C/1000 psi for the solution 0.6 *m* in UO_3 and 1.0 *m* in SO_3. These pressure coefficients are within the limits estimated previously.[10] They are in agreement with our expectations that pressure effects would be large in the vicinity of 300°C and may become very large near the critical temperature of the solutions (i.e., near 374°C, the critical temperature of pure H_2O).

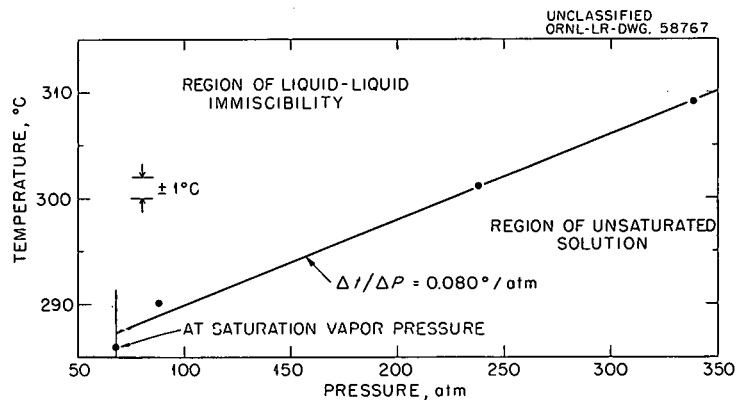

Fig. 7.2. Effect of Hydrostatic Pressure on the Temperature of Liquid-Liquid Immiscibility of a 1.4 *m* UO_2SO_4 in H_2O Solution.

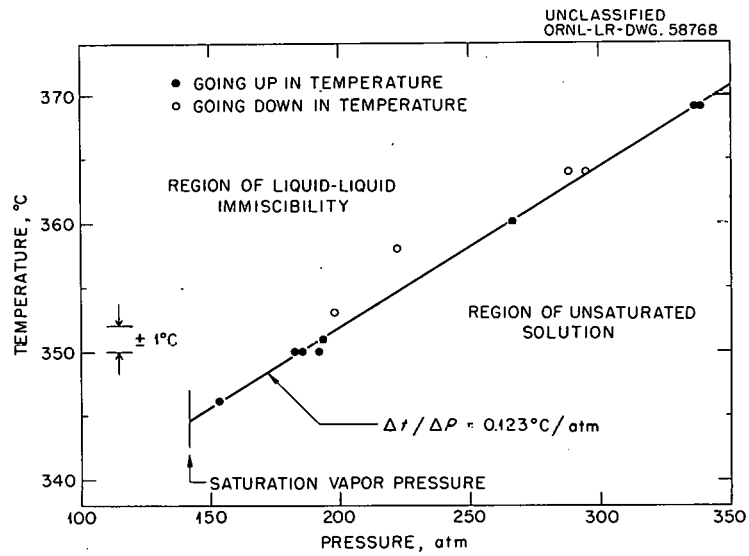

Fig. 7.3. Effect of Hydrostatic Pressure on the Temperature of Liquid-Liquid Immiscibility of a D_2O Solution 0.6 *m* in UO_3 and 1.0 *m* in SO_3.

7.3 CRITICAL PHENOMENA AND LIQUID-LIQUID IMMISCIBILITY IN THE SYSTEMS UO_3-CuO-SO_3-D_2O, UO_3-NiO-SO_3-D_2O, AND UO_3-CuO-NiO-SO_3-D_2O, 280-410°C

The ultimate purpose for the determination of the temperatures of liquid-liquid immiscibility in D_2O systems containing UO_3, CuO, NiO, and SO_3 components is to define limits of stability of aqueous homogeneous reactor fuels over a very wide range of composition. By a systematic approach, empirical equations may be developed to express boundary limits. Later, theoretical equations may be applied to determine thermodynamic values.

Previously, temperatures at which second liquid phases or critical phenomena were observed were reported for the systems UO_3-SO_3-H_2O,[11] UO_3-SO_3-D_2O,[12] CuO-SO_3-D_2O,[13] and UO_3-CuO-SO_3-D_2O; $m_{UO_3}/m_{SO_3} = 1.0$.[14] Temperatures of immiscibility and

critical temperatures (i.e., the temperature at which the meniscus between liquid and vapor disappears) were plotted against the saturation molal ratio, $m_{\text{metal oxide}}:m_{SO_3}$, or the sum of these ratios at various selected concentrations of SO_3. The molalities of SO_3 were varied from 0.02 to 1.0.

These investigations have now been extended to the system UO_3-CuO-SO_3-D_2O at $m_{CuO}:m_{UO_3} = 0.333$, to the system UO_3-NiO-SO_3-D_2O at $m_{NiO}:m_{UO_3} = 1$ and $= 0.333$, and finally to the system UO_3-CuO-NiO-SO_3-D_2O. In the study on the five-component system, values of $m_{CuO}:m_{UO_3}$ and $m_{NiO}:m_{UO_3}$ were held constant at 0.25. All experiments were carried out by the synthetic method described previously.[9]

The results for the various systems are shown in Figs. 7.4 through 7.7, plotted as the summation of the molal ratios, $\Sigma(m_{\text{metal oxide}}:m_{SO_3})$, against either the observed critical temperature or the temperature of liquid-liquid immiscibility. The curves for each system are similar and also correspond to the curves presented previously for the other systems.[11-14] In all cases very large concentrations of metal oxide components were observed in the supercritical fluids.

The systems which contained an NiO component gave results which were not as precise as those from systems not containing NiO. These variations may be related

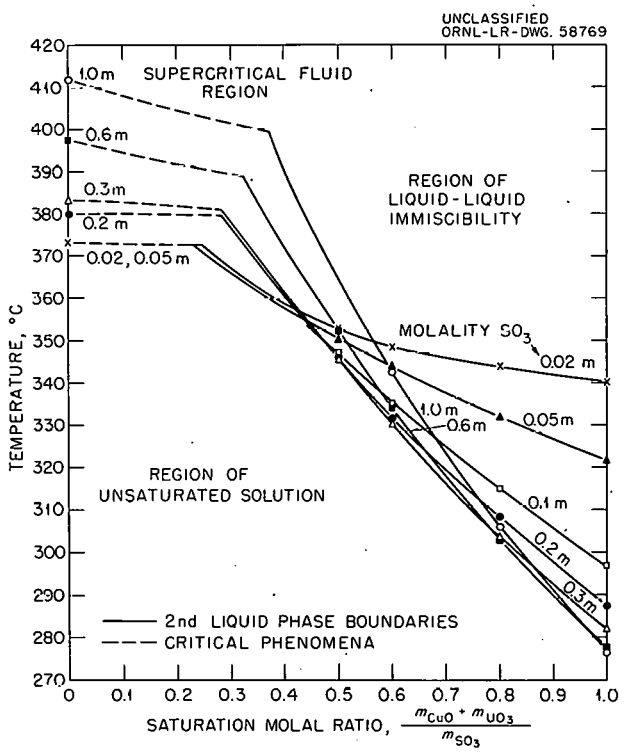

Fig. 7.4. Temperatures of Liquid-Liquid Immiscibility in the System UO_3-CuO-SO_3-D_2O; $m_{CuO}:m_{UO_3} = 0.333$.

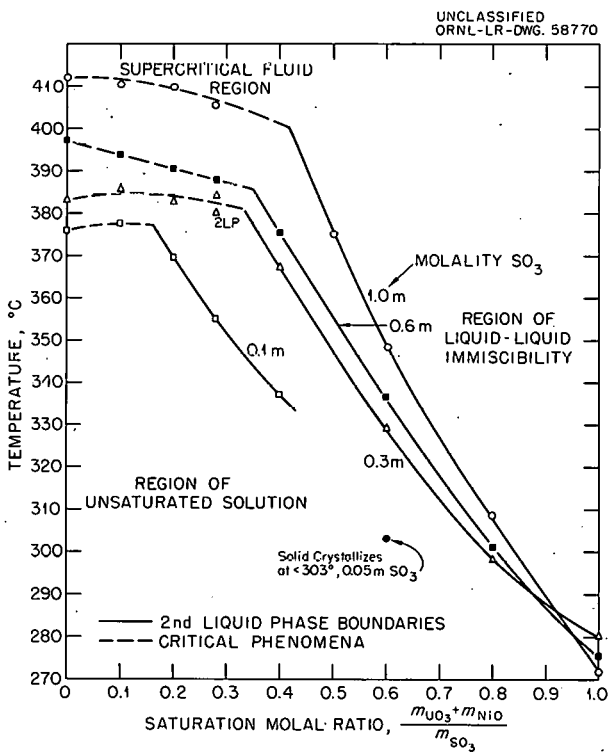

Fig. 7.5. Critical Phenomena and Temperatures of Liquid-Liquid Immiscibility in the System UO_3-NiO-SO_3-D_2O; $m_{NiO}:m_{UO_3} = 1.00$.

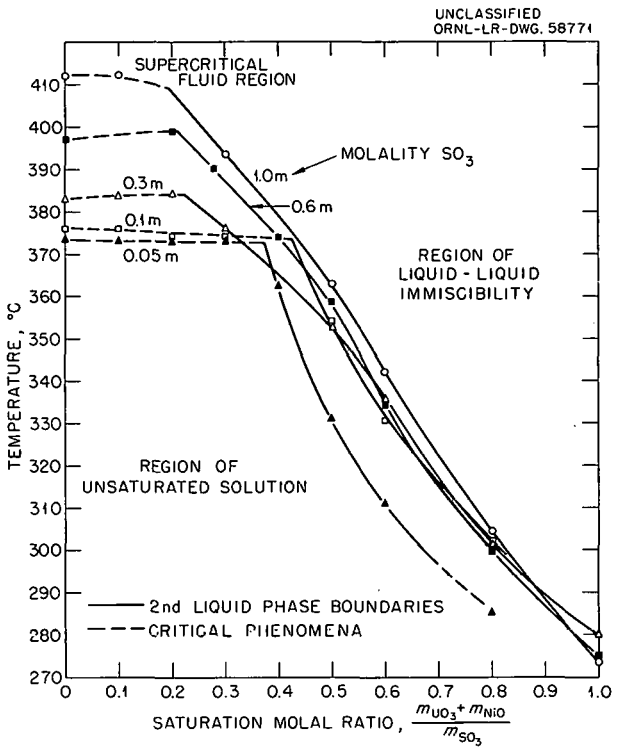

Fig. 7.6. Critical Phenomena and Temperatures of Liquid-Liquid Immiscibility in the System UO_3-NiO-SO_3-D_2O; $m_{NiO}:m_{UO_3} = 0.333$.

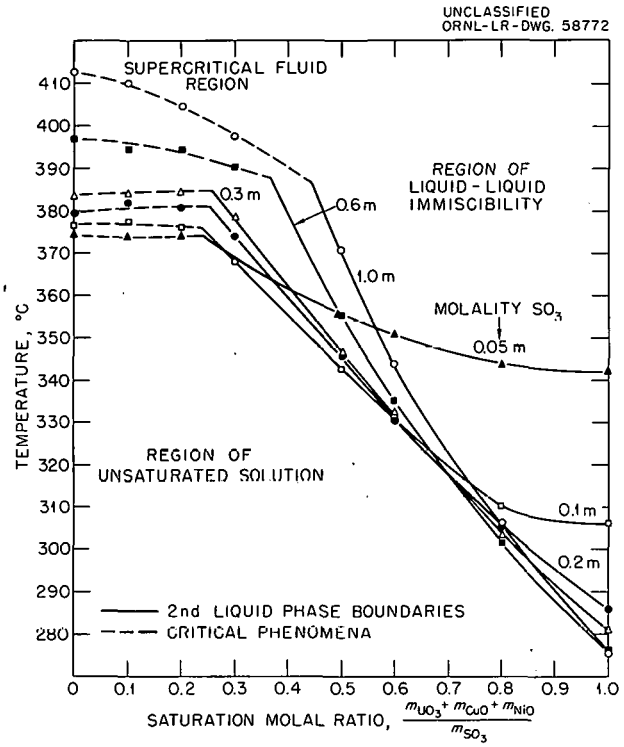

Fig. 7.7. Critical Phenomena and Temperatures of Liquid-Liquid Immiscibility in the System UO_3-CuO-NiO-SO_3-D_2O; $m_{CuO}:m_{UO_3} = m_{NiO}:m_{UO_3} = 0.250$.

to the fact that the system NiO-SO_3-H_2O was not found to show a region of liquid-liquid immiscibility under saturation vapor pressures.[15] Furthermore, variations in composition were found in other investigations of systems containing an NiO component.[16]

Upon completion of these investigations, volume models may be constructed from the data to show limits of composition and temperature for aqueous homogeneous reactor fuels.

7.4 SOLUBILITY OF UO_3 IN SUPERCRITICAL FLUIDS ABOVE 374°C

The observations that high concentrations of UO_3, as well as other metal oxide components, are soluble in a supercritical fluid of SO_3 and H_2O--a gaseous mixture in all respects--open a new region for exploration. This region of temperature and composition extends from approximately 374°C, the critical temperature of H_2O, to the vicinity of 800°C and encompasses metal oxides showing moderate solubilities in systems containing three or more components. In Fig. 7.8 is a compilation of the majority of solubilities for systems of stoichiometric salts in H_2O (two components) above 200°C. These were compiled in 1959[17] and do not include investigations at ORNL or investigations by geochemists of solubilities in the range of parts per million to several weight per cent. It is evident that very little information exists above 374°C. With sufficient study above this temperature, regions of stability may be defined for solutions containing UO_3 and other components. Fuel compositions could then be specified which would be stable at 25°C, as well as at temperatures considerably above 374°C. The continuing, fundamental aspect of the phase-equilibria program will lie in this direction.

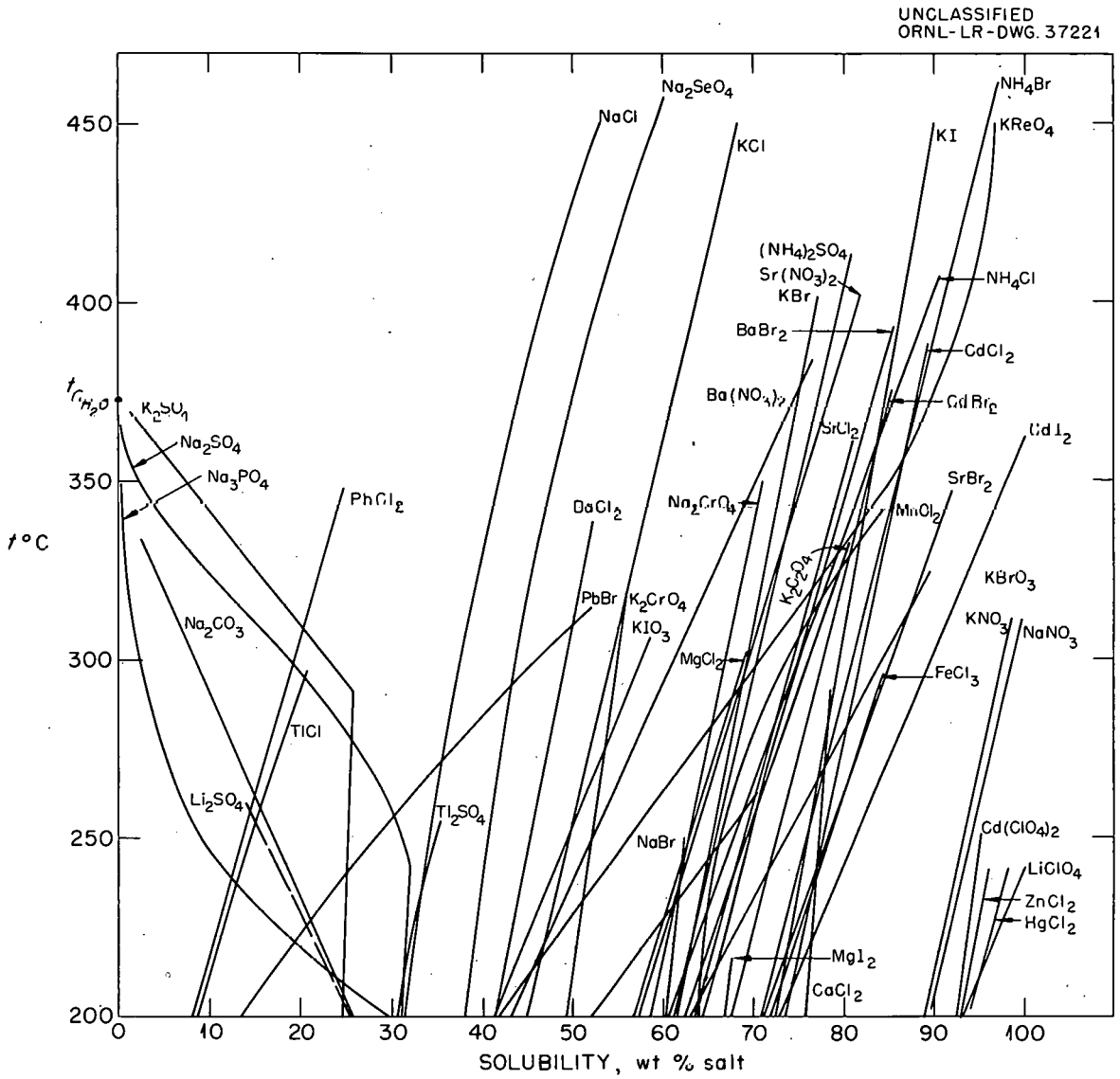

Fig. 7.8. Compilation of the Majority of Salt Solubilities in Two-Component H_2O Systems Above 200°C (Exclusive of ORNL Data and of Salts Showing Very Low Solubilities). Compiled by W. L. Marshall, 1959.

7.5 SOLUBILITY OF ThO_2 IN SOLUTIONS OF HNO_3 AND H_2O AT 150 AND 200°C

Solutions of ThO_2 in DNO_3 and D_2O have long been considered[18] as media for the breeding of U^{233} from Th^{232}. Some experimental programs were re-initiated in view of the potentiality for large-scale production of low-cross-section N^{15} (ref 19) and the possibility that radiolytic N_2 and O_2 may be recombined economically by commercial processes.[20] M. J. Kelly et al.[21] have been investigating processes for removal of the intermediate protactinium before this product absorbs further neutrons to be converted to nonfissionable Pa^{234}. In view of the success of their program, additional solubilities of ThO_2 in HNO_3-H_2O were determined at 150 and 200°C. These data are supplementary to those reported previously[22] at 200 and 300°C. Experimental and analytical procedures were the same.

The over-all results are given in Table 7.2. Solubilities of ThO_2 determined after the longest intervals of time at the respective equilibration temperatures are shown in Fig. 7.9. The current values at 200°C are in good agreement with those obtained previously using ThO_2 fired at 650°C (ORNL Pilot Plant batch No. DT-58-650). The earlier values, as well as those obtained previously at 300°C using the same ThO_2 product, are included in Fig. 7.9. Inspection and comparison of the results in Table 7.2 with the previous values show a moderately fast rate

Table 7.2. Solubility of ThO_2 in HNO_3-H_2O Solutions at 150 and 200°C

(Initial Mixtures: ThO_2 Fired at 650°C + HNO_3-H_2O Solutions)

Temperature (°C)	Rocking Time (hr)	HNO_3 (M)	Molal Ratio, ThO_2/HNO_3
150	23	2.442	0.177
		0.941	0.105
		0.448	0.076
		0.224	0.018
		0.057	<0.0003*
200	65	9.740	0.243
		4.864	0.226
		2.442	0.187
		0.930	0.098
		0.441	0.024
		0.201	0.001
		0.060	<0.00028*

*ThO_2 less than 1.7×10^{-5} m.

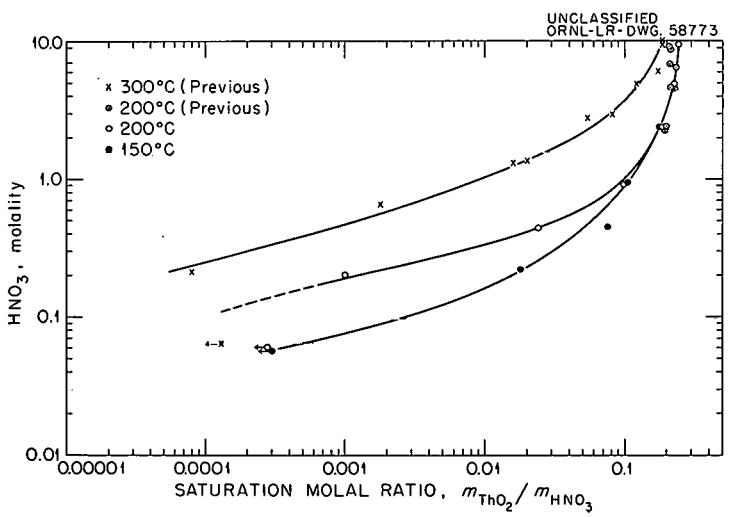

Fig. 7.9. Solubility of ThO_2 in HNO_3-H_2O Solutions at 150, 200, and 300°C.

of dissolution of refractory ThO_2 in HNO_3-H_2O solution at 150 as well as 200 and 300°C. This constitutes further evidence that aqueous solutions of HNO_3 at temperatures between 150 and 300°C may be useful for dissolving refractory ThO_2 in chemical processing.

REFERENCES

1. W. L. Marshall, Anal. Chem. 27, 1923 (1955).

2. W. L. Marshall and J. S. Gill, Investigation of the System UO_3-CuO-NiO-SO_3-H_2O at 300°C, ORNL CF-59-12-60, Rev. 1.

3. W. L. Marshall and J. S. Gill, "Aqueous Systems at High Temperature. III. Investigations on the System UO_3-CuO-NiO-SO_3-H_2O at 300°C," in press, Journal of Inorganic and Nuclear Chemistry (1961).

4. J. K. Dawson, E. Wait, K. Alcock, and D. R. Chilton, J. Chem. Soc. 1956, 3531.

5. G. W. Watt, S. L. Achorn, and J. L. Marley, J. Am. Chem. Soc. 72, 3341 (1950); L. O. Gilpatrick and H. F. McDuffie, ORNL-2931, p 125 (Apr. 29, 1960), Office of Technical Services, Dept. of Commerce, Washington, D. C.; L. Silverman and R. A. Sallach, J. Phys. Chem. 65, 370 (1961).

6. M. D. Silverman, G. M. Watson, and H. F. McDuffie, Ind. Eng. Chem. 48, 1238 (1956).

7. F. E. Clark et al., J. Chem. Engr. Data 4, 12 (1959).

8. J. Timmermans and J. Lewin, Disc. Faraday Soc. 15, 195 (1953).

9. C. J. Barton, G. M. Hebert, and W. L. Marshall, Liquid-Liquid Immiscibility Above 300°C in the System UO_3-SO_3-N_2O_5-H_2O, ORNL CF-59-11-64 (Nov. 17, 1959); also "Aqueous Systems at High Temperature. II. Liquid-Liquid Immiscibility Above 300°C in the System UO_3-SO_3-N_2O_5-H_2O," in press, Journal of Inorganic and Nuclear Chemistry (1961).

10. W. L. Marshall and J. S. Gill, HRP Quar. Prog. Rep. Jan. 31, 1960, ORNL-2920, p 70-71.

11. W. L. Marshall and G. M. Hebert, Reactor Chemistry Div. Ann. Prog. Rep. Jan. 31, 1960, ORNL-2931, p 100-103.

12. E. V. Jones and W. L. Marshall, HRP Quar. Prog. Rep. July 31, 1960, ORNL-3004, p 49.

13. W. L. Marshall and F. Smith, HRP Quar. Prog. Rep. Nov. 30, 1960, ORNL-3061, p 54.

14. E. V. Jones and W. L. Marshall, HRP Quar. Prog. Rep. July 31, 1960, ORNL-3004, p 53.

15. W. L. Marshall and F. Smith, HRP Quar. Prog. Rep. July 31, 1960, ORNL-3004, p 49-51.

16. E. V. Jones and W. L. Marshall, "Aqueous Systems at High Temperature. V. Distribution of CuO and NiO Components in the System UO_3-SO_3-H_2O and its D_2O Analog, 300-350°C," submitted for publication in the Journal of Inorganic and Nuclear Chemistry (1961).

17. W. L. Marshall, "Aqueous Solubility Equilibria, 200 to 374°C," presented at the 135th National Meeting of the American Chemical Society, Boston, Mass. (April 1959).

18. H. F. McDuffie, "Properties of Aqueous Fuel Solutions," Fluid Fuel Reactors, chap. 3, J. A. Lane, H. G. MacPherson, and F. Maslin (eds.), Addison-Wesley, Reading, Mass., 1958.

19. J. S. Drury, Results of Pilot Plant Production of N-15, Oak Ridge National Laboratory (1957-Present).

20. Conferences between P. H. Emmett, Johns Hopkins University, and H. F. McDuffie et al., Reactor Chemistry Division, Oak Ridge National Laboratory (1960).

21. M. J. Kelly et al., HRP Prog. Rep. Nov. 30, 1960, ORNL-3061, p 43-47.

22. W. L. Marshall and R. Slusher, HRP Quar. Prog. Rep. July 31, 1960, ORNL-3004, p 51-54.

8. SOLUTION CORROSION

J. C. Griess H. C. Savage
J. M. Baker

8.1 CHEMICAL EQUILIBRIA AND CORROSION IN HIGH-TEMPERATURE URANYL SULFATE SOLUTIONS

A small, high-pressure titanium loop, previously described,[1] was used to demonstrate the chemical stability of a dilute uranyl sulfate solution containing copper sulfate and sulfuric acid at 360°C and to determine the corrosion resistance of titanium and Zircaloy-2 in such a solution. The room-temperature composition of the heavy-water solution was 0.085 *M* UO_2SO_4, 0.020 *M* $CuSO_4$, and 0.245 *M* D_2SO_4. At 365°C, the solution contained about 10 g of uranium per liter. It was reported by McDuffie[2] that the solution was chemically stable to at least 365°C and that the copper concentration would be adequate to recombine the radiolytic gas at a power density of 50 kw/liter at this temperature.

Specimens of titanium-75A and Zircaloy-2 were exposed to the flowing solution. The titanium specimens were machined from an annealed plate, and the Zircaloy-2 specimens were cut from a welded plate in such a manner that the specimens were composed almost entirely of weld metal. These same specimens had been exposed to a less-concentrated uranyl sulfate solution containing less acid for 157 hr. The corrosion rates were negligible during this period.[1]

The solution was circulated for 553 hr at 360°C in the main loop and 365°C in the pressurizer. During this time several samples were withdrawn from the main circulating line and from the underflow pot of a hydroclone. Within the precision of the chemical analyses, no changes in chemical composition of the solution were observed. Toward the end of the run a small amount of a white solid was found in the samples removed from the underflow pot of the hydroclone. Spectrographic analysis showed the material to contain mostly aluminum, which originated from the aluminum oxide bearings used in the pump, and a small amount of zirconium.

On heating up the loop and while the loop was operating, samples of the vapor above the solution in the pressurizer were withdrawn, condensed, and analyzed. Table 8.1 shows the concentration of the condensate collected at various temperatures.

The second and third columns represent the actual analytically determined concentrations in the condensate. The fourth column represents the net sulfate concentration (presumably as H_2SO_4). This figure was obtained by assuming that all the uranium in the condensate samples got there by entrainment of solution in the vapor and carried with it sulfate in the same ratio in which it was present in the solution and then subtracting this amount of sulfate from the total. While these data are not highly accurate, they do show that sulfuric acid (and possibly uranium at the higher temperatures) will be present in the vapor above highly acidified uranyl sulfate solutions at temperatures much above 300°C.

The corrosion rates observed on the Zircaloy-2 specimens during the run are shown in Table 8.2. The titanium specimens developed thin black-blue films and showed essentially negligible weight changes except for the lead coupon which corroded at a rate of 0.4 mpy. The Zircaloy-2 specimens were white to gray in color

and showed significant corrosion rates independent of flow rate. The Zircaloy-2 holder in which the specimens were held had a similar appearance, indicating that there was no difference in behavior between weld metal (specimens) and wrought material (holder).

Table 8.1. Concentrations of Uranium and Sulfate in the Vapor Above a Uranyl Sulfate Solution

Pressurizer Temperature (°C)	U Concentration (ppm)	SO_4 (ppm)	Corrected Sulfate (ppm)
300	8.2	12.2	(-1.5)
320	5.8	18.3	8.6
340	5.1	45.7	37
360	9.2	228	210
365	16.7	365	340
365	323	1010	470
365	30	610	550

Table 8.2. Corrosion of Zircaloy-2 Specimens in a Uranyl Sulfate Solution* at 360°C

Velocity Range (fps)	Weight Loss (mg/cm^2)	Corrosion Rate (mpy)
7.4 - 8.6	8.4	8.1
8.6 - 11	7.9	7.6
11 - 13	9.3	8.9
13 - 17	8.2	7.9
17 - 24	9.2	8.8
24 - 31	8.6	8.3
31 - 39	8.4	8.1
39 - 22	9.8	9.4
22 - 15	8.5	8.2
15 - 12	8.4	8.1
12 - 9.3	9.2	8.8
9.3 - 7.6	8.1	7.8

*The room-temperature concentration of the heavy-water solution was 0.085 *M* UO_2SO_4, 0.020 *M* $CuSO_4$, and 0.245 *M* D_2SO_4.

The run was terminated by failure of the pump, which resulted from excessive corrosion of the front aluminum oxide bearing by the relatively concentrated sulfuric acid solution. An autoclave test with a portion of the bearing showed that at 200°C the aluminum oxide corroded at a rate of 150 mpy during a 500-hr test.

Except for the aluminum oxide and the Zircaloy-2, corrosion of the system was immeasurably small. However, before additional tests in the high-acid system can be run, a suitable pump bearing material must be found.

REFERENCES

1. J. C. Griess, H. C. Savage, et al., HRP Prog. Rep. Aug. 1 - Nov. 30, 1960, ORNL-3061, p 61-63.

2. H. F. McDuffie, private communication, Oct. 31, 1960.

9. RADIATION CORROSION

G. H. Jenks H. C. Savage

A. L. Bacarella T. H. Mauney
R. J. Davis

9.1 AUTOCLAVE TESTS

One in-pile autoclave (L5Z-141) was assembled and operated during the report period. The experiment was designed primarily to provide information on the radiation corrosion of Zircaloy-2 by a uranyl sulfate fuel solution at temperatures to 360°C. This objective was not achieved because a leak caused termination of the in-pile exposure before any 360°C operation. However, data of interest were obtained, and they are summarized here. These include: out-of-pile corrosion at 360°C, surface sorption of uranium during out-of-pile exposure, and radiolytic-gas recombination during in-pile exposure. A duplicate experiment is planned to accomplish the 360°C in-pile exposure.

The autoclave was fabricated of Zircaloy-2 and contained five Zircaloy-2 corrosion test specimens. A solution of 0.08 *m* UO_2SO_4, 0.02 *m* $CuSO_4$, and 0.24 *m* D_2SO_4 in D_2O was charged to the autoclave, and an oxygen gas overpressure was used. The excess acid was required[1] to maintain the chemical stability of the solution at 360°C.

Before operation in-pile, the autoclave was operated at 360°C for 350 hr out-of-pile to obtain corrosion data for comparison with that observed under irradiation. After 124 hr at 360°C, the autoclave was opened and the amount of uranium sorption in the surface film on the test specimens was determined by alpha counting.

The in-pile tests completed were concerned with a determination of the activity of the copper catalyst for recombination of radiolytic gas. Recombination rates at temperatures of 230, 250, and 280°C were obtained, after which a leak in the autoclave caused termination of the experiment.

9.1.1 Out-of-Pile Corrosion

The average over-all penetration of the Zircaloy-2 during 350 hr at 360°C was 0.07 to 0.08 mil. For the last 300 hr, the corrosion rate was about 1.5 mpy, based on oxygen uptake. This rate is in line with an extrapolation of rates observed for Zircaloy-2 in a previous autoclave experiment[2] with uranyl sulfate solution at 290°C. However, the rate is considerably below the 8 mpy obtained on Zircaloy-2 weld metal with a similar solution in a pump-loop test (see Chap. 8).

9.1.2 Uranium Sorption on Specimen Surfaces

After 124 hr of operation at 360°C (out-of-pile) the quantity of uranium sorbed on the water-washed Zircaloy-2 specimen surfaces averaged 0.24 $\mu g/cm^2$. Values obtained for the ten surfaces (two sides of five specimens) ranged between 0.19 and 0.29 $\mu g/cm^2$. These values are small compared to a few tens of micrograms per square centimeter previously found[3,4] on specimens irradiated with solutions containing about one-tenth as much excess acid as that in this test. Correlation of the in-pile corrosion data[5] and out-of-pile tests of uranium sorption on hydrous zirconia[6]

also indicate marked reduction of uranium sorption with increased excess-acid concentration.

9.1.3 Rates of Recombination of Radiolytic Gas

Recombination rate constants as a function of temperature for the copper-catalyzed recombination of radiolytic gas were estimated by analyses of the rate of pressure increase following initiation of irradiation. The values obtained at 230, 250, and 280°C are shown in Fig. 9.1. The analysis does not require a knowledge of G_{D_2}, but does include the solubility of D_2. Values employed for D_2 solubility were 0.454, 0.377, and 0.283 psi cc^{-1} liter (volumes at STP) at 230, 250, and 280°C, respectively.

The values in Fig. 9.1 are lower by about one-third to one-half than those predicted for uranyl sulfate solutions (D_2O solvent) with lower acid concentrations.[7-10] Thus it appears that the results are in agreement with rates obtained in other tests, which indicate a decrease in K_{Cu} with increased excess-acid concentrations.[10,11]

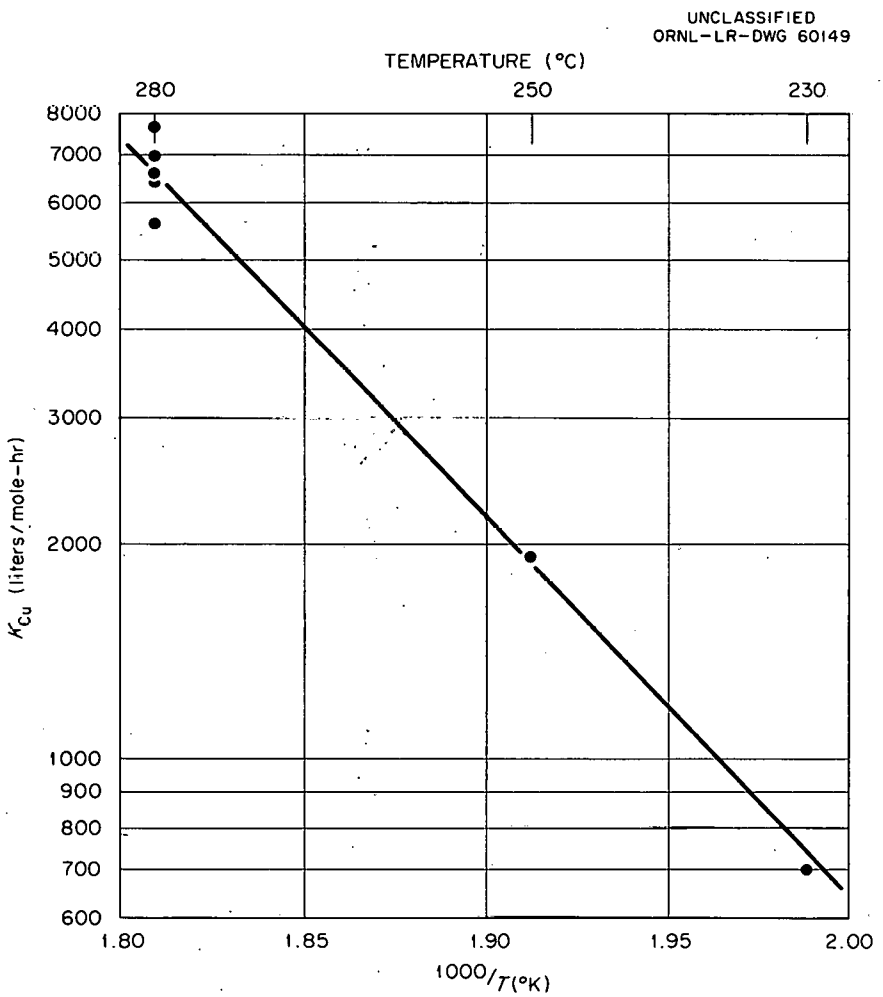

Fig. 9.1. K_{Cu} Values in 0.08 *m* UO_2SO_4, 0.24 *m* Excess D_2SO_4, D_2O Solution.

9.2 ELECTROCHEMICAL STUDIES OF ZIRCALOY-2 CORROSION

A previous report[12] mentioned the difficulties which arose when the electrochemical measurements of Zircaloy-2 corrosion were extended to temperatures above 250°C. White oxide formed near and on a welded section of the small quartz-tube-insulated lead wire, and it was then assumed that this portion of the Zircaloy-2 test specimen corroded at an accelerated rate and that the measured rate after long exposure times could be due entirely to corrosion at this area. The white oxide formation has subsequently been shown to occur on unwelded lead wires and is now believed to result from oxygen depletion in the thin layer of solution between wire and quartz tube. It was hoped that a modification of the apparatus to allow solution flow past the portion of the specimen where the accelerated attack occurred would result in more uniform corrosion.

Such a modification was made, and an experiment was performed in the temperature range 150 to 300°C with Zircaloy-2 in the usual oxygenated 0.05 *m* H_2SO_4 solution. In addition to the type of measurements previously reported,[12] some constant-potential measurements were made after the rate leveled off at the initial temperature of 293°C. These measurements were made with a potentiostat, an instrument which automatically maintains the potential of a test electrode (cathode) at a chosen constant value with respect to a reference electrode. The net current necessary to maintain the potential constant is measured by recording the voltage drop across precision resistors. The reference electrode was a platinum wire in oxygenated 0.05 *m* H_2SO_4 at about 30°C which was bridged into the autoclave cell containing the Zircaloy-2 test electrode. The potential of the reference was constant and independent of the temperature (150 to 300°C) of the autoclave.

After the experiment was terminated, an examination of the specimen again revealed white-oxide attack at the same area of the test specimen. It is believed that the modification did not correct for the flow difficulty, and another change in design in which the quartz tube is eliminated has been made for the next experiment.

Although the rate-time measurements could not be mechanistically interpreted or related to a uniformly corroding specimen, they are nevertheless valid rate measurements for the over-all specimen, and the results of the measurements are summarized here.

Posey[13] has derived several expressions for the effect of temperature in electrode kinetics. One expression for the simple case of one anodic and one cathodic process occurring at an electrode interface can be modified to give:

$$J_p = (J_a - J_c) = K_a' \exp - \left(\frac{\Delta H_a^{o\ddagger} - (\alpha\lambda)_a F\Delta\phi}{RT} \right) - K_c' \exp - \left(\frac{\Delta H_c^{o\ddagger} + (\alpha\lambda)_c F\Delta\phi}{RT} \right). \quad (1)$$

Here J_p is the net current, the K's contain the potential and temperature-independent portions of the specific rate constants of partial processes and the concentration of reactants, and $\Delta H_a^{o\ddagger}$ and $\Delta H_c^{o\ddagger}$ are the (standard) enthalpies of activation of the anodic and cathodic partial processes, respectively. The $(\alpha\lambda)$'s and $\Delta\phi$ have the usual meaning: $(\alpha\lambda)$ the electrochemical transfer coefficient for the anodic or cathodic reaction, and $\Delta\phi$ the electrode-solution potential difference.

In Figs. 9.2 and 9.3 the measured currents are plotted as a function of temperature for various fixed potentials. The general interpretations of these data, based on the relationships shown in Eq. (1), are the following: At the

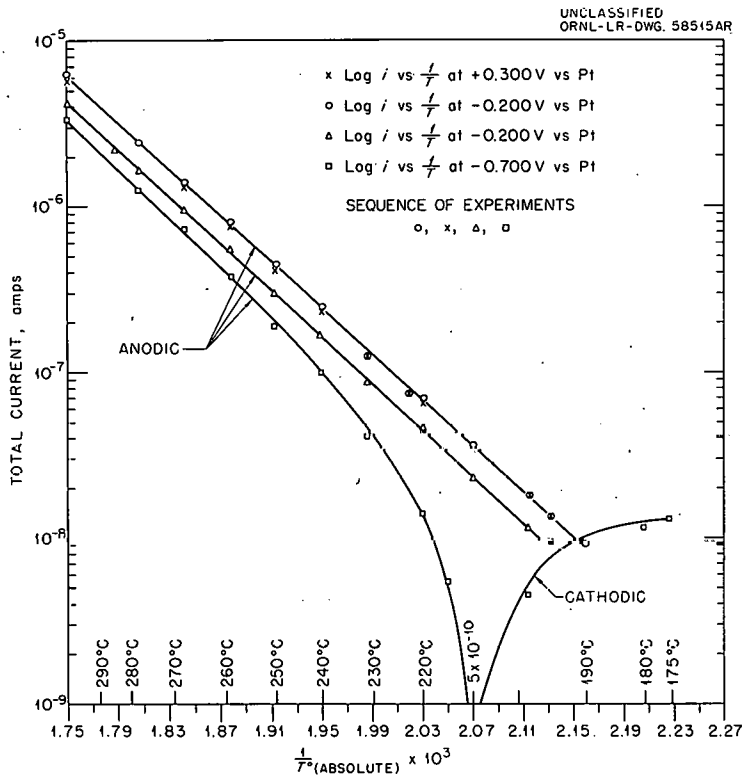

Fig. 9.2. Logarithm of Current vs Reciprocal of Temperature for Passivated Zircaloy-2 in Oxygenated 0.05 *m* H_2SO_4 at Various Fixed Potentials.

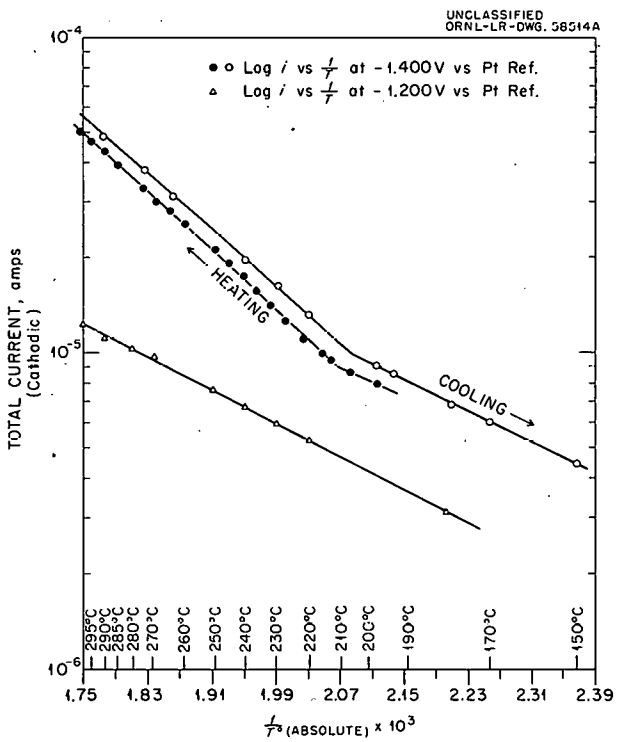

Fig. 9.3. Logarithm of Current vs Reciprocal of Temperature for Passivated Zircaloy-2 in Oxygenated 0.05 *m* H_2SO_4 at Various Fixed Potentials.

more anodic potentials ($\Delta\phi$ more positive), the contribution of the cathodic current to the measured net current becomes negligible, and similarly at the more cathodic potentials ($\Delta\phi$ more negative), the contribution of the anodic current to the measured net current becomes negligible. At intermediate potentials, for example, -0.700 v to Pt, Fig. 9.2, the contribution of the cathodic current to the total measured net current is negligible from 300 to 240°C, but at lower temperatures the cathodic current becomes more and more significant, and at 212°C the anodic and cathodic currents are equal and $J_p = 5 \times 10^{-10}$ amp, or nearly zero. At still lower temperatures the measured net current reverses sign, becoming more cathodic as the temperature is further decreased. At potentials between -0.700 to -1.200 v to Pt, the measured net current is a complicated function of temperature and is probably explained by contributions from two or more of the factors entering into Eq. (1).

It was found that the activation energy for the anodic reaction (oxidation of zirconium) is 31.1 kcal/mole, and is independent of potential and temperature. The activation energy for the cathodic reaction (reduction of oxygen) is, however, a function of potential and temperature, 10.8 kcal/mole at -1.400 v to Pt and between 220 and 300°C, changing to 5.4 kcal/mole at temperatures below 220°C. At -1.200 v to Pt the activation energy is 5.4 kcal/mole over the entire temperature range, 180 to 300°C.

As experimental data, the temperature dependence of the anodic and cathodic currents are remarkably reproducible. For the anodic currents the measured values are identical with both heating and cooling at all potentials. Furthermore, the rate at which the temperature was changed was not uniform; certain temperatures were maintained for periods of 30 min, while some others were obtained in passing at rates of about a degree per minute. On the cathodic side at -1.400 v to Pt, Fig. 9.3, there was some small difference in the measured currents on heating versus cooling; the slopes, however, were the same.

Figure 9.4 further demonstrates the self-consistency and reproducibility of the data. Here the current-potential behavior was determined at two fixed temperatures, 299 and 260°C, each of which was maintained for several days during the measurements. At 260°C on the cathodic side two determinations of the current-potential relationships were made; in one (+) the potential was varied and the currents were measured, and in the other (O) the current was varied and the potentials were measured.

Table 9.1 summarizes the experimental agreement between the several types of measurements.

A more complete analysis of the data will be presented upon completion of further experiments with the modified apparatus.

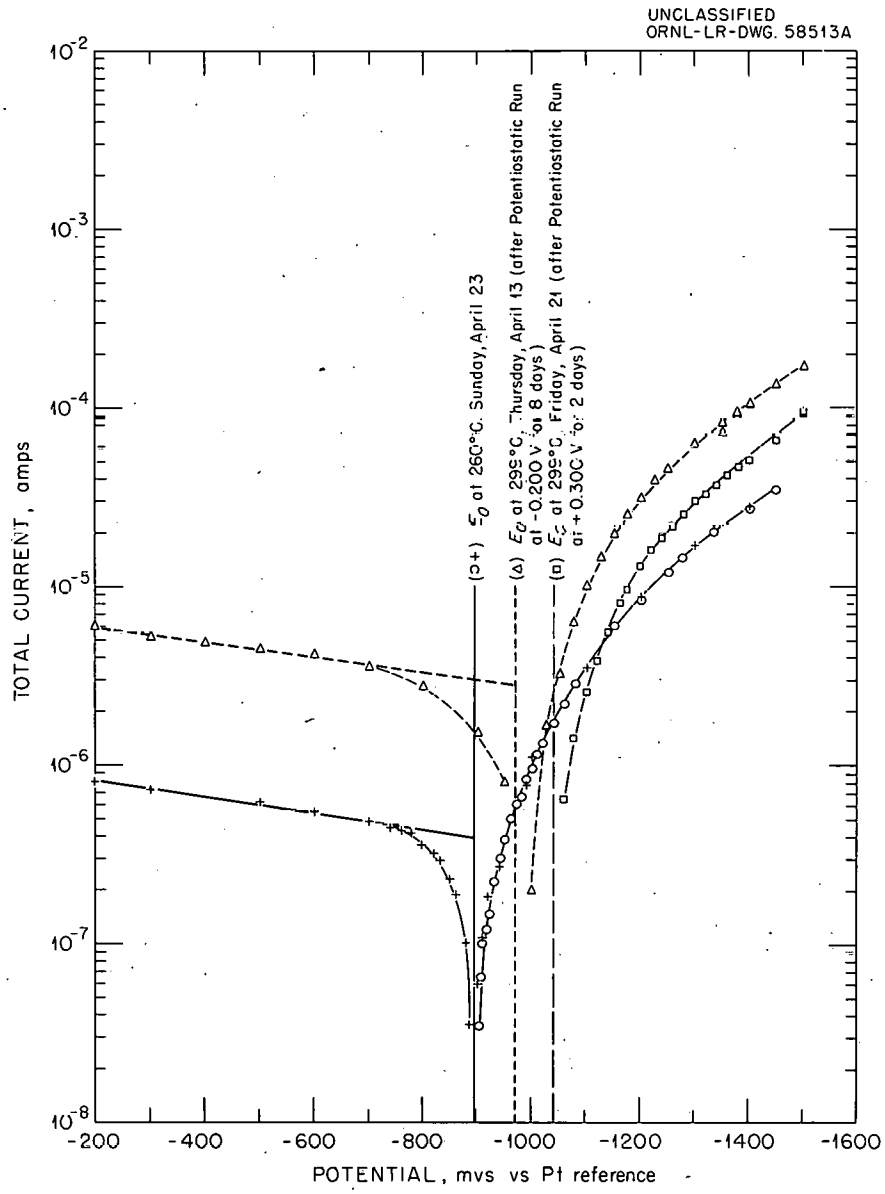

Fig. 9.4. Logarithm of Current vs Potential for Passivated Zircaloy-2 in Oxygenated 0.05 *m* H_2SO_4 at Various Fixed Temperatures

Table 9.1. Comparison Between Galvanostatic and Potentiostatic Results

Temperature (°C)	Potential vs Pt (v)	Total Current (amp) Galvanostatic[a]	Potentiostatic[b]
299	-0.200	4.8×10^{-6} (estimated)	4.2×10^{-6}
260	-0.200	8.0×10^{-7}	6.0×10^{-7}
299	-0.700	3.1×10^{-6} (estimated)	3.5×10^{-6}
260	-0.700	4.8×10^{-7}	4.1×10^{-7}
299	-1.200	1.3×10^{-5}	1.2×10^{-5}
260	-1.200	8.5×10^{-6}	8.5×10^{-6}
299	-1.400	5.2×10^{-5}	5.2×10^{-5}
260	-1.400	2.7×10^{-5}	2.6×10^{-5}

[a]Galvanostatic results are obtained from data presented in Fig. 9.4.

[b]Potentiostatic results are obtained from data presented in Figs. 9.2 and 9.3.

REFERENCES

1. W. L. Marshall et al., HRP Prog. Rep. Nov. 30, 1960, ORNL-3061, p 53.
2. G. H. Jenks, Effect of Radiation on the Corrosion of Zircaloy-2, ORNL CF-57-9-11 (Sept. 30, 1957), p 14.
3. G. H. Jenks et al., HRP Quar. Prog. Rep. Jan. 31, 1958, ORNL-2493, p 125.
4. G. H. Jenks et al., HRP Quar. Prog. Rep. Apr. 30, 1959, ORNL-2743, p 162.
5. G. H. Jenks, Review and Correlation of In-Pile Zircaloy-2 Corrosion Data and a Model for the Effect of Irradiation, ORNL-3039 (in press).
6. R. J. Davis et al., unpublished work.
7. R. J. Davis et al., Summary and Discussion of Results of Twenty-Four Zircaloy-2 HRP In-Pile Corrosion Test Autoclaves (in preparation).
8. M. J. Kelly et al., The Effectiveness of Cupric Ion as a Homogeneous Catalyst in the UO_3-HNO_3-H_2O Systems for the Recombination of Hydrogen and Oxygen Produced by Radiolytic Decomposition, ORNL CF-59-9-15 (Sept. 3, 1959).
9. G. H. Jenks and J. E. Baker, Apparent Copper Rate Constants in In-Pile Loop Experiment L-2-22, ORNL CF-60-3-88 (Mar. 23, 1960).
10. M. J. Kelly et al., HRP Prog. Rep. Oct. 31, 1959, ORNL-2879, p 94.

11. H. F. McDuffie et al., The Radiation Chemistry of Homogeneous Reactor Systems. III. Homogeneous Catalysis of the Hydrogen-Oxygen Reaction, ORNL CF-54-1-122 (Jan. 26, 1954), p 32.

12. G. H. Jenks et al., HRP Quar. Prog. Rep. July 31, 1960, ORNL-3004, p 75-77.

13. F. A. Posey, private communication.

PART IV. SLURRY FUELS

10. THORIUM OXIDE IRRADIATIONS

J. P. McBride
S. D. Clinton W. L. Pattison

10.1 THORIA-PELLET IRRADIATIONS

10.1.1 Previous Pellet Irradiations

The black vitreous material formed on irradiation in D_2O of 1750°C-fired alumina-coated (0.5 wt % aluminum) thoria pellets[1] was identified spectrographically as carbonaceous. Approximately 1 wt % of the total solids recovered had a density of 1.18 g/cc and was >76% volatile. It contained 0.23 wt % Th, 0.07% Fe, and 0.007% U. The material was formed in a 2900-hr irradiation in the LITR of 50 of the pellets in D_2O at a thermal-neutron flux of ~2 x 10^{13} neutrons/cm^2·sec, during which considerable pellet damage occurred. The material is probably the carbon residue of the polyvinyl alcohol binder used in the pellet fabrication, which was not removed by the 1750°C firing, although repeated analyses of the irradiated pellets did not show sufficient carbon to account for the amount of material found in the autoclave. The analytical method included measuring the CO_2 produced on firing at 1600°C in an oxygen stream in the presence of a fluxing agent that completely destroyed the pellets.

10.1.2 Present Status

An irradiation experiment was performed with "pure" thoria pellets under D_2O in the LITR. The pellets, P-82, are the best sintered compacts that have been prepared to date by the Ceramics Section of the Metallurgy Division. They have a pycnometric density of 9.2 g/cc and a surface area of 0.011 m^2/g. Several different thoria powder and pellet preparations are scheduled for irradiation in an attempt to determine their resistance to damage by reactor radiation under D_2O (see Sec. 10.4).

10.2 SLURRY IRRADIATIONS

Nearly all the oxide in a D_2O slurry of classified ThO_2 - 0.4% $U^{235}O_2$ (DT-22) irradiated five weeks at 280°C in the LITR at a flux of ~2 x 10^{13} neutrons/cm^2·sec to a total nvt of 5 x 10^{19} neutrons/cm^2 appeared to be somewhat degraded. Twelve per cent of the irradiated material (initially 2.1 μ average size and 0.5% <1 μ) was recovered as a dispersed suspension with an average particle size of 0.25 μ (Fig. 10.1). About 6% of the material had settled to the bottom of the autoclave and been resuspended by stirring; this material had an average size of 1.6 μ but a very steep size-distribution curve. An additional 40% of the total solids was recovered by drying the autoclave and shaking it to release dried solids from the bottom and sides. Other adhered solids were dissolved in acid, but a 100% material balance has not yet been obtained.

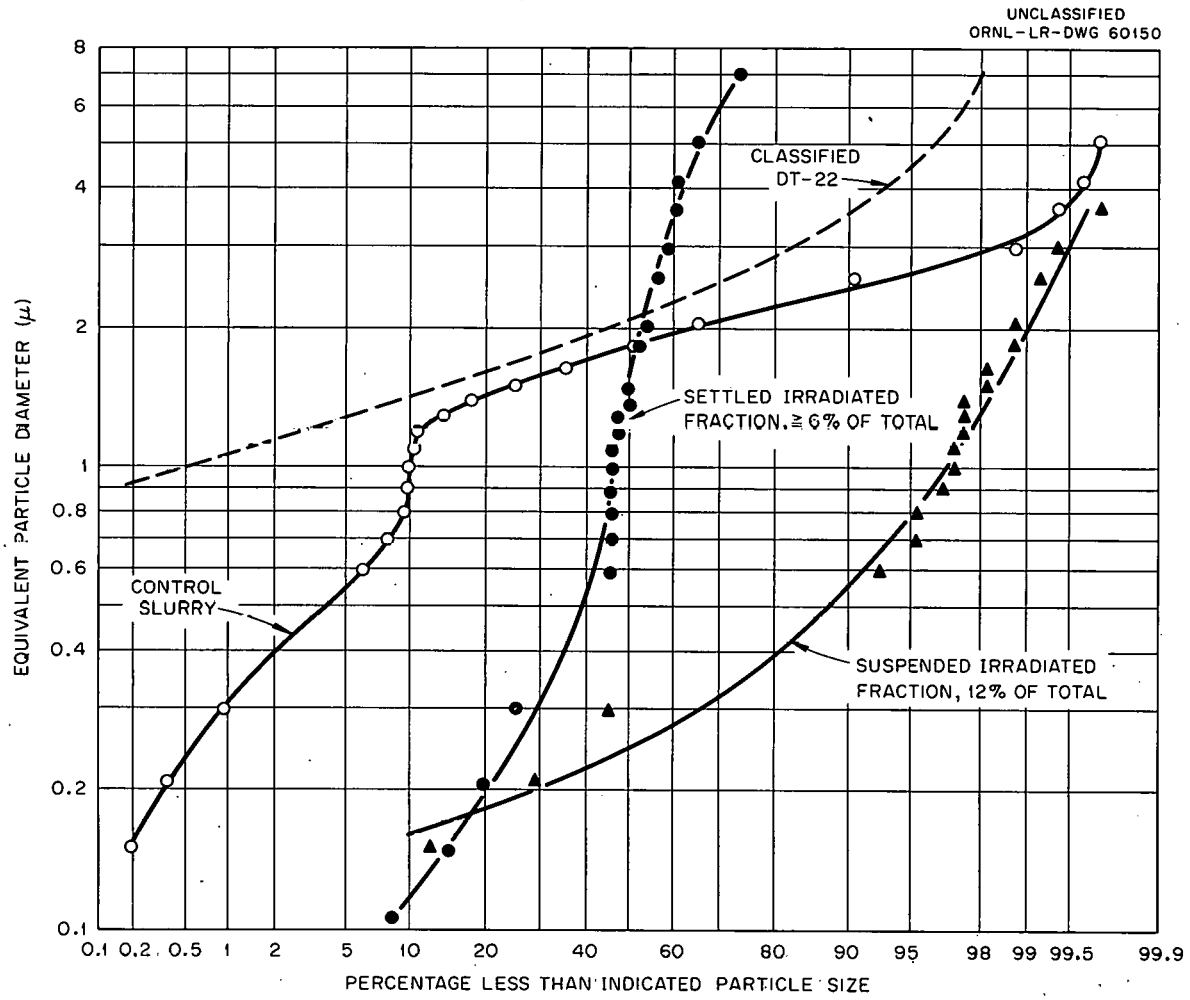

Fig. 10.1. Particle Size Distribution in Irradiated Slurry of ThO_2–0.4% $U^{235}O_2$ (DT-22). Total *nvt*, 5×10^{19} neutrons/cm^2.

Slurry from a control experiment run in the laboratory had an average particle size of 1.8 μ, with 10% of the particles smaller than 1 μ (Fig. 10.1). Apparently, treatment in high-temperature water released fines held on the classified solids which were not released by the dispersing agent (0.001 *M* $Na_4P_2O_7$) used in the particle size analysis. (Particle size analysis was carried out in the Analytical Chemistry Division by neutron-activation-sedimentation.) It is not known whether these fines have any relation to the dispersed material observed in the irradiated slurry.

The irradiation was carried out in a stainless steel autoclave with the slurry (7 ml of D_2O per gram of solid) in a settled condition. An overpressure of 100 psi O_2 and 700 psi He was added at room temperature. No radiolytic gas pressure was observed during the experiment.

The mixed oxide was a portion of the original oxide used in the in-pile slurry loop experiment[2] and had been carefully classified to remove particles smaller than 1 μ (Fig. 10.2). Classification was by elutriation with oxalic acid at pH 2.6 and then ammonium hydroxide at pH 10.5, the solid being washed with water in between and on completion of the classification. After classifi-

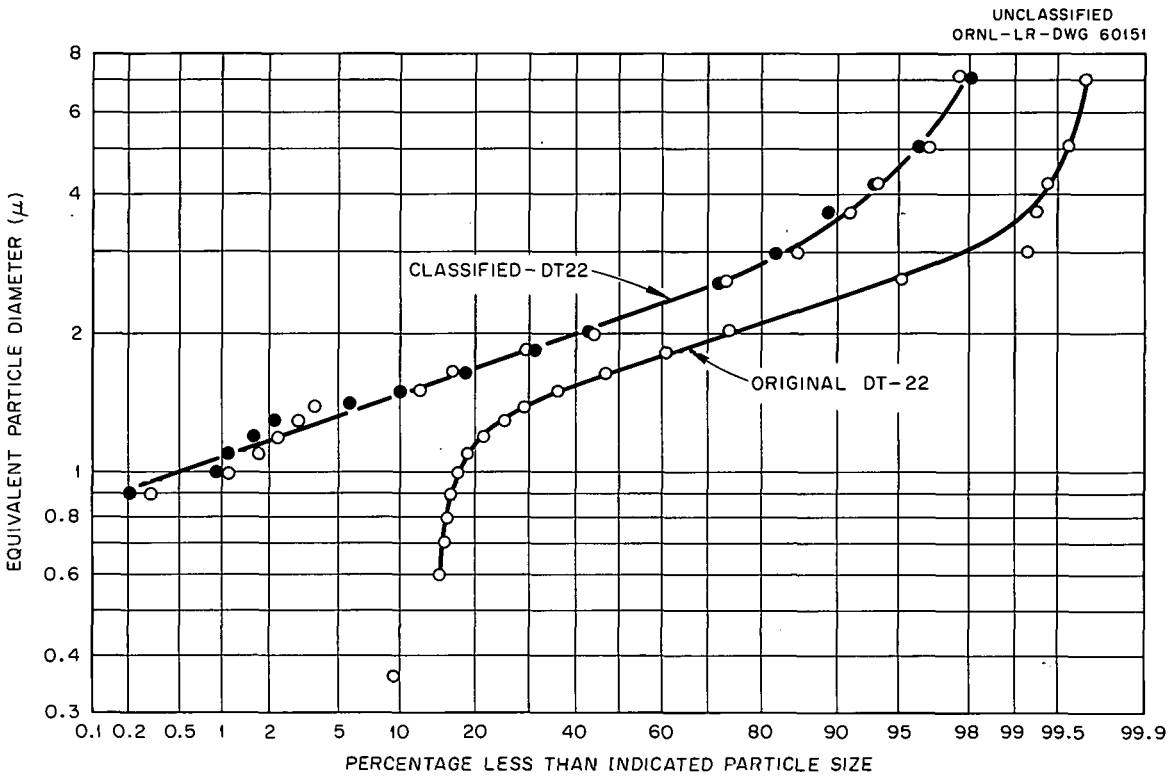

Fig. 10.2. Classification of Thoria-UO_2 Powder for Reactor-Irradiation Damage Experiments.

cation the oxide was fired at 650°C to remove adsorbed materials. There was some selective removal of uranium-rich fractions, the fines eluted with oxalic acid having a U/Th ratio of 0.0060 and that with ammonia of 0.0064. The classified solids contained 87.0% Th, and had a U/Th ratio of 0.0044 and a specific surface area measured by nitrogen adsorption of 2.1 m^2/g. Before classification the surface area was 2.5 m^2/g.

10.3 PARTICLE DAMAGE BY REACTOR IRRADIATION

Data obtained in some 55 slurry irradiations (reported in previous HRP Quarterly Progress Reports) and a few dry thoria-powder irradiations[3] carried out in the LITR over the last several years are being assembled for preparation of a progress report on these studies. A review of the particle-size information obtained in 18 of the irradiations (Table 10.1) suggests particle damage in some cases. Pure oxide preparations fired at 1600°C were resistant to radiation damage. The amount of damage observed in the wet irradiations, as opposed to the apparent stability demonstrated by the dry oxide in tests carried out here and elsewhere, suggests a radiation-water-solid interaction to produce damage, although definitive comparisons between wet and dry tests have not yet been made.

The slurry irradiations referred to above were carried out primarily to determine whether or not there was a gross deterioration of slurry behavior under reactor irradiation rather than to assess particle damage as such. The choice of slurry investigated was determined by the current opinion on what was the best slurry oxide and the particular reactor concept envisaged. All slurry irradiations were carried out in a dash-pot-stirred stainless steel autoclave[4] at 280°C, and the principal information developed was whether or not the slurry could be

Table 10.1. Particle Size Effects in Reactor-Irradiated Slurries

Temperature: 280°C
Flux: ~2 x 10^{13} neutrons/cm^2·sec

Exp. No.	Slurry Solids	Slurry Conc. (g Th/kg H_2O)	Irradiation Time (hr)	Fissions g ThO_2 x 10^{15}	Stirring Time[a] (hr)	Solids Recovered[b] (%)	Average Particle Size (μ)		% Less than 0.7 μ		Fractional Increase in % <0.7 μ, Irradiated / Unirradiated	Ref.[d]
							Unirradiated Solids[c]	Irradiated Solids	Unirradiated Solids[c]	Irradiated Solids		
3	650°C-fired ThO_2	500	258	0.2	120	(67)	2.0	<0.7	11	64	6.1	4,5
5	900°C-fired ThO_2	500	175	0.05	12	(79)	(1.1)	0.9	(32)	37	1.2	5
8	650°C-fired ThO_2	500	165	0.05	165	-	2.0	1.7	11	31	2.9	5,6
9	1600°C-fired pumped ThO_2	500	200	0.08	200	(73)	0.8	0.6	43	53	1.3	5,6
17	900°C-fired Th - 0.5% U^{235} oxide	1000	92	49	9	28	2.0	1.0	11	34	3.1	7,8
21	900°C-fired Th - 0.4% U^{235} oxide	750	168	72	168	52	(0.9)	1.9	(17)	31	1.8	8,10
26	900°C-fired ThO_2	750	198	0.08	198	33	0.8	0.8	40	47	1.2	9,10
27	800°C-fired ThO_2	750	344	0.4	344	21	(2.0)	3.4	(15)	24	1.6	9,10
33	1600°C-fired pumped ThO_2	500	336	0.4	320	(21)	(1.3)	1.3	(16)	16	1.0	11
38	1000°C-fired Th - 0.4% nat. U oxide	750	332	1.4	62	(50)	(0.8)	0.6	(44)	60	1.4	12,13
40	1300°C-fired Th - 0.4% U^{235} oxide	500	322	138	322	55	(1.7)	1.5	(32)	23	<1.0	13
44	1000°C-fired Th - 4% nat. U oxide	750	49	1.5	49	76	1.1	0.8	10	40	4.0	13,14
46	1000°C-fired Th - 4% nat. U oxide	500	361	11	361	97	1.1	1.0	10	34	3.4	13,14
47	1000°C-fired Th - 4% nat. U oxide	250	354	11	354	65	1.1	1.1	10	32	3.2	13,14
48	1000°C-fired Th - 4% nat. U oxide	250	310	9	310	(14)	1.1	0.4	9	73	8.1	14,15
49	1000°C-fired Th - 4% nat. U oxide	250	350	11	350	-	1.1	3.0	9	34	3.8	14,15
54	1050°C-fired Th - 8% nat. U oxide	250	335	20	335	74	1.3	2.0	4	18	4.5	16,17
55	1050°C-fired Th - 8% nat. U oxide	500	370	22	370	28	1.3	0.6	4	56	14	17

[a] Under irradiation.

[b] Values in parentheses estimated from settled volumes of recovered solids assuming constant settled density for all irradiated solids; others based on Th determinations.

[c] Values in parentheses obtained on the solids from a control experiment; others from original materials.

[d] References:

4. ORNL-1943
5. ORNL-2004
6. ORNL-2057
7. ORNL-2096
8. ORNL-2148
9. ORNL-2222
10. ORNL-2272
11. ORNL-2432
12. ORNL-2493
13. ORNL-2561
14. ORNL-2654
15. ORNL-2696
16. ORNL-2743
17. ORNL-2879

stirred under irradiation. The stirrer degraded the particles, particularly those larger than 1 μ, making the particle-size data somewhat difficult to interpret. Since control experiments were run in at least some of the cases and since mechanical degradation out-of-pile by the stirrer did not proceed much below 1 μ, qualitative interpretation of the particle-size data relative to irradiation damage to particles appears permissible. Not all the material was recovered in any experiment; so some bias may have been introduced into the analyses.

The data in Table 10.1 were taken from all the slurry irradiation experiments in which material recovery was good enough and the particle-size analyses on the irradiated material were sufficiently self-consistent to warrant attention. While the average particle sizes of the unirradiated and irradiated material are given, probably the most important information is the increase in the size fraction <0.7 μ, since mechanical action of the stirrer (in the absence of irradiation) probably had little or no effect in producing smaller material. In the two irradiations of 1600°C-fired material, 200 and 336 hr respectively, there was little particle damage (Fig. 10.3). The data indicate that ThO_2 fired at 650 to 800°C was less resistant to particle damage by reactor irradiation than that fired at 900 to 1600°C. A 1300°C-fired Th - 0.5% U^{235} oxide suffered little or no particle damage in a 320-hr irradiation. Mixed thorium-uranium oxides containing 5 to 8% natural uranium, in general, appeared less resistant to damage than those containing 0.4 to 0.5% uranium.

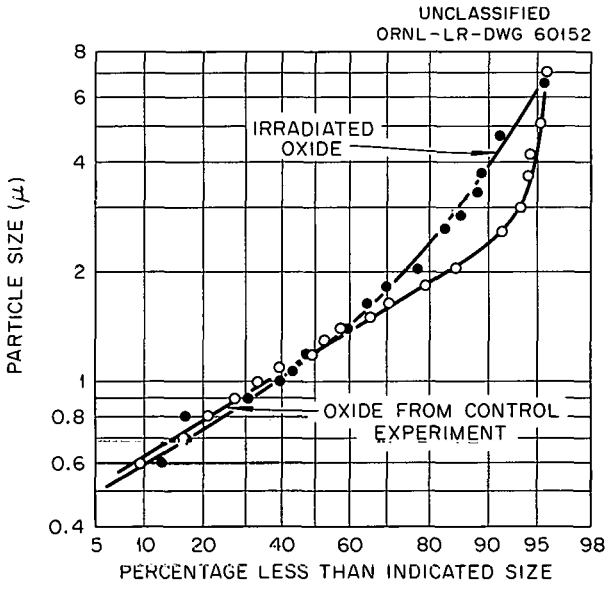

Fig. 10.3. Size-Distribution Curves of 1600°C-Fired ThO_2 Irradiated for 336 hr in H_2O (LITR-33) and Oxide from Control Experiment.

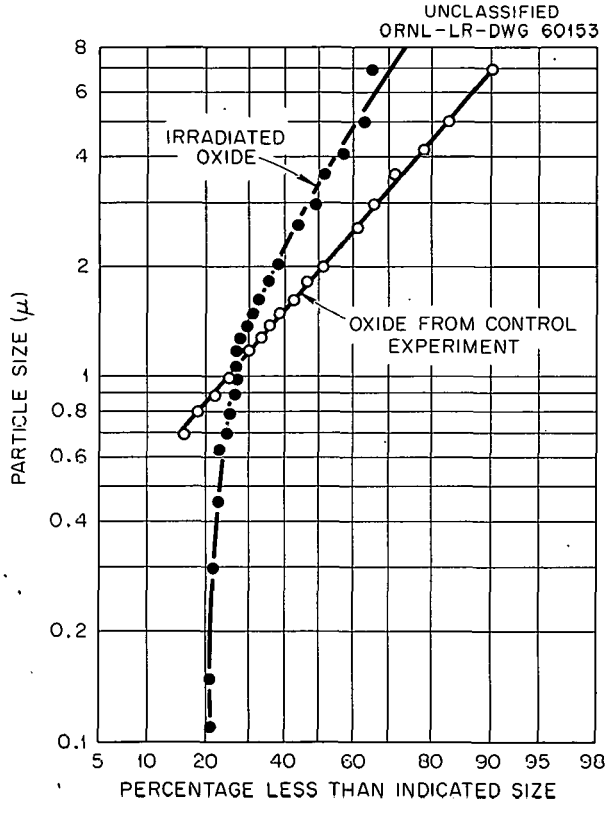

Fig. 10.4. Typical Size-Distribution Curves Showing Evidence of Radiation Damage. Irradiated oxide was 800°C-fired ThO_2 irradiated for 344 hr in H_2O (LITR-27).

Besides the increase in the fine fraction less than 0.7 μ, evidence of radiation damage was indicated by the marked change in the size-distribution curves of nearly all the irradiated samples when compared with those of the original materials. In general, where the size-distribution curve was much steeper and agglomeration had apparently occurred, it was believed that particle damage had taken place (Fig. 10.4). The apparent discrepancies in Table 10.1 in which a large increase in the fraction of material less than 0.7 μ is accompanied by little or no change, and sometimes even an increase, in average size result from such agglomeration. There is some evidence that treating a slurry in a reducing atmosphere will affect the results of the subsequent particle-size analysis such that particle growth will appear to have occurred. This may account for some of the agglomeration seen in the irradiated materials, many of which were irradiated under reducing conditions.

10.4 DEVELOPMENT OF IRRADIATION FACILITIES

Facilities are being developed for both the dry and wet irradiation of thoria powders and pellets. For the dry irradiation the materials will be contained in 2.5-in.-long 0.48-in.-OD aluminum capsules in a helium atmosphere. For mechanical protection and ease of handling, seven of the capsules will be contained in a second perforated can so that reactor water will cool the capsules. Fourteen capsules may be irradiated simultaneously in a partial fuel element in LITR lattice position C-41. Seven capsules that are now under irradiation contain Th - 2% U^{235} oxide pellets, P-82 thoria pellets, arc-fused ThO_2 (10 to 12 mesh), fired thoria gel fragments (10 to 12 mesh), and Th - 0.5% U^{235} oxide powders (DT-22). A cobalt flux monitor and a small quantity of silvered Yorkmesh for an iodine trap were inserted in each capsule.

An autoclave to permit irradiation of multiple "wet" samples of oxide is being developed and fabricated for insertion in the C-43 irradiation facility. While each material will be separately contained in the irradiation autoclave, they will all be exposed to a common gas and liquid phase by means of a sintered stainless steel filter in each container. The initial experiment will contain sintered thoria powder compacts, fired sol-gel thoria, shaped arc-fused thoria, arc-fused thoria fragments (300 to 500 μ), thoria single crystals, and 1600°C-fired thoria powder (DT-46). Another irradiation facility analogous to C-43 to permit long- and short-term multiple wet irradiations is also under development.

REFERENCES

1. J. P. McBride, HRP Prog. Rep. Nov. 30, 1960, ORNL-3061, p 75.

2. E. L. Compere, H. C. Savage, et al., HRP Prog. Rep. Nov. 30, 1960, ORNL-3061, p 89.

3. J. P. McBride, HRP Quar. Prog. Rep. July 31, 1960, ORNL-3004, p 81.

4. J. A. Lane, H. G. MacPherson, and Frank Maslan (eds.), Fluid Fuel Reactors, p 180, Addison-Wesley, Reading, Mass., 1958.

11. DEVELOPMENT OF GAS-RECOMBINATION CATALYST

J. P. McBride L. E. Morse W. L. Pattison

11.1 GAS-INJECTION APPARATUS

Calibration of the gas-injection apparatus[1] used in the gas-recombination-catalyst development studies continued. Partial holdup of gas in the capillary connecting the charging system to the reaction autoclave has been suggested[2] as an explanation for certain anomalies that have been observed (e.g., incomplete recombination and threshold reaction pressures). The results of a series of gas-recombination experiments, in which the holdup of the second gas charged (D_2) was controlled by displacing the gas in the capillary with a measured quantity of water forced in behind the gas, appear to support this conclusion.

In the calibration experiments essentially constant quantities of O_2 and D_2 were charged to the capillary system connecting the pressurizable gas burette with the reaction autoclave (first O_2 and then D_2), displaced with various quantities of water, and allowed to recombine to apparent steady state. At the end of each recombination experiment the autoclave was cooled to room temperature, and a sample of the residual gas in the reaction system was taken for O_2 and D_2 analysis and the remainder was released prior to resealing the autoclave and heating it to temperature for the succeeding experiment. As the amount of water injected was increased, the initial D_2 pressure in the reaction system increased, initial recombination rates increased, and the total quantity of D_2 combined increased until essentially complete reaction of the D_2 added to the reaction vessel was indicated (i.e., the percentage of D_2 in residual gas approached zero; see Table 11.1).

The holdup volume between the pressurizable gas burette and the reaction autoclave had been estimated at 0.92 ml, 0.36 ml in the capillary tubing between the gas burette and the charging valve, and 0.56 ml in the capillary between the charging valve and the reaction autoclave. The data of Table 11.1 suggest that the holdup volume is probably closer to 1.1 ml.

11.2 PALLADIUM CATALYSIS

In support of the in-pile slurry corrosion studies by the Corrosion Section of the Reactor Chemistry Division, gas recombination was studied with slurries containing the oxide projected for the next in-pile study and added palladium catalyst. The slurry to be irradiated will contain 782 g of Th per kg of D_2O as Th - 12.4% U^{235} oxide and 1460 ppm Pd (based on Th) of the sol-prepared palladium catalyst.[3] The power density during irradiation in the LITR will be about 26 w/ml. Out-of-pile data indicate that the catalytic activity of the proposed slurry will be sufficient to maintain the pressure of radiolytic D_2 gas at 100 psi or less at 280°C during the in-pile experiment.

Two series of experiments were carried out. One used a laboratory-prepared slurry containing 68 g of Th per kg of D_2O of the Th - 12.4% U^{235} oxide and 154 ppm Pd (based on Th). The second used the slurry from a mockup of the in-pile experiment carried out by the Corrosion Section diluted to give 86.3 g of Th per kg of D_2O of the Th - 12.4% U^{235} oxide and containing 1460 ppm Pd (based on Th).

Table 11.1. Calibration of Gas-Injection Apparatus

Slurry oxide: 1225°C-fired Th - 0.5% U^{235} oxide
Slurry concentration: 483 g of Th per kg of D_2O; 640 ppm Pd (based on Th)
Reaction temperature: 280°C

Gases Charged (moles)		Water Injected	Residual-Gas Analysis (vol %)		D_2 Reacted
O_2	D_2	(ml)	D_2	O_2	(%)
x 10^{-3}	x 10^{-3}				
4.46	2.89	0	37.1	62.9	12.6
4.51		0.23	38.6	61.4	
4.58	2.83	0.46	32.3	67.7	29.4
4.58	2.84	0.575	28.9	71.1	43.4
4.66	2.84	0.69	25.0	75.0	53.4
4.68	2.80	0.805	12.8	87.2	81.5
4.72	2.78	0.92	4.4	95.6	90.2
4.79	2.83	1.04	2.1	97.9	95.3
4.77	2.86	1.15	1.8	98.2	97.8
4.39	2.72	1.09	2.1	97.9	97.6

Prior to its use in the recombination studies, the laboratory-prepared slurry was heated in O_2 (600 psi above steam pressure) at 280°C for 68 hr. The mockup slurry had been heated about three weeks under approximately the same conditions. The initial reaction rates were correlated by a kinetic expression involving a first-power dependence of rate on the hydrogen partial pressure and a 0.5-power dependence on oxygen partial pressure $(-dP/dt) = kP_{D_2}P_{O_2}^{1/2})$. The molar recombination rate, moles of D_2 per hour per liter of slurry, for a given D_2 partial pressure was calculated from the expression:

$$\frac{dD_2}{dt} = \frac{kP_{D_2}P_{O_2}^{1/2}}{Rt} \cdot \frac{V_g}{V_s} ,$$

where

dD_2/dt = molar recombination rate,
V_g = volume of the gas phase in the reaction vessel (280°C),
V_s = volume of the slurry phase in the reaction vessel (280°C),
k = rate constant.

A limited number of experiments were made with the laboratory-prepared slurry at 700 psi O_2 and 62 to 108 psi D_2 initial pressure. The rate data (Table 11.2, Fig. 11.1) showed reasonable agreement with the proposed kinetic expression. The reaction rate constant was obtained from the slope obtained by plotting $(dP/dt)/P_{O_2}^{1/2}$ vs P_{D_2} (Fig. 11.1). The average CPI (catalyst performance index) for this slurry was 1.2 w/ml at 280°C for a 60%-filled autoclave. Using the rate constant to calculate the CPI at 100 psi D_2 partial pressure and assuming a linear dependence of catalytic activity on slurry and catalyst concentration, this indicates a CPI under the conditions of the LITR irradiations of better than 100 w/ml.

For the diluted slurry from the mockup of the in-pile experiment, the initial reaction rate was studied as a function of the initial O_2 partial pressure from 200 to 800 psi above steam at 280°C and a constant D_2 partial pressure of about 110 psi (Table 11.3). Figure 11.2 is a linear plot of $(dP/dt)/P_{D_2}$ vs $P_{O_2}^{1/2}$

Table 11.2. Reaction Rates of D_2-O_2 Mixtures in an Aqueous Th - 12.4% U^{235} Oxide Slurry Containing Palladium Catalyst

Slurry composition: 68.0 g of Th per kg of D_2O; 151 ppm Pd (based on Th)
Reaction temperature: 280°C
Slurry pretreatment: Heated with O_2 (600 psi above steam pressure) at 280°C for 68 hr

Gases Charged (moles)		Initial Pressures (psi)		Initial Reaction Rates		
O_2	D_2	O_2	D_2	psi/hr	moles/hr	CPI
x 10^{-3}	x 10^{-3}					
9.49	11.0	688	84	191	0.21	0.9
8.87	11.7	705	108	270	0.29	1.3
8.90	10.7	728	62	149	0.14	0.6

$$-\frac{dP}{dt} = kP_{D_2}P_{O_2}^{1/2}$$

$$k = 0.101 \text{ psi}^{-1/2} \text{ hr}^{-1}$$

Table 11.3. Effect of Oxygen Partial Pressure on Recombination Rate in Th - 12.4% U^{235} Oxide Slurry Containing Palladium Catalyst

Slurry composition: 86.3 g of Th per kg of D_2O; 1460 ppm Pd (based on Th)
Reaction temperature: 280°C
Slurry pretreatment: Heated with O_2 (~600 psi above steam pressure) at 280°C for approximately three weeks

Gases Charged (moles)		Initial Pressures (psi)		Initial Reaction Rates		
O_2	D_2	O_2	D_2	psi/hr	moles/hr	CPI
x 10^{-3}	x 10^{-3}					
8.97	1.12	797	108	2356	1.9	8.4
8.90	1.00	822	106	2262	1.6	7.0
8.40	0.98	822	106	2271	1.3	5.7
6.74	1.10	380	104	2000	1.7	7.7
6.61	1.11	601	117	2280	1.7	7.2
4.11	1.16	371	112	1725	1.4	6.3
4.08	1.22	382	120	1950	1.4	6.2
3.72	1.23	376	114	1764	1.1	4.9
2.73	1.22	240	96	1249	0.9	3.8
2.42	1.26	218	110	1364	1.1	4.8

$$-\frac{dP}{dt} = kP_{D_2}P_{O_2}^{1/2}$$

$$k = 0.66 \text{ psi}^{-1/2} \text{ hr}^{-1}$$

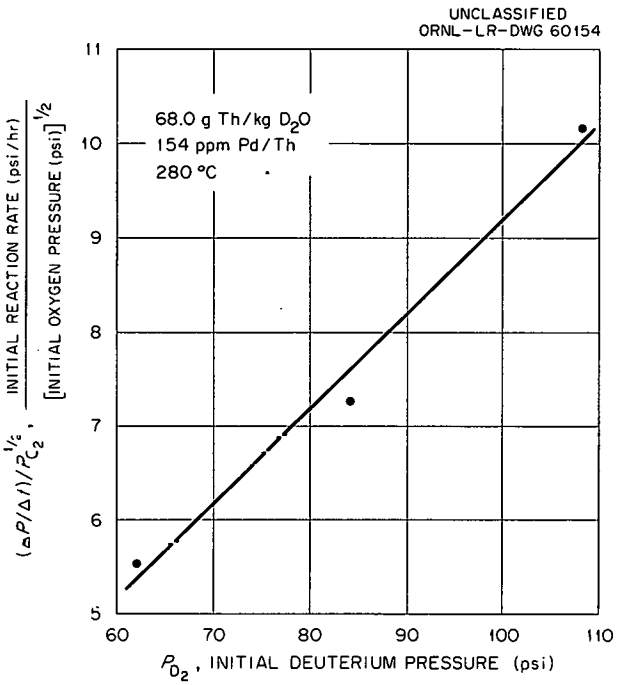

Fig. 11.1. Effect of Deuterium Partial Pressure on Recombination Rate in Thorium – 12.4% Uranium Oxide Slurry.

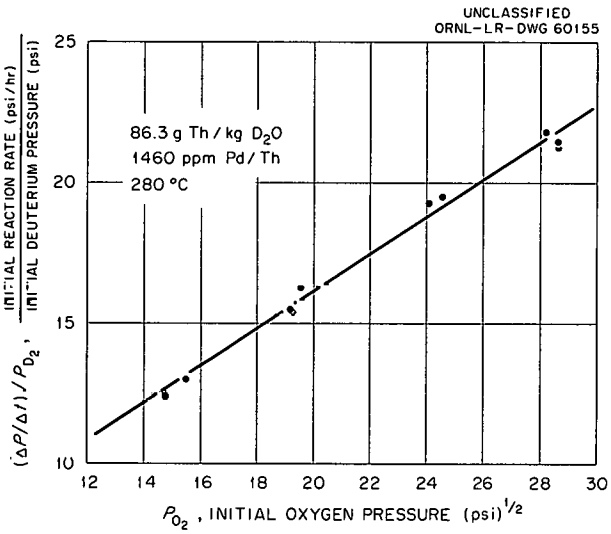

Fig. 11.2. Effect of Oxygen Partial Pressure on Recombination Rate in Thorium – 12.4% Uranium Oxide Slurry.

in agreement with the proposed kinetic expression. Using the k obtained from the slope of this line, the calculated CPI at 280°C and a gas mixture of 700 psi O_2 and 100 psi D_2 in a 60%-filled autoclave was 6.8 w/ml. Again, assuming a linear dependence of rate on concentration, a CPI greater than 60 w/ml is indicated for the in-pile experiment. When the reaction rate was measured at about 200 psi O_2 above steam at 280°C the first reaction in the group of three after distillation of the excess water proceeded at a measurable rate, but in the following two experiments the D_2 reacted as rapidly as it was charged. The series was repeated again after removal of the excess water with the same results. This may indicate that the true kinetic expression of low O_2 partial pressures or low O_2/D_2 ratios may be somewhat more complicated than the one used to correlate the present data. Enhanced catalytic activity at low O_2 partial pressures is in agreement with data presented in a previous report.[2]

Experiments with the two slurries were made in the same way. Residual gases from any previous experiments were removed by heating (or cooling) the slurry to ~100°C, bleeding off the gases, closing the system, and heating to 280°C. The desired amount of O_2 was injected into the bomb, and the heating was continued 1 hr. Deuterium followed by water in slight excess of the charging-capillary volume was then injected. Analysis of the residual gas at the end of each experiment showed that more than 90% of the D_2 was consumed in the reaction. The injection of water to displace the D_2 from the capillary resulted in the introduction of a small quantity of water in the slurry. In order to avoid excessive dilution of the slurry, experiments were performed in groups of three, and the excess water was removed by distillation at the conclusion of the third experiment.

REFERENCES

1. J. P. McBride and L. E. Morse, HRP Prog. Rep. Oct. 31, 1959, ORNL-2879, p 175.

2. J. P. McBride, L. E. Morse, and W. L. Pattison, HRP Prog. Rep. Nov. 30, 1960, ORNL-3061, p 78-83.

3. J. P. McBride and L. E. Morse, HRP Quar. Prog. Rep. Apr. 30, 1960, ORNL-2947, p 87.

12. SLURRY CORROSION AND BLANKET MATERIALS TESTS

E. L. Compere H. C. Savage

J. M. Baker S. A. Reed
R. E. McDonald* A. J. Shor
T. H. Mauney L. F. Woo

12.1 THORIA-PELLET TEST PROGRAM

12.1.1 Evaluation of Code P-82 Pellets

The method of fabrication and the results of initial evaluations of code P-82 pellets were discussed previously.[1,2] This batch of pellets displayed the highest integrity of any pellets made up to that time and on this basis was chosen for further evaluation in an in-pile test (see Sec. 10.1.2). Therefore supplementary data were obtained during the present report period to better characterize the pellets and to evaluate their relative integrity under other test conditions.

Physical characteristics of the pellets were determined by measurements of their specific surface area by a modified BET[3] method using krypton-gas adsorption, by estimation of their pore volume and pore radius by mercury intrusion,[4] and by determination of pellet density by water immersion. The homogeneity of the pellets was determined by conventional metallurgical polishing and etching techniques. Results of the examinations are presented in Table 12.1 and Fig. 12.1.

Table 12.1. Physical Properties of Code P-82 ThO_2 Pellets

Right Cylinders with Hemispherical Ends, 0.219-in. Diameter x 0.205-in. Length; Calcined at 1650°C for 2 hr

Surface area (BET, krypton)	0.011 m^2/g
Average pore radius (Hg intrusion)	0.964 μ
Pore volume (Hg intrusion)	0.0055 cc/g or 5.1 vol %
Density (H_2O immersion)	9.14 g/cc

The average grain size as shown in Fig. 12.1 is approximately 10 to 15 μ. The surface area of 15-μ cubes is 0.04 m^2/g. The observed surface area of 0.011 m^2/g implies the accessibility to krypton of a substantial fraction of internal surface.

The observed pore volume of 0.0055 cc/g, coupled with a density of 10.0 computed from crystal lattice parameters, leads to an estimated density of 9.49

*Postirradiation Examination Group, Metallurgy Division

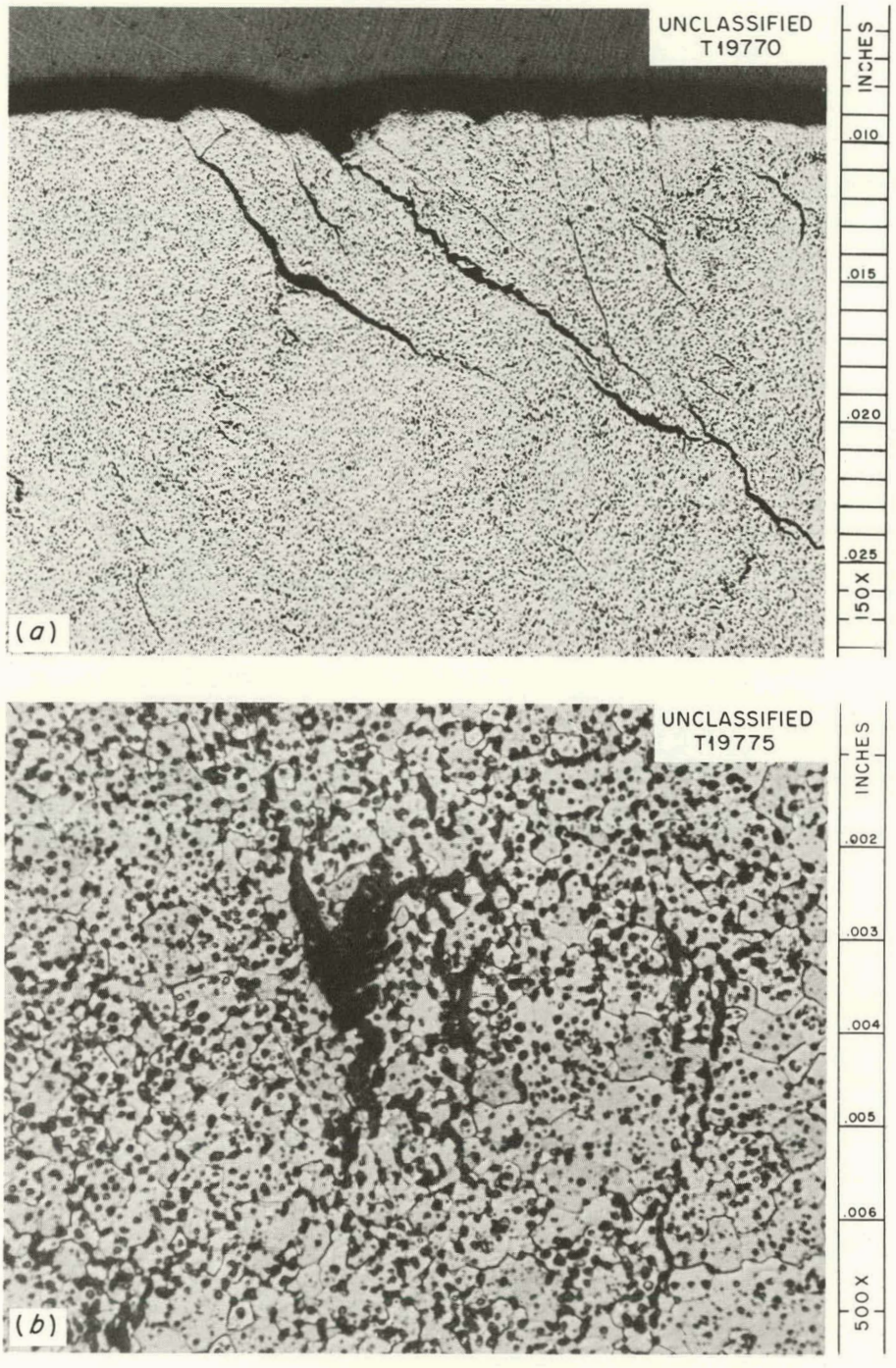

Fig. 12.1. Photomicrographs of Interior of Code P-82 ThO_2 Pellets. (*a*) Cracks Originating at Junction of Cylindrical and Hemispherical Sections of Pellet. As polished. 150X. (*b*) Void in Center of Pellet. Etchant: $HF\text{-}HNO_3$. 500X.

if there are no internal voids inaccessible to mercury intrusion. The observed density by water immersion was obtained without outgassing; water doubtless did not intrude in the pores, and the density of 9.14 may be compared with the above estimate. The discrepancy between them implies the existence of internal voids. Such voids may be seen in the photomicrographs of Fig. 12.1.

Supplementary attrition data from spouted-bed tests after autoclaving the pellets in 350°C water and from a small fluidized-bed test are summarized in Table 12.2. Data from previous tests are also included for comparison.

Table 12.2. Attrition Rates of Code P-82 ThO_2 Pellets in Various Tests

Test	Average Weight Loss Rate (%/hr)
Accelerated Tests	
Spouted bed (10 pellets); superficial velocity, 0.37 fps; two 1-hr exposures	
Before autoclaving	0.27
After autoclaving in	
260°C water	0.49
350°C water	0.51
Ball mill (10 pellets), 3.75-in.-ID rubber-lined mill, 150 rpm	0.06
Fluidized bed (2- by 2-in. static bed); 30% bed expansion; 12-hr exposure; superficial velocity, 0.56 fps	0.014

Although pellets autoclaved in water at 260°C showed a substantial increase in attrition rates, further increase to 350°C autoclaving temperature did not augment this effect.

Small fluidized beds have been considered as one method for exposing pellets in a dynamic in-pile test. The attrition rate (0.014% per hour) shown in Table 12.2 was the average weight-loss rate observed over a 12-hr period using 430 pellets (2- by 2-in. static bed) which were fluidized at a 30% bed expansion with water at room temperature. The value is considerably below the rates obtained in accelerated tests.

A loss rate of 0.06% per day could be tolerated[5] in a reactor pellet blanket. Although the experimental rate of 0.014% per hour was obtained at room temperature, it appears likely that reactor beds containing pellets of this quality could be fluidized a few hours a day.

12.1.2 Evaluation of Experimental Pellets

As part of the cooperative program with the Ceramics Group of the Metallurgy Division, samples of 11 different experimental pellet preparations were subjected

to routine laboratory accelerated attrition tests as an aid to evaluating new fabrication techniques. Test data for the series are summarized in Table 12.3. Descriptions of fabrication variables and detailed test data are reported elsewhere[6,7].

With the exception of one preparation, code P-97, all the specimens displayed considerably higher weight-loss rates in spouted-bed tests than the code P-82 pellets discussed previously. Code P-97 pellets, which were pressed as right cylinders, had been preattrited by milling for 4 hr to remove sharp edges prior to testing. It is known that such pretreatment of cylinders generally reduces wear rates.[8] Similarly, spheroidal pellets (code P-98) displayed comparatively good attrition resistance.

No correlation with pellet density was manifested in the series.

12.2 IN-PILE SLURRY AUTOCLAVES

12.2.1 Introduction

In-pile slurry autoclave experiment L5Z-155S was performed to evaluate the radiation effect on the degradation of particles in a thoria-urania slurry gently agitated in a rocking autoclave in comparison with that observed in the slurry pumped in in-pile slurry loop experiment L-2-27S. Irradiation in the HB-5 facility of the LITR has been completed. The Zircaloy-2 autoclave contained a thoria-urania slurry (0.4% U, based on Th) prepared from the same oxide batch (DT-22) used in the in-pile slurry loop experiment. The oxygen-pressurized autoclave, loaded with slurry at a concentration of 996 g of Th per kg of D_2O and 0.014 m in Pd, was operated for a total of 770 hr at 280°C. The autoclave was irradiated for 453 hr, achieving an effective full-flux time of 87.2% of this.

From activation of a cobalt flux monitor located inside the autoclave in a type 347 stainless steel tube, the thermal-neutron flux in the autoclave was estimated to be 7.7×10^{12} neutrons/cm^2·sec (corresponding to an nvt of 1.1×10^{19}). At this flux, the slurry particles should develop 5.1×10^{16} fissions per gram of solids.

Based on radiochemical analyses of Zr^{95} and Cs^{137} in the irradiated slurry, the fission dose developed in the slurry was estimated to be 3.1×10^{16} and 4.2×10^{16} fissions per gram of solids, respectively. Neutron captures by thorium, based on Pa^{233} counting, were 1.73×10^{17} captures per gram of solids, leading to an estimated thorium cross section of 8.5 barns (based on total fissions from Cs^{137} counting, and a U^{235} cross section of 582 barns). This agrees favorably with the activation cross section of 7.7 ± 0.4 barns cited[9] by Weinberg and Wigner.

12.2.2 Operation

The autoclave was pretested at Y-12 for 198 hr and in beam hole HB-5 for 14 hr before irradiation. After 1.5 hr of smooth irradiation in the fully inserted position, pressure-temperature aberrations developed. During a shutdown of the reactor and experiment, the pressure system was recalibrated and found to be correct. After the completion of the experiment, a major source of the problems was found to be in the use of unsuitable instrument cables leading to the experiment. The aberrations involved temperature discrepancies of several degrees, but did not interfere substantially with continued irradiation at maximum flux.

Table 12.3. Summary of Evaluation Tests of Experiment ThO_2 Pellets

Code	Shape[a]	Pressed from ThO_2 Powder Batch	Binder	Final Calcn. Temp. (°C)	Density[b] (g/cc)	Spouted Bed Test[c] Average Weight Loss Rate (%/hr) Pre-autoclave	Post-autoclave[d]
P-86	Rt. cyl; domed ends	D-40, 650°C-calcined	PVA[e]	1650	8.8C	0.66	1.09
P-87	Rt. cyl; domed ends	D-40, 650°C-calcined	PVA[e]	1650	8.41	0.75	1.25
P-88	Rt. cyl; domed ends	D-40, 650°C-calcined	PVA[e]	1650	8.2E	0.82	1.24
P-89	Rt. cyl; domed ends	D-40, 650°C-calcined	Carbowax	1650[f]	9.24	2.25	1.48
P-90	Rt. cyl; domed ends	D-40, 650°C-calcined	Carbowax	1650[f]	9.22	3.19	1.22
P-91	Rt. cyl; domed ends	D-40, 650°C-calcined	Carbowax	1650[f]	9.05	1.11	1.15
P-92	Rt. cyl; domed ends	D-40, 650°C-calcined	Carbowax	1650[f]	9.05	1.46	1.14
P-95	Rt. cyl; domed ends	D-40, 1425°C-calcined	Carbowax	1790 (Ar atmos)	9.2C	0.92	1.11
P-96	Rt. cyl; domed ends	D-40, 1425°C-calcined	Carbowax	1790 (H_2 atmos)	9.24	1.37	1.64
P-97	Rt. cyl	DT-102, 1000°C-calcined	Carbowax	1425[g]	8.8E	0.48	0.47
P-98	Spheroidal[h]	DT-102, 1000°C-calcined	Carbowax	1900	9.8E	0.84	0.89

[a] All preparations were approximately 0.2 in. in diameter by 0.2 in. in length.

[b] Measured by water immersion.

[c] Ten pellets; superficial velocity, 0.33 to 0.37 fps; two 1-hr tests.

[d] Exposed in static autoclave, 72 hr, 260°C water, after initial spouted-bed tests.

[e] Polyvinyl alcohol.

[f] Milled 4 hr with Al_2O_3 balls after calcination.

[g] Milled 4 hr after calcination.

[h] Formed by tumbling cubes.

The autoclave was equipped with an Al_2O_3 filter[10] protecting the capillary line to the pressure instrument. No indication of any plugging of this line was noted during in-pile operation. However, a venting lag was encountered, and when the autoclave was later opened the filter was found cracked off.

12.2.3 Radiolytic Gas

Due to the aberrations in temperature readings during the experiment, knowledge of the radiolytic gas generated was not as well defined as in earlier slurry autoclave experiments. Some few observations appear to be reliable. During the first 1.5 hr of irradiation with the autoclave in the fully inserted position, no buildup of radiolytic gas was noted. Furthermore, following shutdown of the experiment and reactor over the weekend, irradiation fully inserted for over 34 hr produced no pressure rise. Later, near the end of the irradiation, an insertion experiment observed for 2 hr indicated no radiolytic gas.

Between these three observations, discrepancies in readings of thermocouples (including the temperature-controlling couple) were noted, and pressure drifts were generally associated with the temperature aberrations.

It is believed that catalytic and gamma recombination were sufficient in the experiment to prevent the development of observable radiolytic-gas pressures.

12.2.4 Autoclave Corrosion

Generalized corrosion was followed in the usual manner by measuring the decrease in oxygen pressure during periodic shutdowns. As indicated in Fig. 12.2, an out-of-pile corrosion rate of 4.4 mpy for the first 48 hr was observed. The rate decreased to 1 mpy for the remaining period out-of-pile. Upon irradiation the corrosion rate remained essentially constant at 1 mpy. Thus no effect of irradiation on the generalized corrosion was indicated in this experiment.

12.2.5 Recovery of the Irradiated Slurry

A primary purpose of the experiment was to recover as much of the irradiated slurry as possible for the assessment of radiation effects. Since the irradiated slurry had been settled for 30 days for its radioactivity to decay, resuspension of the slurry was attempted by inverting the autoclave 100 times. The autoclave head was then removed, and a 4.5 ml portion of the slurry was removed with a pipette. After filling the autoclave with distilled water, the contents of the autoclave were further mixed by repeatedly drawing the slurry into the pipette and forcing it back into the autoclave. During the transfer of this slurry to a centrifuge cone, the pipette became plugged. The slurry in the pipette subsequently was recovered by back-flushing the pipette and rubber tubing. The autoclave was inverted over a funnel, and slurry remaining on the inside walls of the autoclave was rinsed with jets of water from small holes drilled at the closed end of a 3/8-in. copper tube inserted into the autoclave. A small amount of thickened slurry was noted on the autoclave head before cleaning.

All the recovered slurry was composited in a single beaker, and the water volume was reduced to 100 ml under a heat lamp. While the slurry was thoroughly agitated, two samples were removed for particle-size analyses. Then a dried sample was removed for surface-area determination.

12.2.6 Effect of Irradiation On Particle Integrity

The surface area of the original thoria-urania (92%) was 2 m^2/g, and that of the finely divided palladium-thoria catalyst (8%) was 53 m^2/g. The surface

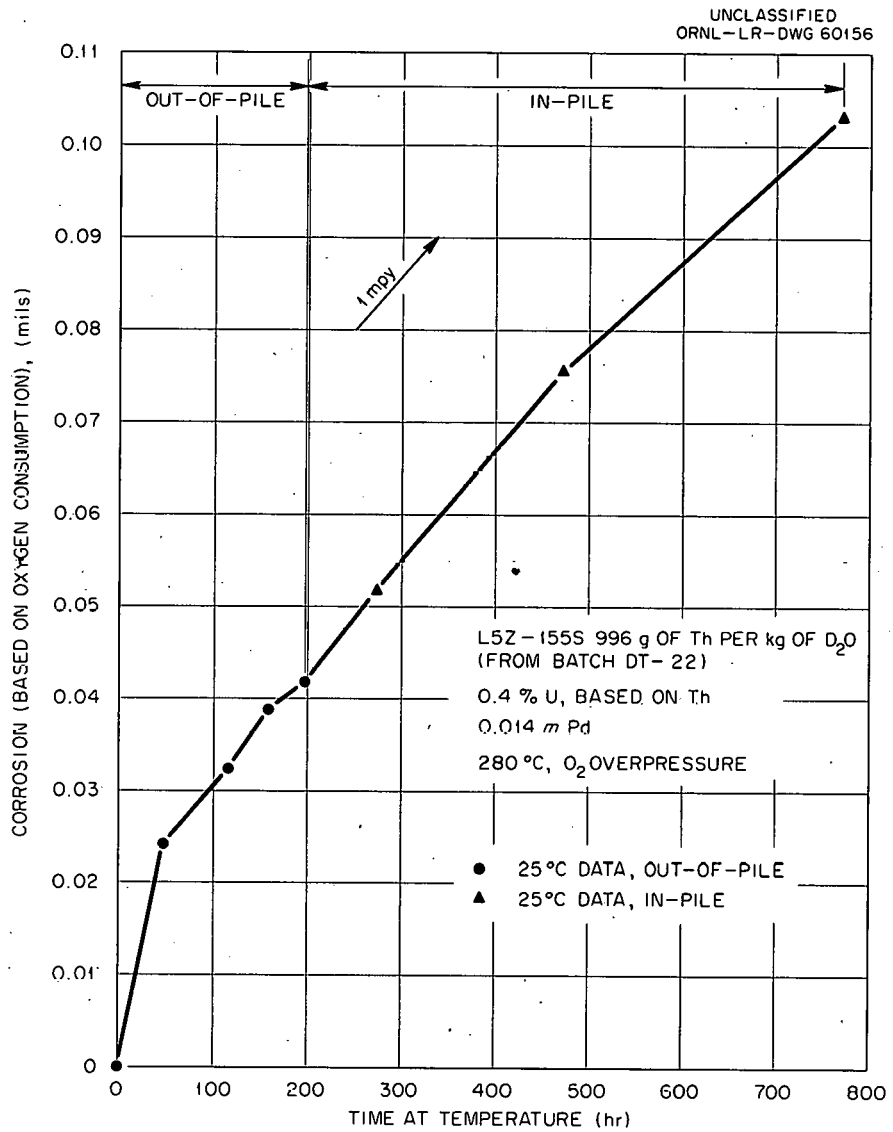

Fig. 12.2. Generalized Corrosion in Experiment L5Z-155S, Autoclave Control for In-Pile Slurry Loop L-2-27S.

area of the unirradiated m xture was 8 m^2/g. After irradiation, the surface area of the slurry was 30 m^2/g. Thus irradiation resulted in an increase in surface area similar to that shown by loop samples at an equivalent nvt.

The results of the particle-size analyses of the irradiated slurry and an unirradiated replicate mixture (control) are shown in Fig. 12.3. Although some agglomeration of fines was indicated in the irradiated slurry, as compared with the unirradiated material, no particular degradation of the slurry was seen.

From the results of the physical analyses so far, it is inferred that irradiation does indeed cause submicroscopic defects in the slurry particles, as observed by an increase in surface area, but that particle agitation more severe than that experienced in a rocking autoclave is necessary to actually break up the slurry particles.

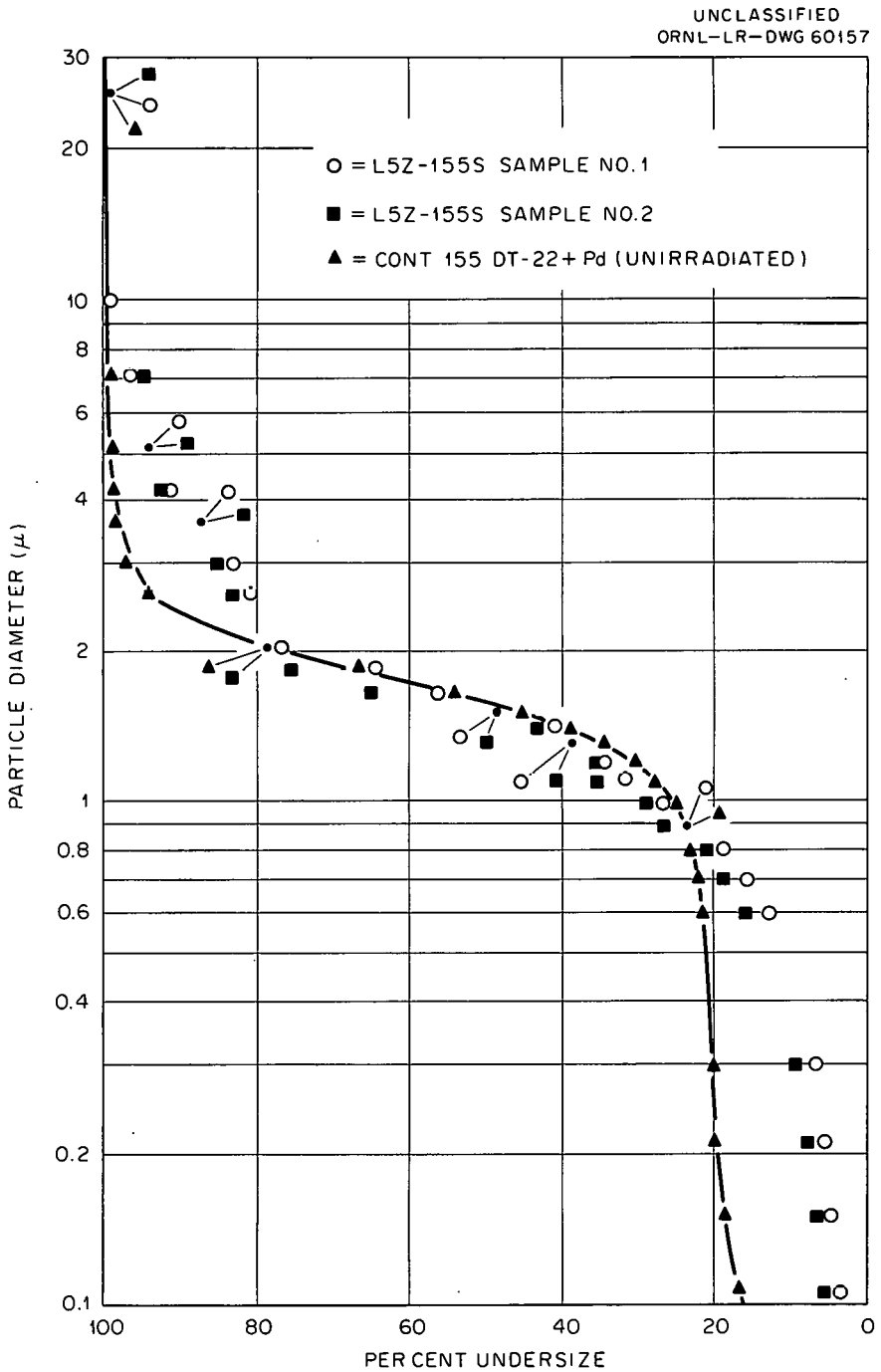

Fig. 12.3. Effect of Irradiation (10^{19} nvt) on Particle Size of Slurry Mixture.

12.3 IN-PILE SLURRY LOOP

12.3.1 Introduction

Additional information from the examination of slurry samples from the first in-pile slurry loop[11-13] includes final radiochemical data, particle size distribution, surface area, and crystallite size. Indications by these techniques of particle breakdown have been confirmed by electron micrographs of slurry samples from throughout the run.

Postirradiation examination of the core region has begun. Weight-change data on coupons, permitting the estimation of corrosion-erosion attack in this region, have not indicated particularly severe attack on any specimens, although entrance effects were noted on specimens in 22-fps holders. The question of possible slurry caking in the core or other regions is of considerable interest. No indication of any noteworthy deposits in the core region is reported.

12.3.2 Radiochemical Considerations

The ingrowth of various fission products, corrected for decay and reactor shutdown periods, permits a calculation of total fissions and other related dose data. Data for Zr^{95} and Ce^{144} were used in the estimates, Cs^{137} being regarded as less reliable since it was partitioned between solid and liquid phases in an inadequately defined way in the high-temperature slurry system. As shown in Table 12.4, approximately 7×10^{16} fissions per gram of solids were obtained, with a total U^{235} burnup of 0.92% of that originally present. An exposure of 1.6×10^{19} nvt was calculated, with a flux averaged over the entire slurry mainstream of 2.4×10^{12} nv.

Only Cs^{137} was found in appreciable concentrations in the liquid phase relative to the solids phase, distribution coefficients of approximately unity being obtained. Zirconium-95, Ce^{144}, and Pa^{233} were strongly adsorbed on the solids. Adsorption on metallic loop surfaces remains to be studied.

12.3.3 Particle Integrity

Additional data on the effect of irradiation and circulation on slurry particle size distribution and surface area are shown in Fig. 12.4, extending data previously reported[11] from the time 2617 hr of slurry circulation to the termination of the run, after 3111 hr of circulation.

Table 12.4. Radiochemical Data, In-Pile Slurry Loop L-2-27S
(Irradiated 1839 hr)

Fissions per gram of solids				7×10^{16}
Burnup				0.9% of orig. U^{235} or 0.003% of metal atoms
Average flux				2.4×10^{12}
nvt				1.6×10^{19}
Distribution of fission products				
	Cs-137	Zr-95	Ce-144	Pa-233
K, solids/liquid	~1	$>10^5$	10^4	10^4

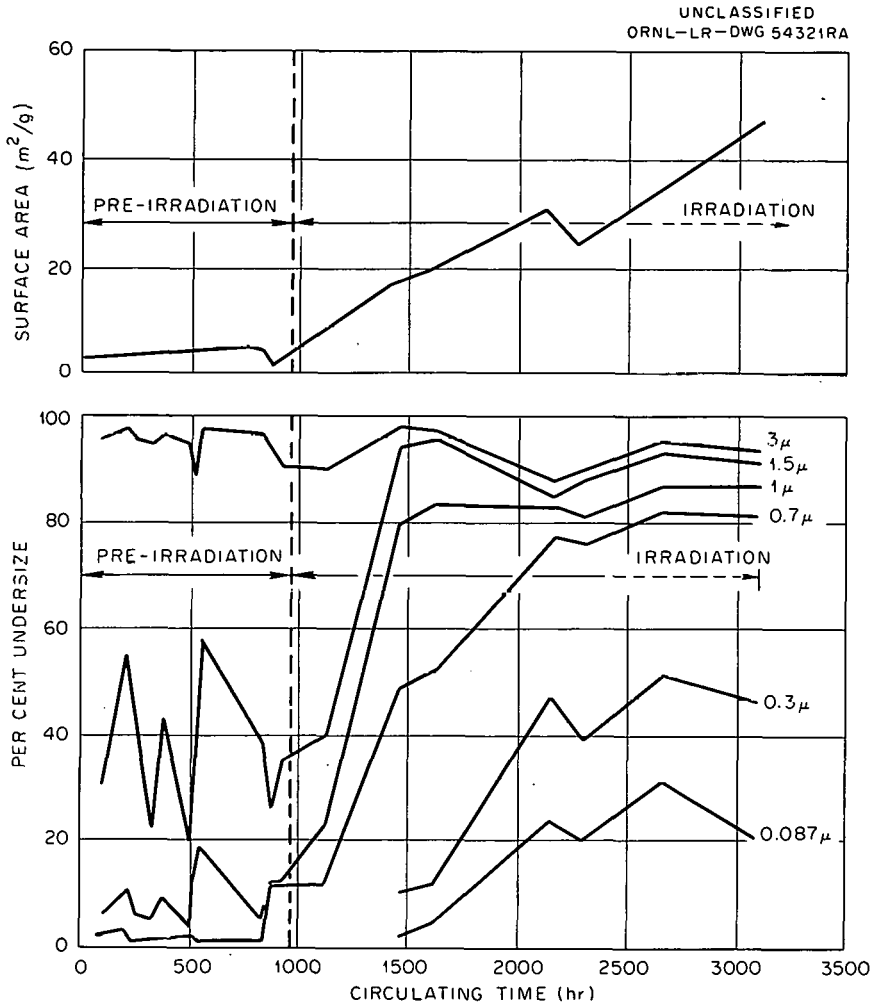

Fig. 12.4. Effect of Irradiation and Circulation on Slurry Particle Size Distribution and Surface Area.

Crystallite size as determined by x-ray line-broadening techniques showed a steady decrease during the entire period of in-pile operation. (Fig. 12.5). These data may be compared with the corresponding surface-area measurements. An inverse relationship has been found (Fig. 12.6) similar to that suggested for low-fired thorias at various firing temperatures.[14] Lines corresponding to single-thickness cubes, rods, and plates are shown for reference.

Direct observation by electron micrography has been used to show the relative changes in the shape and size of the circulated particles. Figure 12.7 presents a series of such photographs of the irradiated slurry and also an example of unpumped, unirradiated material. The rounding of sharp edges and the production of fine particulate matter after about 400 hr of in-pile irradiation is apparent. The progressive nature of the particle degradation is also evident. The large particles in several photographs in Fig. 12.7, apparently 5 μ or larger, may be real agglomerates or may be artifacts resulting from sample preparation procedures prior to exposure in the electron microscope.

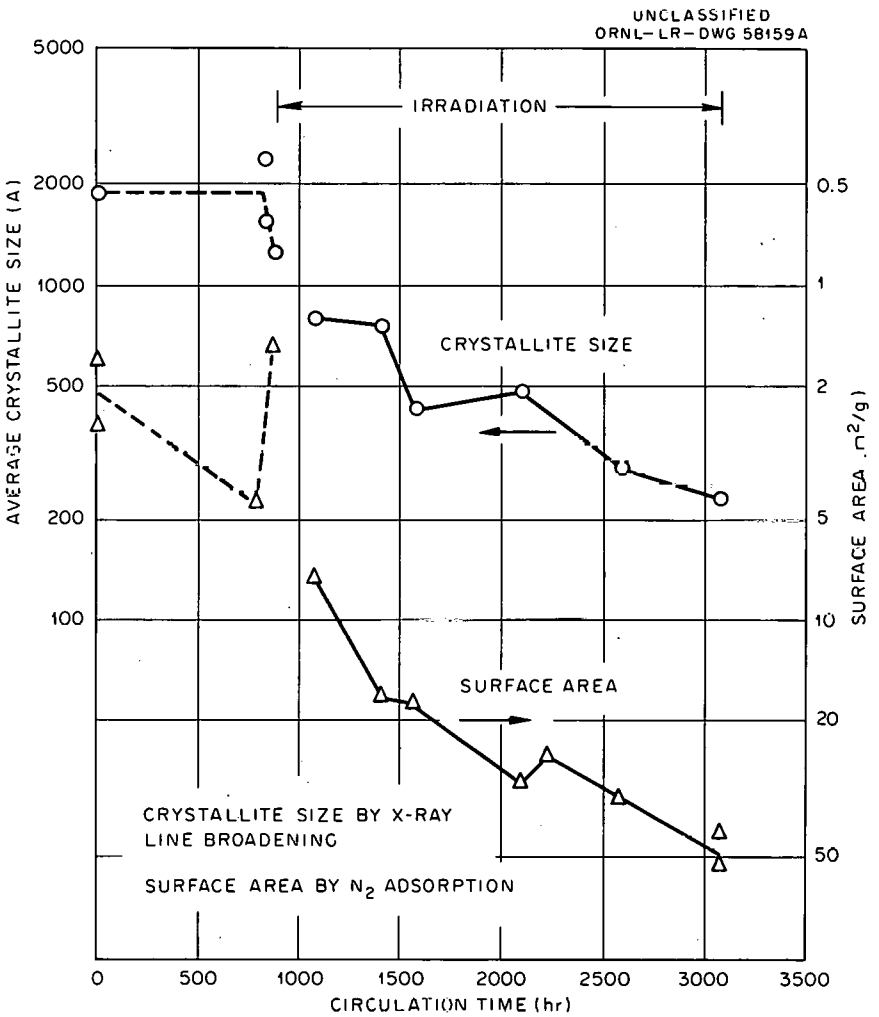

Fig. 12.5. Changes in Properties of Solids, In-Pile Loop L-2-27S.

12.3.4 Postirradiation Examination

After the loop can was removed, but prior to removal of specific sections of the loop for direct inspection, a collimated gamma-ray spectrometer survey was made at various positions along the piping, filter, core, pressurizer, and pump. As expected, some fission-product activity, notably Zr^{95}-Nb^{95}, was found in the region of the filter. Calibration to permit determination of the quantities of slurry on the filter is to be made and compared with the results of a direct cutup. In other regions of the apparatus, the presence of fission products was not detected in any significant amount. Cobalt-58, 60 activities were detected in the stainless steel at the high-flux region of the core.

Direct observation of the internal surface of the piping at the inlet and outlet of the core, particularly at a welded reducer section, has shown only a small amount of dispersed material of a metallic appearance (presumably produced while cutting) near the edges of the pipe cuts.

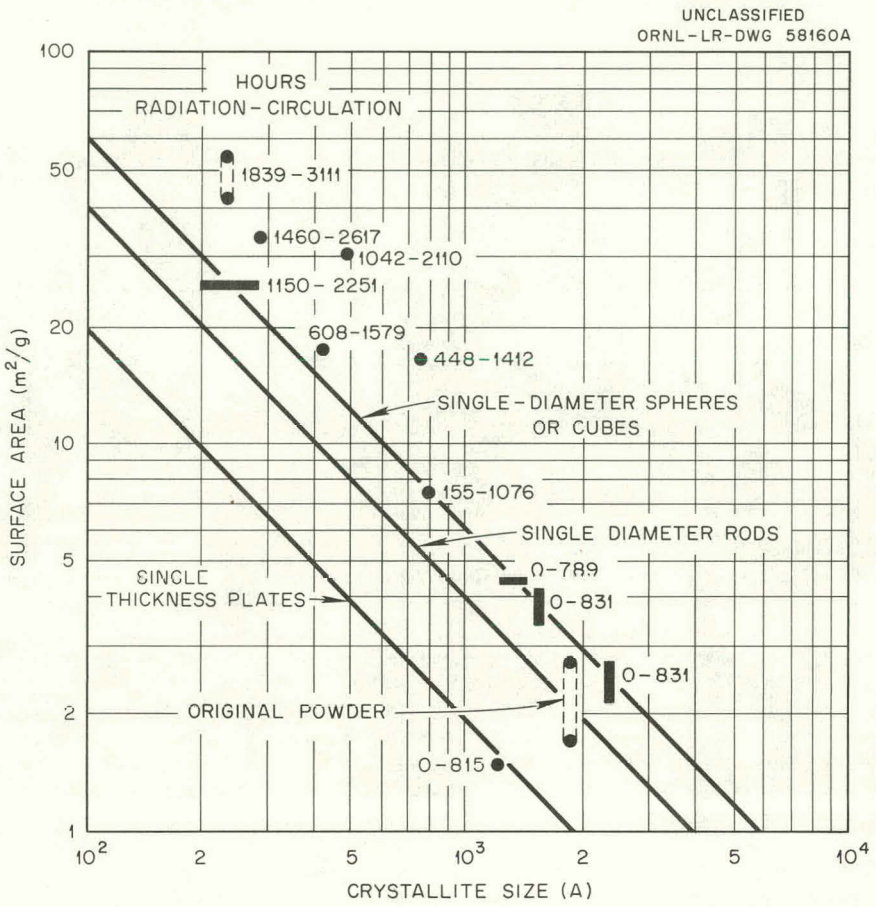

Fig. 12.6. Effect of Irradiation on Properties of Slurry Particles in In-Pile Loop Experiment.

12.3.5 Corrosion

Corrosion specimens of Zircaloy-2, type 347 stainless steel, and titanium alloys 45A and 110AT were exposed at three different flux levels and at two different velocities, 8 and 22 fps. Each specimen holder contained an identical array of coupons of the same geometry. Zircaloy-2 specimens were located at the inlet and outlet positions, with stainless steel specimens in adjacent positions. Two Zircaloy-2 specimens were placed on each side of the center line, and the two titanium coupons filled the remaining locations.

Observation of the specimens and adjacent internal surfaces of the loop piping with stero-optics did not show any marked accumulations of solids. Besides the normal oxide coloration a number of specimens showed lighter shaded regions, which might be very thin deposits of thoria solids. Several Zircaloy-2 specimens showed markings having the appearance of stringer-corrosion striations across the length of the specimens perpendicular to the flow.

Table 12.5 shows the weight-change data obtained. The flow of the slurry was from the lower to the higher position number. The total area of the 1/4- by 5/8- by 1/16-in.-thick coupons was 2.7 cm^2, and the wetted area was 1.6 cm^2. Comparison of the as-removed weights, the scrubbed-specimen weights, and the original weights indicate that loose solids on the surface ranged from 2 to 5 mg per specimen or about 1 to 3 mg/cm^2. In general, the Zircaloy-2 specimens after scrubbing showed weight gains up to 2 mg/cm^2. However, in a number of cases,

UNCLASSIFIED
ORNL-LR-DWG. 58164

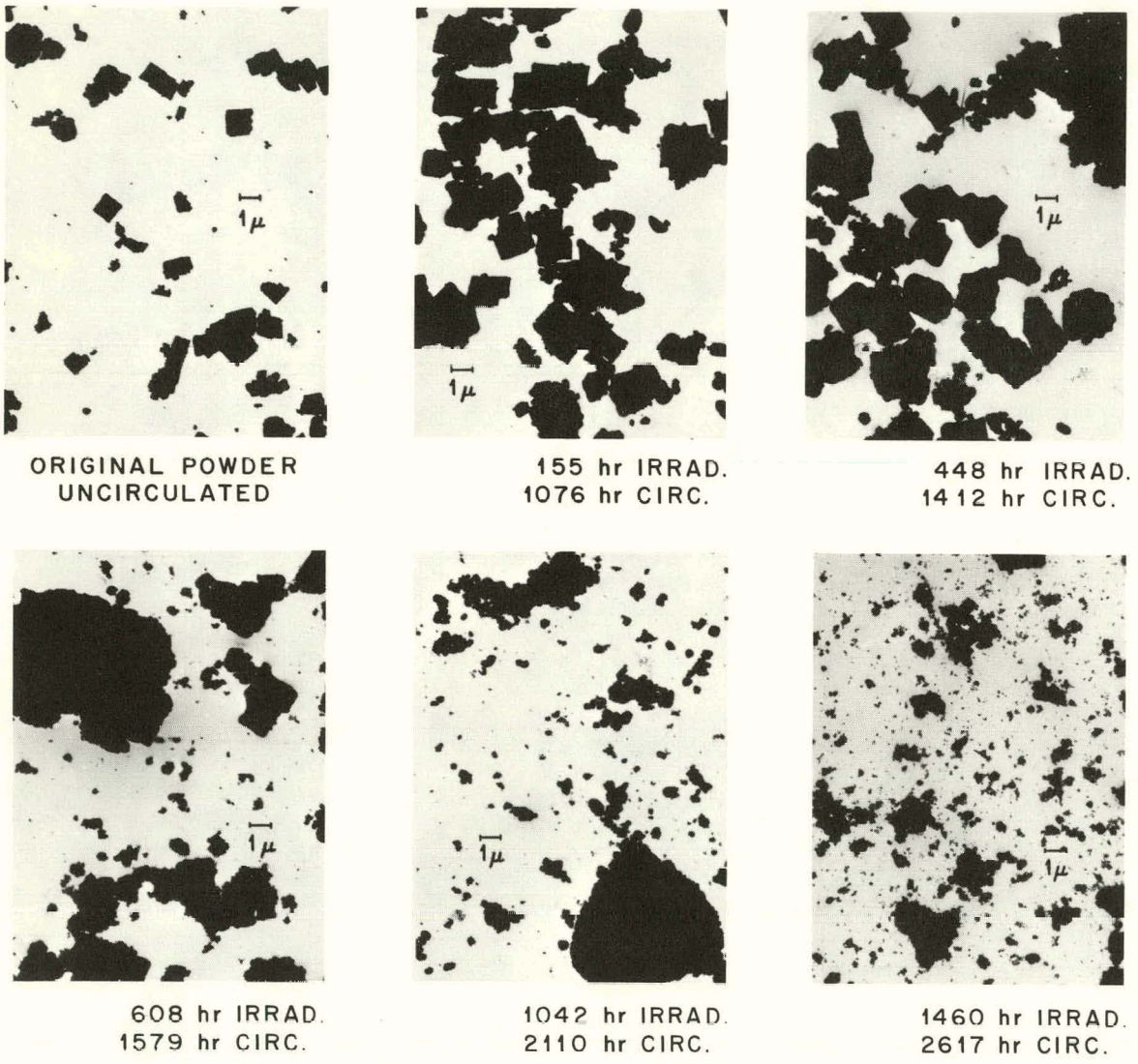

Fig. 12.7. Electron Photographs of Slurry from In-Pile Loop L-2-27S.

particularly for those specimens at the entrance region of an array, weight losses were indicated. The weight data show that the corrosion rate during the run probably averaged less than 1 mpy.

The rate of decrease of O_2 pressure and the rate of accumulation of iron during the run, as shown in a previous report,[10] indicated a generalized corrosion rate of stainless steel of 0.4 mpy.

Table 12.5. Weight Changes of Corrosion Coupons from Core of In-Pile Slurry Loop L-2-27S

	Position	Weight Change of Scrubbed Specimen		Weight Removed By Scrubbing	
		8 fps	22 fps	8 fps	22 fps
Zircaloy-2					
Low flux (~10^{12} nv)	1	+3.7 mg	-17.8 mg	3.7 mg	3.1 mg
	4	+4.0	+ 1.5	4.0	2.3
	5	+3.7	+ 2.0	4.0	1.7
	8	+3.9	+ 3.1	5.0	2.4
High flux (~10^{13} nv)	1	-3.5 mg	-	2.3 mg	-
	4	+5.0	-	4.7	-
	5	+4.7	-	3.8	-
	8	-	-	-	-
		1 mpy* = 9 mg metal lost or 3 mg oxygen pickup			
Titanium 110-AT					
Low flux	2	-0.4 mg	- 7.9 mg	3.8 mg	2.2 mg
High flux	2	-1.0	-	1.4	-
Titanium-45A					
Low flux	7	+0.5 mg	+ 0.5 mg	4.3 mg	4.7 mg
High flux	7	+0.7	-	3.3	-
		1 mpy* = 7 mg metal lost or 4 mg oxygen pickup			
Type 347 stainless steel					
Low flux	3	+0.5 mg	-10.1 mg	2.2 mg	1.6 mg
	6	+0.5	- 5.0	1.8	2.5
High flux	3	+0.3 mg	-	3.4 mg	-
	6	+0.5	-	4.2	-
		1 mpy* = 12 mg metal lost or 4 mg oxygen pickup			

*Based on exposure of two surfaces (1/4 x 1/2 in.) to flowing slurry for 3115 hr.

REFERENCES

1. R. A. McNees et al., HRP Prog. Rep. Nov. 30, 1960, ORNL-3061, p 101.

2. S. A. Reed et al., HRP Prog. Rep. Nov. 30, 1960, ORNL-3061, p 86-87.

3. J. M. Dallavalle, Micromeritics, 2nd ed., p 337, Pitman Publishing Co., New York, 1953.

4. This work was performed by P. G. Dake of the Technical Division, ORGDP.

5. R. B. Briggs, Attrition Requirements of Thoria Pellets and Coatings, ORNL-HRP-60-132 (Oct. 20, 1960).

6. S. A. Reed et al., Summary of Evaluation Tests of Code P-86-92 Thoria Pellets Prepared from Batch D-40 ThO_2 Powder, ORNL-CF-60-12-74.

7. S. A. Reed et al., Summary of Evaluation Tests of Code P-95-98 Experimental Thoria Pellets, ORNL-CF-61-3-107.

8. E. L. Compere et al., HRP Quar. Prog. Rep. July 31, 1960, ORNL-3004, p 90.

9. A. M. Weinberg and E. P. Wigner, The Physical Theory of Neutron Chain Reactors, p 83, University of Chicago Press, Chicago, 1958.

10. E. L. Compere et al., HRP Prog. Rep. Nov. 30, 1960, ORNL-3061, p 88.

11. Ibid., p 89-94.

12. H. C. Savage et al., HRP Quar. Prog. Rep. July 31, 1960, ORNL-3004, p 96-97.

13. H. C. Savage et al., HRP Quar. Prog. Rep. Apr. 30, 1960, ORNL-2947, p 101-107.

14. J. P. McBride, "Preparation and Characterization of Thorium Oxide and Its Aqueous Suspensions," p 147, in Fluid Fuel Reactors, J. A. Lane et al., editors, Addison-Wesley, Reading, Mass., 1958.

PART V. FUEL MANUFACTURE

13. THORIUM OXIDE PRODUCTION

O. C. Dean C. E. Schilling

Methods of preparing rounded 1/8- to 1/4-in. attrition-resistant thoria and thoria-urania particles are being investigated. The most promising method at present appears to be the sol-gel process.

13.1. PREPARATION OF OXIDE SOLS

Sols were prepared from ThO_2 made by 650°C firing of thorium oxalate and by steam stripping of the nitrate from thorium nitrate crystals.

13.1.1 Preparation from Oxalate-Derived Thoria

Thorium oxalate fired at 650°C was dispersed in hot 1-2 *M* HNO_3 and then evaporated at 135°C and redispersed in water or settled and decanted at room temperature until sufficient nitrate had been removed to form a stable sol (Fig. 13.1a). When uranium was included, it was added to the sol, prior to evaporation, as $UO_3 \cdot H_2O$ or as ammonium diuranate. Approximately 1 hr of blending at 90°C was required to distribute the uranium homogeneously on the thoria particles.

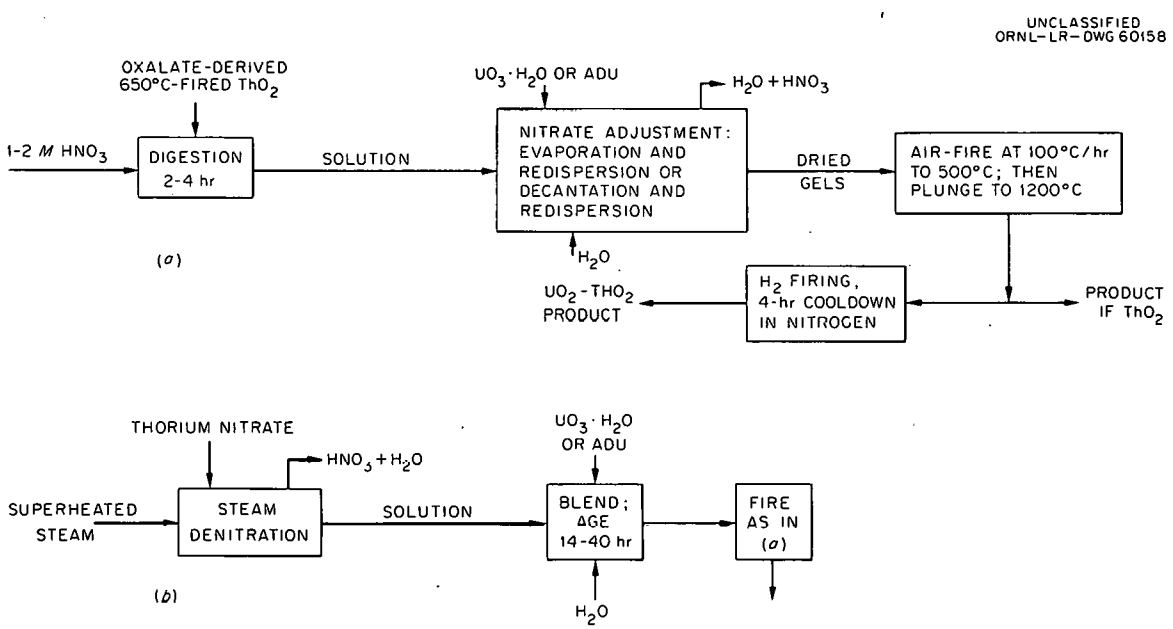

Fig. 13.1. Schematic Flowsheets for Sol-Gel Process from (*a*) Oxalate-Derived ThO_2 and (*b*) Steam-Denitrated ThO_2.

13.1.2 Preparation from Steam-Denitrated Thoria

From 1-kg batches of thorium nitrate crystals in a 4- by 12-in. rotary reactor, about 97% of the nitrate was stripped with steam at 390 to 400°C, about 3 hr being required. The oxide was then dispersed in water (Fig. 13.1b).

13.1.3 Properties of Sols of Thoria Prepared from Nitrate by Steam Stripping

The N/Th atom ratio of the oxide from which the sol is prepared is important to the strength, shape, and density of the oxide particles prepared from it. The optimum N/Th ratio is 0.13 to 0.15 and appears to be that which saturates the surface of the solid and gives only enough thorium nitrate in solution to produce a pH not less than 3 at any time during the evaporation. The optimum soluble-thorium concentration appears to be 10^{-4} *M*. Oxide products with N/Th atom ratio >0.15 dispersed readily in water, but on standing overnight part of the solids separated as a soft floc. When separated from the sol supernatant, this floc could be easily dispersed by dilution with water. Evaporation of this type of sol led to the deposition of more flocs. The ThO_2 particles produced were strained (Fig. 13.2). Frequently they fractured in a glass-like pattern. The fired product had small, dense particles. The diametral shrinkage factor from gel to fired-fragment stage was ~1.8.

When a steam denitration temperature >400°C was used with a longer exposure time, or when air denitration was used, a low-nitrate (<0.13) precursor was prepared in which a relatively large fraction of particles could not be readily dispersed by water. The nondispersed particles were chalky or granular. When prepared at low temperature, they were chalky and could be dispersed by addition of small amounts of HNO_3, but when made at high temperature (>425°C) or by air denitration, long refluxing with 1-2 *M* HNO_3 was required. Aging at 90°C for 14 to 40 hr slightly increased the small particle suspension. Evaporation of such sols without removal of nondispersed particles led to the deposit of nonhomogeneous gels with glassy particles embedded in a chalky matrix. When fired, such particles were weak and had low particle density.

Three ~2 *M* ThO_2 sols, having N/Th ratios of 0.35, 0.14, and 0.104, were supercentrifuged in a centrifugal field of ~50,000 G for 4 hr to separate intermicellar liquid from solids. Analyses and states of sols, supernatant liquids, and separated solids are summarized in Table 13.1. The sol with an N/Th ratio of 0.14 gave strong, vitreous particles on firing, and they showed little cracking. Particles prepared from the lower nitrate sol were chalky, and those from the higher nitrate material were small and strained.

Table 13.1. Supercentrifugation of Sols

Initial ThO_2 concentration: ~2 *M*

Sol		Supernatant		Undispersed Material	
N/Th Atom Ratio	State	Th Conc. (*M*)	pH	N/Th Ratio[a]	Appearance
0.35	Flocculated	0.11	2.1	0.13	Clear, glassy
0.143	Well dispersed	0.5×10^{-4}	3.1	0.11	Mostly clear, glassy
0.104	Poorly dispersed	4×10^{-4}[b]	3.7	0.08	Chalky, overlaid with ~5% clear

[a]Corrected for nitrate in adhering solution.

[b]Supernatant not entirely clear.

Fig. 13.2. Strained 900°C-Fired Thoria Gels from Steam-Stripped Sol Precursors Which Contained Excessive Nitrate. 18X.

13.2 CALCINATION OF THORIA GELS

Unexpectedly, the density of ThO_2 particles prepared by the sol-gel process was slightly higher when calcined in hydrogen at 825 to 1255°C than when calcined in air (Table 13.2). Hydrogen-fired products were purplish-black or mottled; air-fired samples were off-white. No color-producing cationic impurity >2 ppm was detected by spectrographic analysis. All samples were prefired at 500°C, and since the ThO_2 samples were dispersed in HNO_3 on preparation of the sol, the possibility of the presence of carbon was ruled out. Because of the unexpected results of the first series, a second series of parallel firings was conducted; the results were the same. Additional test samples, fired in hydrogen from room temperature to 1000°C, gave purplish-black products while those fired in air were white. Refiring the black samples for 3 to 4 hr in air at 1200°C produced the usual off-white ThO_2 characteristic of air-firing. It is possible that the hydrogen reduces residual nitrate to nitride which acts as a flux in the densification of ThO_2.

Table 13.2. Effects of Atmospheres and Temperature on Density and Crystallite Size for Thorium Oxide Prepared by the Sol-Gel Process

Temp. (°C)	Density[a] (g/cc)		X-Ray Crystallite Size (Å)	
	Hydrogen-Fired	Air-Fired	Hydrogen-Fired	Air-Fired
825	9.05	9.00	190	160
940	9.50	9.30	670	460
1040	9.50	9.80	1520	1490
1145	9.95	9.85	1930	2170
1255	9.90	9.80	>2500	>2500

[a]Toluene immersion method; not outgassed by vacuum.

A slight reduction in density on increasing the firing temperature from 1150 to 1250°C was observed consistently for both thoria and thoria-urania gels.

13.3 PREPARATION OF ROUNDED THORIA PELLETS

Both oxalate- and nitrate-derived ThO_2 gels with ThO_2 concentrations of 1-8 *M* were cast into rounded graphite molds or were hand rolled and evaporated at various rates in air, vacuum, or steam at temperatures from 25 to 135°C to form spheres. All spheres cracked during drying because of the large volume shrinkage (a factor of 3 to 8). Sols containing obviously high nitrate concentrations had the highest shrinkage rate, and gels produced from them by evaporation had the highest cracking incidence. Sols extremely low in nitrate gave chalky gel deposits which tended to crumble.

In experiments to explore methods of reducing shrinkage on evaporation, sols were loaded with oxalate-derived ThO_2 powders that had been fired at 650, 1000, and 1400°C, nitrated oxalate-derived powders, and nitrate-derived ThO_2 powders that had been heated 10 min at 350, 400, 450, and 500°C. When added to sols already formed, oxides that had not been nitrated and nitrate-derived oxides that had been heated to above 450°C destabilized the sols to granular materials. When such sols were evaporated and fired, the products were weak, chalky fragments. Although products made by slow evaporation and firing of sols containing powders were the strongest preparations, none survived processing without some cracking. Steam and vacuum drying did not improve the integrity of the products.

13.4 EVALUATION OF SOL-GEL FRAGMENTS FOR STRENGTH AND ATTRITION RESISTANCE

Thoria-urania fragments prepared by the sol-gel process are of promising hardness and strength. Ten fragments containing nominally 5% uranium and having approximately the shape and the size desired were subjected to six successive 1-hr spouted-bed attrition tests with corresponding weight losses of 2.13, 0.88, 0.68, 0.96, 1.13, and 0.28%. Microscopic examination after testing showed that most of the loss was due to the grinding-off of sharp points and edges (Figs. 13.3 and 13.4). The surface area of a 10-g sample was lower than could be measured by nitrogen adsorption methods.

Fig. 13.3. Thorium–5 wt % Uranium Fragments Prepared from Oxalate-Derived Thoria Sols Before Grinding in Spouted Bed. 12X.

Fig. 13.4. Thorium–5 wt % Uranium Fragments Prepared from Oxalate-Derived Thoria Sols After Grinding 6 hr in Spouted Bed. 12X.

13.5 FORMATE-STABILIZED SOLS

Strong particles of 9.83-g/cc density, with few cracks, were produced from a low-nitrate-content ThO_2 (N/Th ratio of 0.039) prepared by steam denitration of thorium nitrate. The production method consisted in aging a 3 *M* ThO_2 suspension in 2 *M* formic acid for 72 hr, evaporation of the sol, and firing of the gel produced.

When a 4 *M* sol of high-nitrate steam-stripped thoria was refluxed in 3.5 *M* formic acid for six days to remove all nitrate, considerable chalky solids separated. These were ball-milled to redisperse them and then added to the suspension. Evaporation, prefiring, and 1200°C firing produced blocky but large chalky particles.

PART VI. METALLURGY

14. METALLURGY

A. Taboada

F. W. Cooke R. A. McNees
A. J. Taylor

14.1 EFFECT OF PREFERRED ORIENTATION ON MICROHARDNESS OF ZIRCALOY-2

A study was undertaken to determine to what extent Knoop microhardness was affected by and could be correlated with the deformation characteristics and anisotropy of properties of Zircaloy-2 sheet exhibiting a high degree of preferred orientation. The texture of the sheet used in the study was characterized by a maximum concentration of basal poles near the sheet normal, a maximum concentration of first-order prism poles in the transverse direction (the short dimension of the prism being parallel to the rolling direction), and a maximum concentration of second-order prism poles in the rolling direction and at 60° from the rolling direction in the plane of the sheet (Figs. 14.1 and 14.2). This was a complex texture in that there was a distribution of basal poles in a zone about the rolling direction so that there were some basal poles in the transverse direction, some first-order prism poles in the sheet normal direction, and a more or less random distribution of second-order prism planes about the rolling direction.

The slip system in pure zirconium is $\{10\bar{1}0\}\langle\bar{1}2\bar{1}0\rangle$; that is, the slip plane is the primary prism plane and the slip direction is in the basal plane.[1] Deformation by twinning is also significant in this metal. The deformation systems for Zircaloy-2 have not been determined but are presumed to be the same as those for pure zirconium.

Specimens were prepared metallographically having orientations such that the normal to the plane of polish was in the rolling direction for one specimen (rolling-direction specimen), in the transverse direction for the second (transverse-direction specimen), and near the direction of the maximum concentration of basal poles for the third (basal-plane specimen). After polishing, the cold-worked surface layer was removed by etching.

Knoop hardness measurements were obtained at 37 orientations of the indenter for each specimen. These orientation changes consisted of 5° rotations about the specimen normal with one of the standard sheet directions taken as a reference. The reference direction for the basal-plane and transverse-direction specimens was the rolling direction, and for the rolling-direction specimen it was the transverse direction.

In an attempt to correlate the hardness data with the known texture of the sheet and its assumed deformation systems, a model was proposed to describe the deformation that occurs when a Knoop hardness indentation is made. It was proposed that plastic deformation tends to occur by slip parallel to the plane of polish and in a direction perpendicular to the major axis of the indenter. This implies

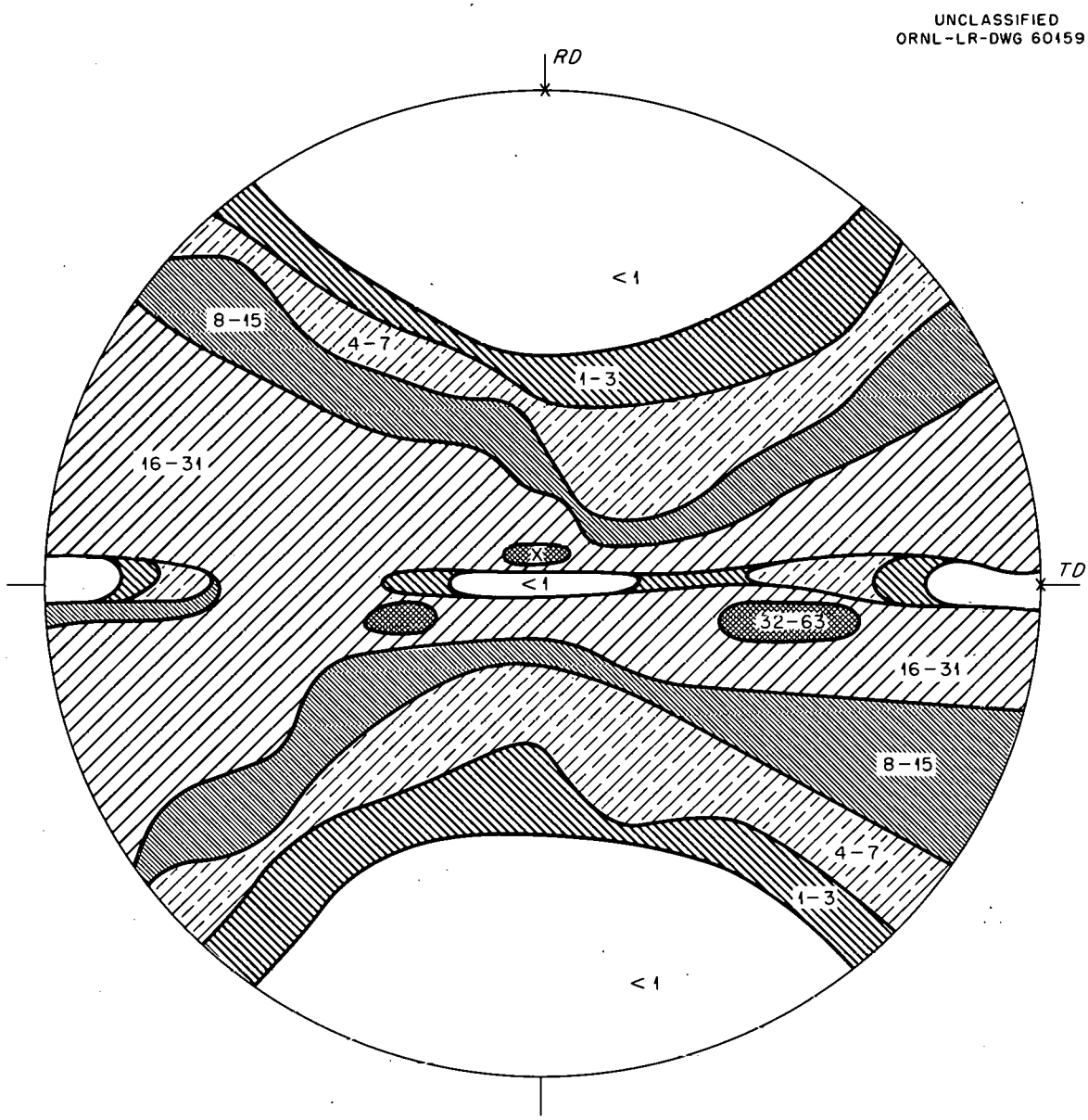

Fig. 14.1. (002) Pole Figure for Zircaloy-2 Schedule 62. X indicates specimen orientations.

that deformation is caused by a wedging action of the indenter. Although this model does not take deformation by twinning into consideration, it was found to correlate well with the observed behavior.

Figures 14.3, 14.4, and 14.5 are plots of Knoop hardness as a function of indenter orientation for the rolling-direction, transverse-direction, and basal-plane specimens, respectively.

The plane of polish of the rolling-direction specimen was parallel to the maximum concentration of second-order prism planes, which were more or less randomly distributed about the specimen normal. It would therefore be expected that the hardness would change only slightly with rotation of the indenter about the specimen normal. The data presented in Fig. 14.3 show that this was indeed the case.

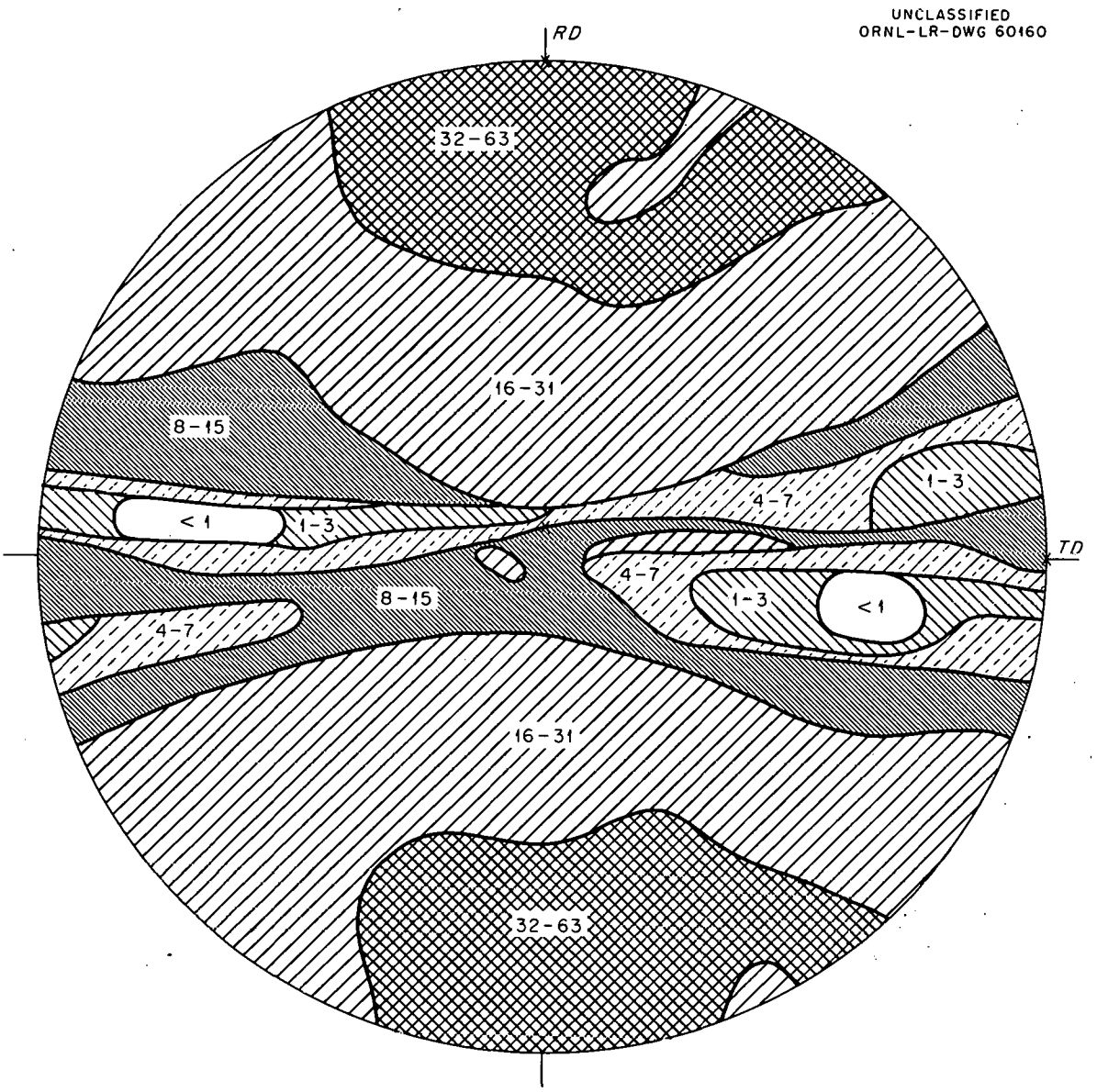

Fig. 14.2. (110) Pile Figure for Zircaloy-2 Schedule 62. X indicates specimen orientations.

The plane of polish of the transverse-direction specimen had the same orientation as that of the maximum concentration of first-order prism planes, with some basal planes also being present. According to the deformation model, the hardness should have been a maximum for this specimen when the major axis of the indenter was parallel to the rolling direction. For this orientation, the proposed direction of deformation was perpendicular to the rolling direction, which was the slip direction. Furthermore, the Knoop hardness should have decreased as the indenter was rotated away from the rolling direction, to a minimum when its major axis was in the direction of the sheet normal. The data in Fig. 14.4 show that the hardness did vary in this manner.

The basal-plane specimen had the maximum concentration of basal planes and some first-order prism planes parallel to its plane of polish. The data recorded in Fig. 14.5 show that the hardness of this specimen is a maximum at 0 and 180°

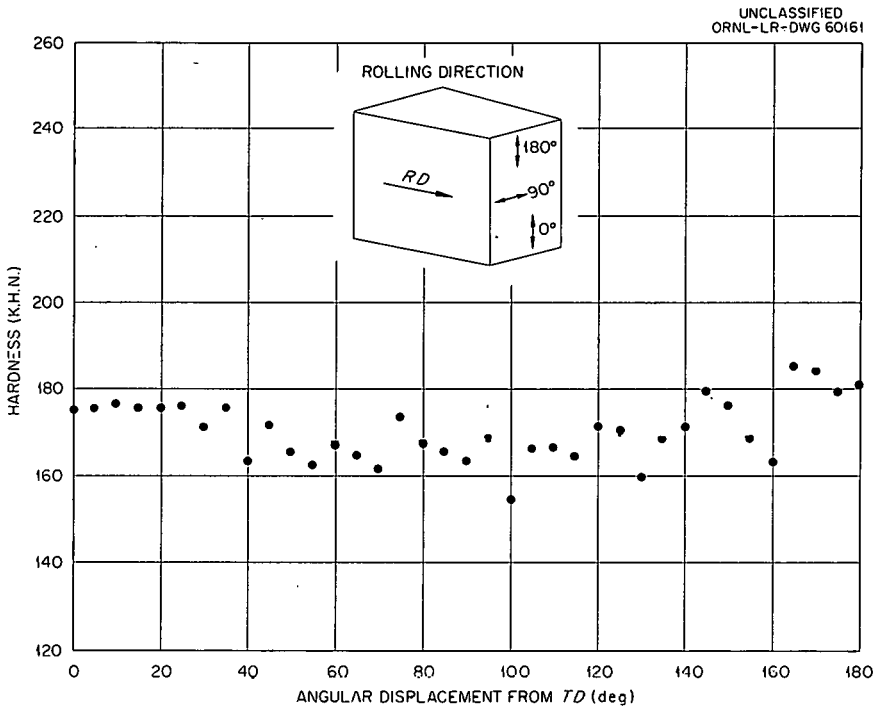

Fig. 14.3. Knoop Hardness as a Function of Indenter Orientation for the Rolling-Direction Specimen.

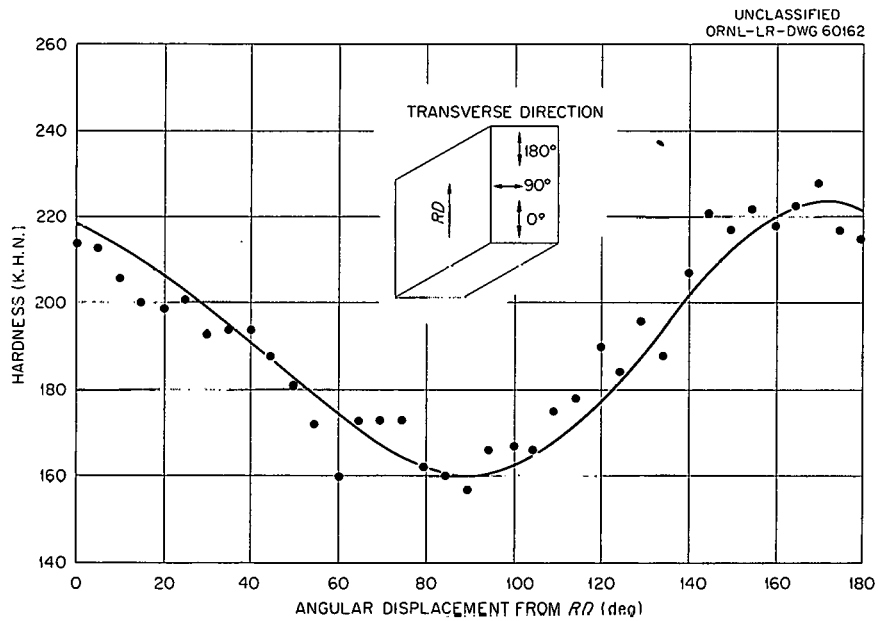

Fig. 14.4. Knoop Hardness as a Function of Indenter Orientation for the Transverse-Direction Specimen.

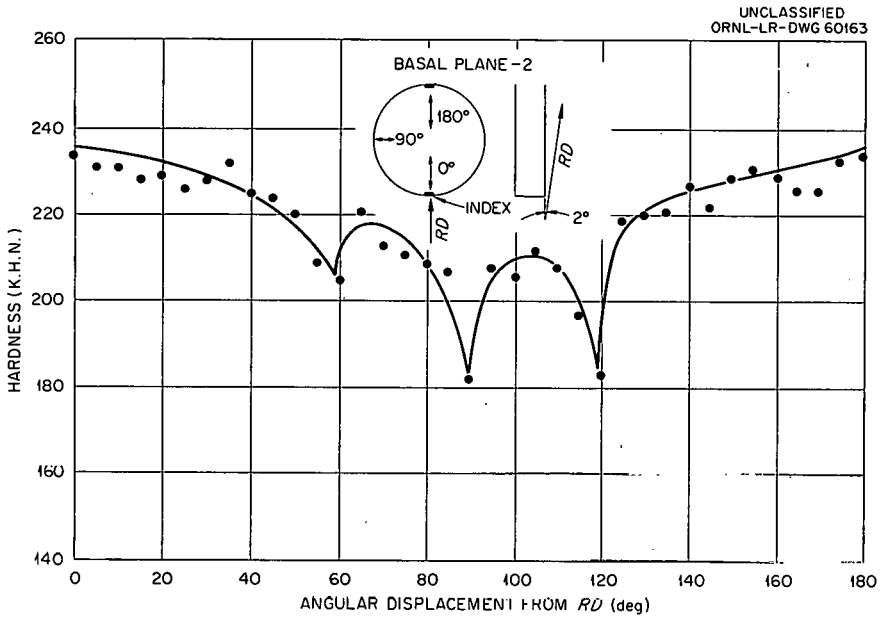

Fig. 14.5. Knoop Hardness as a Function of Indenter Orientation for Basal-Plane Specimen.

and a minimum at 90°, which is similar to the behavior of the transverse-direction specimen. This behavior is apparently due to the presence of the first-order prism planes.

Since the grains oriented with their basal planes in the plane of polish are not able to deform by slip according to the deformation model, it is not too surprising that their presence does not affect the hardness variations more strongly. These grains probably deform by twinning, which may account for the hardness minima which occur with hexagonal symmetry at 60 and 120°. The absence of hardness minima at 0 and 180°, which would be consistent with a hexagonal symmetry, can be explained by the overshadowing effect of grains having first-order prism planes in the plane of polish. The extremely short range of orientations over which the minima at 60, 90, and 120° occur was not expected. Nonetheless, several indentation hardness transverses, including transverses at 1° increments in the vicinity of 60, 90, and 120°, have verified that significant minima occur at these orientations.

14.2 THORIA-PELLET FABRICATION

Two different methods have been investigated for forming rounded bodies of thorium oxide for use in the blanket region of a breeder reactor. The problems associated with one approach were very well defined, and the method was shown to be extremely difficult to control. The other method appears to be very promising and amenable to the necessary controls.

The method, previously described,[2] whereby slurry-type oxides can be modified for use in pressing dome-end pellets was used with several different lots of one particular batch (D-40) of thorium oxide. Persistent difficulties were experienced during the pressing of each of these lots, however, and consistent production of sound lamination-free bodies was not possible. Figure 14.6a shows typical variations between pellets produced from a single, superior batch of modified D-40 oxide, while Fig. 14.6b shows the great variation between pellets formed from other batches of modified D-40 oxide. The experience with these modified

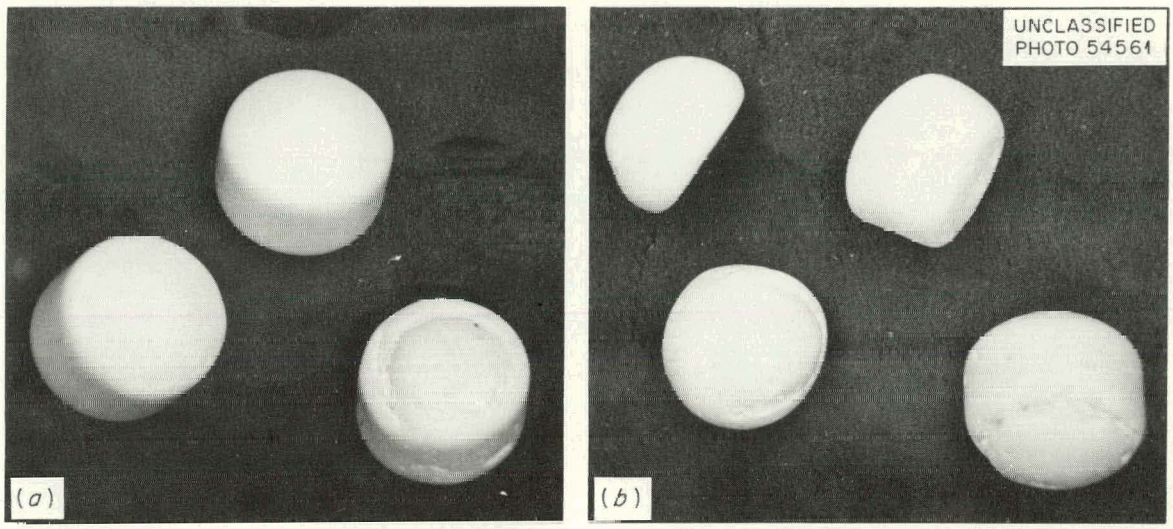

Fig. 14.6. Domed-End Cylinders Pressed from Modified D-40 Thorium Oxide and Fired to 1650°C. (a) Variations between pellets produced from a single, superior batch of modified D-40 ThO_2. (b) Variations between pellets produced from four other batches of modified D-40 ThO_2. Magnification 5X.

powders showed clearly that it is extremely difficult to partially sinter ThO_2 to the point that it will not laminate while being pressed into a hemispherical shape and at the same time retain sufficient sinterability to allow for firing the pressed object to a high density. These difficulties are magnified by the fact that small differences in temperature or heating time in the region of 1450°C markedly affect the properties of the powder. Likewise, the ball-milling operation subsequent to the 1450°C heating step is neither easily reproducible nor precisely adjustable to correct for variations introduced during the heating step. Because of these difficulties, this method of forming pellets was abandoned in favor of a more promising method. However, several batches of pellets prepared in this fashion were submitted to the Reactor Chemistry Division for physical testing (see Sec. 12.1).

The more promising method consists of forming, with the aid of an organic binder, a very reactive powder into cubes at pressures low enough to avoid laminations and then abrading these cubes into spherical shapes. The cubes are first tumbled dry while still in the unfired state, and the abraded powder is collected, repressed into cubes, and the cycle repeated, thereby avoiding reprocessing chemically the material removed during reduction of the cubes to spheres. These rough spherical shapes are fired to 1300°C and then tumbled in water to polish the surface of the spheres. A final firing to temperatures in the range of 1650 to 1800°C produces a body with a density as high as 9.8 g/cm^3. The several stages in preparing spheres by this method are shown in Fig. 14.7.

Studies with a single-action press, a slurry-type oxide, and a die case 0.211 in. square have shown that a better body--i.e., higher green density without laminations--is produced if the oxide is heated to 1000°C for 2 hr before being pressed. A fine, smooth powder, free of hard agglomerates, produces cubes which abrade more uniformly into a spherical shape than does a powder which contains such lumps. Use of about 2% Carbowax 4000 as a binder produces a body of good green strength, yet one which will abrade at a reasonable rate. With 4 or 5% binder, the milling time necessary to produce spherical shapes is 5 to 10 times longer than when only 2% binder is used.

UNCLASSIFIED
PHOTO 54562

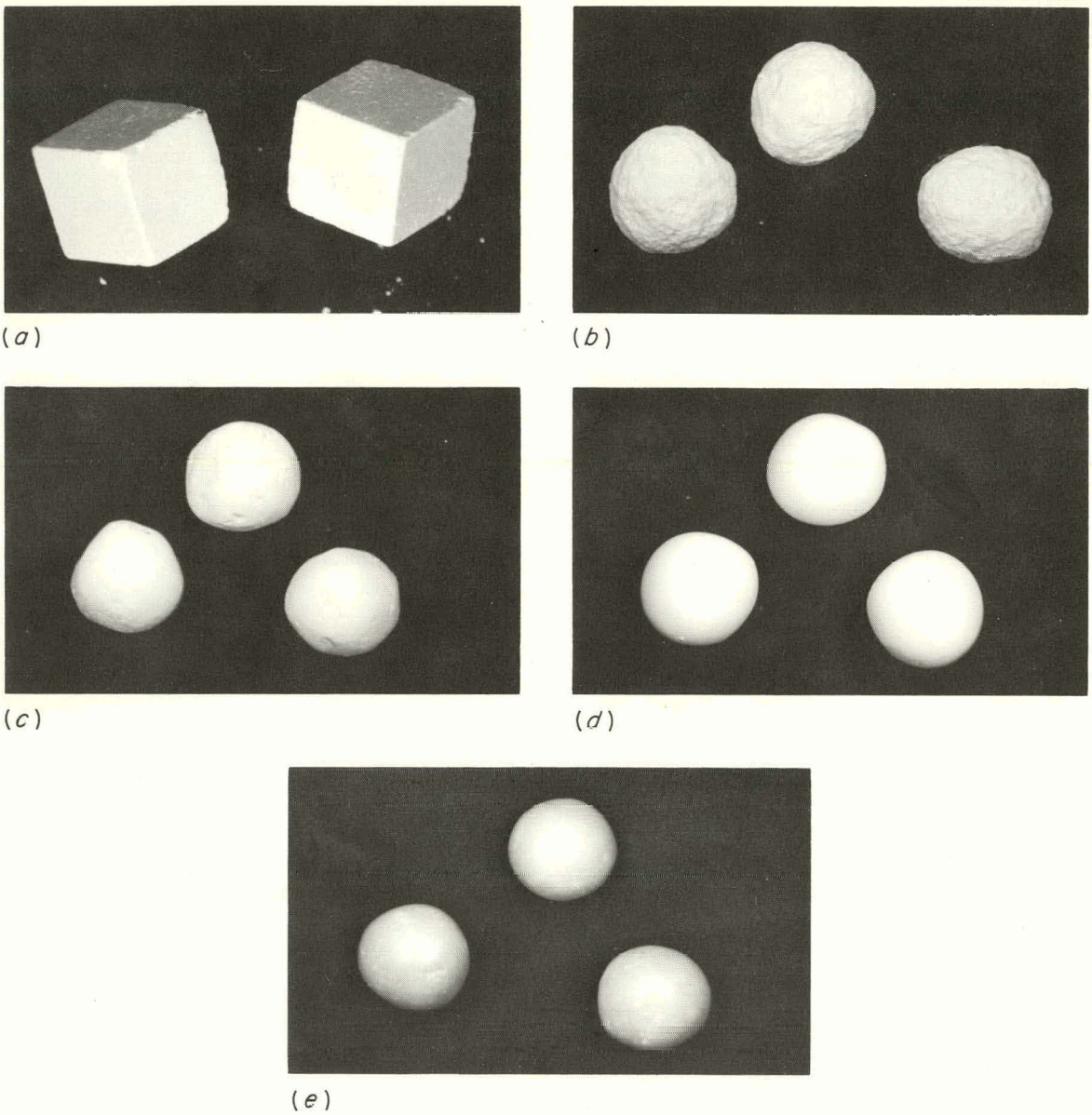

Fig. 14.7. Five Stages in Preparation of ThO_2 Spheres from Cubes. (a) As-pressed cubes. (b) After tumbling. (c) After firing to 1300°C. (d) After polishing. (e) After firing to 1800°C. Magnification 3.3X.

Soft firing the tumbled shapes to 1300 to 1350°C produces a body which can be polished readily by wet tumbling either alone or with alumina balls. Firing to 1200°C produces a chalky body which does not polish satisfactorily and which abrades rapidly; bodies fired to 1400 to 1450°C are difficult to polish. Final firing may be done in air-controlled atmosphere to any desired temperature. Twenty-five pounds of pellets have been prepared by this technique, and an additional 25 lb are now being prepared for use in large-scale loop and fluidized-bed studies to be conducted by the Reactor Chemistry Division. In addition, several small batches of pellets prepared in this manner were submitted to the Reactor Chemistry Division for preliminary evaluation (see Sec. 12.1). Studies are in progress to

determine the effect of such variables as green density, sintered density, chemical composition, and powder characteristics on the mechanical and chemical properties of the spheres in an effort to improve their usefulness as a blanket material for breeder reactors.

A batch of mixed ThO_2 - 1% UO_2 spheres was prepared by using the pressed-cube technique. The powder for this purpose was prepared by mixing the pure oxides in a Waring Blendor along with an aqueous solution of Carbowax. After the green cubes had been tumbled to spherical shapes, the spheres were fired to 600°C slowly in air and then to 1350°C in hydrogen. After wet polishing, the spheres were fired to 1750°C for 2 hr in hydrogen. With the exception of a few regions which contained particles of UO_2 that had not been rendered sufficiently small during the blending operation, a uniform solid solution was obtained by this method. It is planned to investigate other methods of blending in order to obtain even better dispersions.

REFERENCES

1. E. J. Rapperport, Room Temperature Deformation Processes in Zirconium, NMI-1199 (Feb. 24, 1958).

2. A. Taboada et al., HRP Prog. Rep. Nov. 30, 1960, ORNL-3061, p 101.

PART VII. ANALYTICAL CHEMISTRY

15. ANALYTICAL CHEMISTRY

H. E. Zittel D. L. Manning
G. Goldstein

15.1 AMPEROMETRIC TITRATION OF COPPER AND RARE-EARTH ELEMENTS

An amperometric method previously described[1] for the titration of thorium with ethylenediaminetetraacetic acid in which Fe(II) is used as the indicator has been extended to the determination of copper and some of the rare-earth elements (Tb-earth but not Ce-earth elements).

Copper is titrated by this method in a medium buffered at pH 2.5 with a mixture of chloroacetic acid and sodium chloroacetate. Test results for copper in synthetic homogeneous-reactor core and blanket solutions were as follows:

	Cu (mg)		
Sample	Added	Found	Error
HR core	1.92	1.92	0.00
	1.92	1.92	0.00
HR blanket	0.90	0.87	-0.03
	1.50	1.50	0.00

Rare-earth elements are titrated with EDTA in a medium buffered at pH 4.5. The following test results were obtained by titrating solutions of 14 rare-earth elements (all except promethium) in the trivalent state:

		mg			
Element	Log K[(a)]	Added	Found	Error	
La	15.5	3.00	(b)	---	
Ce	16.0	4.20	(b)	---	
Pr	16.4	4.00	(c)	---	Not
Nd	16.6	4.00	(c)	---	Quantitative
Sm	17.1	4.00	3.32	-0.68	
Eu	17.4	4.21	3.56	-0.65	
Gd	17.4	3.75	3.51	-0.24	
Tb	17.9	4.00	3.93	-0.07	
Dy	18.3	7.42	7.39	-0.03	
Ho	18.7	4.97	4.95	-0.02	
Er	18.9	3.67	3.70	0.03	Quantitative
Tm	19.3	4.26	4.56	0.30	
Yb	19.5	3.48	3.58	0.10	
Lu	19.8	6.74	6.68	-0.06	

(a) Log of the metal-EDTA stability constant.
(b) Indicator current obtained upon addition of first increment of titrant.
(c) End point poorly defined.

From the foregoing data it is indicated that only those elements of the rare-earth group which form EDTA chelates with stability constants exceeding $10^{17.5}$ (Tb to Lu, atomic No. 65 to 71, inclusive) can be titrated satisfactorily by this method.

This method is adaptable to remote operations and therefore provides an alternative method for the determination of copper in samples of irradiated fuel or blanket solutions from the Homogeneous Reactor Test.

REFERENCE

1. H. E. Zittel, Amperometric Titrations with EDTA Using Iron(II) as the Indicator Application to the Determination of Thorium, ORNL CF-61-2-34 (Feb. 6, 1961).

THIS PAGE

WAS INTENTIONALLY

LEFT BLANK

ORNL-3167
UC-80 - Reactor Technology
TID-4500 (16th ed.)

INTERNAL DISTRIBUTION

1. C. E. Center
2. Biology Library
3. Health Physics Library
4. Metallurgy Library
5-6. Reactor Division Library
7-9. Central Research Library
10-14. Laboratory Records Department
15. Laboratory Records, ORNL R.C.
16. G. M. Adamson
17. L. G. Alexander
18. A. L. Bacarella
19. J. E. Baker
20. S. J. Ball
21. J. C. Banter
22. S. E. Beall
23. L. L. Bennett
24. A. M. Billings
25. D. S. Billington
26. E. P. Blizard
27. R. Blumberg
28. E. G. Bohlmann
29. C. J. Borkowski
30. G. E. Boyd
31. J. C. Bresee
32. F. R. Bruce
33. J. R. Buchanan
34. W. D. Burch
35. S. R. Buxton
36. A. D. Callihan
37. W. L. Carter
38. G. H. Cartledge
39. R. H. Chapman
40. R. A. Charpie
41. E. L. Compere
42. F. L. Culler
43. D. G. Davis
44. R. J. Davis
45. D. M. Eissenberg
46. J. L. English
47. D. E. Ferguson
48. J. H. Frye, Jr.
49. C. H. Gabbard
50. J. L. Gabbard
51. W. R. Gall
52. E. H. Gift
53. H. E. Goeller
54. J. C. Griess
55. W. R. Grimes
56. E. Guth
57. R. H. Guymon
58. P. A. Haas
59. J. Halperin
60. P. H. Harley
61. R. J. Harvey
62. P. N. Haubenreich
63. D. N. Hess
64. J. W. Hill
65. E. C. Hise
66. A. Hollaender
67. P. P. Holz
68. H. P. House
69. A. S. Householder
70. G. H. Jenks
71. J. E. Jones Jr.
72. R. G. Jordan (Y-12)
73. W. H. Jordan
74. P. R. Kasten
75. C. P. Keim
76. M. T. Kelley
77. M. J. Kelly
78. F. Kertesz
79. J. O. Kolb
80. U. Koskela
81. K. A. Kraus
82. J. A. Lane
83. C. G. Lawson
84. S. C. Lind
85. R. S. Livingston
86. M. I. Lundin
87. R. N. Lyon
88. J. L. Marsh (C&CC, South Charleston)
89. W. L. Marshall
90. J. P. McBride
91. H. F. McDuffie
92. H. A. McLain
93. J. R. McWherter
94. E. C. Miller
95. R. L. Moore
96. C. S. Morgan
97. K. Z. Morgan
98. L. E. Morse
99. J. P. Murray (K-25)
100. M. L. Nelson
101. P. D. Neumann
102. A. R. Olsen
103. P. Patriarca
104. F. N. Peebles
105. A. M. Perry

106. M. L. Picklesimer
107. H. B. Piper
108. L. R. Quarles
109. S. A. Reed
110. W. D. Reel
111. P. M. Reyling
112. S. A. Reynolds
113. L. Rice
114. D. M. Richardson
115. R. C. Robertson
116. H. C. Roller
117. H. C. Savage
118. C. E. Schilling
119. H. E. Seagren
120. C. H. Secoy
121. E. D. Shipley
122. A. J. Shor
123. M. D. Silverman
124. M. J. Skinner
125. A. H. Snell
126. I. Spiewak
127. H. H. Stone
128. R. W. Stoughton
129. C. D. Susano
130. J. A. Swartout
131. A. Taboada
132. E. H. Taylor
133. W. Terry
134. P. F. Thomason
135. M. Tobias
136. W. E. Unger
137. R. Van Winkle
138. D. R. Vondy
139. D. W. Vroom
140. H. O. Weeren
141. A. M. Weinberg
142. S. H. Wheeler
143. E. P. Wigner (Consultant)
144. H. D. Wills
145. G. C. Williams
146. J. C. Wilson
147. C. E. Winters
148. C. H. Wodtke
149. T. F. Woo
150. H. E. Zittel
151. ORNL - Y-12 Technical Library, Document Reference Section
152. HRP Director's Office, Y-12

EXTERNAL DISTRIBUTION

153. D. H. Groelsema, AEC, Washington
154. F. P. Self, AEC, ORO
155. M. E. Wadsworth, University of Utah
156. Division of Research and Development, AEC, ORO
157-760. Given distribution as shown in TID-4500 (16th ed.) under Reactor Technology (75 copies - OTS)
761-762. D. F. Cope, Division of Research and Development, AEC, ORO

Reports previously issued in this series are as follows:

ORNL-527	Date Issued, December 28, 1949
ORNL-630	Period Ending February 28, 1950
ORNL-730	Feasibility Report - Date Issued, July 6, 1950
ORNL-826	Period Ending August 31, 1950
ORNL-925	Period Ending November 30, 1950
ORNL-990	Period Ending February 28, 1951
ORNL-1057	Period Ending May 15, 1951
ORNL-1121	Period Ending August 15, 1951
ORNL-1221	Period Ending November 15, 1951
ORNL-1280	Period Ending March 15, 1952
ORNL-1318	Period Ending July 1, 1952
ORNL-1424	Period Ending October 1, 1952
ORNL-1478	Period Ending January 1, 1953
ORNL 1551	Period Ending March 31, 1953
ORNL-1605	Period Ending July 31, 1953
ORNL-1658	Period Ending October 31, 1953
ORNL-1678	Period Ending January 31, 1954
ORNL-1753	Period Ending April 30, 1954
ORNL-1772	Period Ending July 31, 1954
ORNL-1813	Period Ending October 31, 1954
ORNL-1853	Period Ending January 31, 1955
ORNL-1895	Period Ending April 30, 1955
ORNL-1943	Period Ending July 31, 1955
ORNL-2004	Period Ending October 31, 1955
ORNL-2057	Period Ending January 31, 1956
ORNL-2096	Period Ending April 30, 1956
ORNL-2148	Period Ending July 31, 1956
ORNL-2222	Period Ending October 31, 1956
ORNL-2272	Period Ending January 31, 1957
ORNL-2331	Period Ending April 30, 1957
ORNL-2379	Period Ending July 31, 1957
ORNL-2432	Period Ending October 31, 1957
ORNL-2493	Period Ending January 31, 1958
ORNL-2561	Periods Ending April 30 and July 31, 1958
ORNL-2654	Period Ending October 31, 1958
ORNL-2696	Period Ending January 31, 1959
ORNL-2743	Period Ending April 30, 1959
ORNL-2879	Period May 1 Through October 31, 1959
ORNL-2920	Period Ending January 31, 1960
ORNL-2947	Period Ending April 30, 1960
ORNL-3004	Period Ending July 31, 1960
ORNL-3061	Period from August 1 to November 30, 1960